NASA/CR-2001-211025

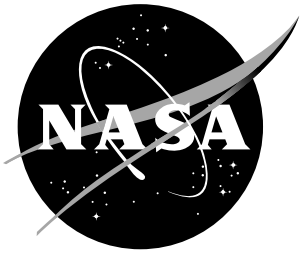

Development and Evaluation of Stitched Sandwich Panels

Larry E. Stanley and Daniel O. Adams
University of Utah, Salt Lake City, Utah

June 2001

The NASA STI Program Office ... in Profile

Since its founding, NASA has been dedicated to the advancement of aeronautics and space science. The NASA Scientific and Technical Information (STI) Program Office plays a key part in helping NASA maintain this important role.

The NASA STI Program Office is operated by Langley Research Center, the lead center for NASA's scientific and technical information. The NASA STI Program Office provides access to the NASA STI Database, the largest collection of aeronautical and space science STI in the world. The Program Office is also NASA's institutional mechanism for disseminating the results of its research and development activities. These results are published by NASA in the NASA STI Report Series, which includes the following report types:

- TECHNICAL PUBLICATION. Reports of completed research or a major significant phase of research that present the results of NASA programs and include extensive data or theoretical analysis. Includes compilations of significant scientific and technical data and information deemed to be of continuing reference value. NASA counterpart of peer-reviewed formal professional papers, but having less stringent limitations on manuscript length and extent of graphic presentations.

- TECHNICAL MEMORANDUM. Scientific and technical findings that are preliminary or of specialized interest, e.g., quick release reports, working papers, and bibliographies that contain minimal annotation. Does not contain extensive analysis.

- CONTRACTOR REPORT. Scientific and technical findings by NASA-sponsored contractors and grantees.

- CONFERENCE PUBLICATION. Collected papers from scientific and technical conferences, symposia, seminars, or other meetings sponsored or co-sponsored by NASA.

- SPECIAL PUBLICATION. Scientific, technical, or historical information from NASA programs, projects, and missions, often concerned with subjects having substantial public interest.

- TECHNICAL TRANSLATION. English-language translations of foreign scientific and technical material pertinent to NASA's mission.

Specialized services that complement the STI Program Office's diverse offerings include creating custom thesauri, building customized databases, organizing and publishing research results ... even providing videos.

For more information about the NASA STI Program Office, see the following:

- Access the NASA STI Program Home Page at ***http://www.sti.nasa.gov***

- E-mail your question via the Internet to help@sti.nasa.gov

- Fax your question to the NASA STI Help Desk at (301) 621-0134

- Phone the NASA STI Help Desk at (301) 621-0390

- Write to:
  NASA STI Help Desk
  NASA Center for AeroSpace Information
  7121 Standard Drive
  Hanover, MD 21076-1320

NASA/CR-2001-211025

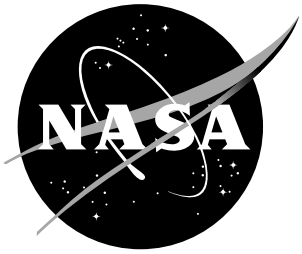

Development and Evaluation of Stitched Sandwich Panels

Larry E. Stanley and Daniel O. Adams
University of Utah, Salt Lake City, Utah

National Aeronautics and
Space Administration

Langley Research Center
Hampton, Virginia 23681-2199

Prepared for Langley Research Center
under Purchase Order L-11332

June 2001

The use of trademarks or names of manufacturers in the report is for accurate reporting and does not constitute an official endorsement, either expressed or implied, of such products or manufacturers by the National Aeronautics and Space Administration.

Available from:

NASA Center for AeroSpace Information (CASI)
7121 Standard Drive
Hanover, MD 21076-1320
(301) 621-0390

National Technical Information Service (NTIS)
5285 Port Royal Road
Springfield, VA 22161-2171
(703) 605-6000

ABSTRACT

This study explored the feasibility and potential benefits provided by the addition of through-the-thickness reinforcement to sandwich structures. Through-the-thickness stitching is proposed to increase the interlaminar strength and damage tolerance of composite sandwich structures. A low-cost, out-of-autoclave processing method was developed to produce composite sandwich panels with carbon fiber face sheets, a closed-cell foam core, and through-the-thickness Kevlar stitching. The sandwich panels were stitched in a dry preform state, vacuum bagged, and infiltrated using Vacuum Assisted Resin Transfer Molding (VARTM) processing. For comparison purposes, unstitched sandwich panels were produced using the same materials and manufacturing methodology. Test panels were produced initially at the University of Utah and later at NASA Langley Research Center. Four types of mechanical tests were performed: flexural testing, flatwise tensile testing, core shear testing, and edgewise compression testing. Drop-weight impact testing followed by specimen sectioning was performed to characterize the damage resistance of stitched sandwich panels. Compression after impact (CAI) testing was performed to evaluate the damage tolerance of the sandwich panels. Results show significant increases in the flexural stiffness and strength, out-of-plane tensile strength, core shear strength, edgewise compression strength, and compression-after-impact strength of stitched sandwich structures

TABLE OF CONTENTS

CHAPTER 1

INTRODUCTION

As technology advances, the need increases for lighter and stronger materials that may be tailored for specific applications. The use of composites, specifically laminated composites, has grown significantly over the last two decades in order to fill the need for lighter and stronger materials in our advancing society. Fabrication and design of these materials is continually evolving to make even stronger and lighter structures. Composite sandwich structures and stitched composites are two examples of composite structures that have evolved to fill some of these needs. This study will focus on the combination of these two types of composite structures.

Laminated composites traditionally consist of layers of unidirectional fibers impregnated with an epoxy resin. The fibers are usually much stronger and stiffer than the resin. Changing the orientation of the fibers significantly changes the directional material properties of the composite. The orientation of fibers can thus be adjusted to achieve desired properties within the plane of the laminate. The properties of the composite in the out-of-plane direction, or through-the-thickness, are highly dependent on the properties of the weaker resin. Delamination between the layers of laminated composites remains a concern and has led to many attempts to increase the properties of the composite in the out-of-plane direction.

One method of increasing the out-of-plane properties receiving particular attention recently has been the addition of through-the-thickness stitching to the composite laminate. Stitched composite materials have been evaluated in recent years for structural applications, including stiffened wing structures for commercial aircraft. Of particular interest to the aerospace industry, as well as to this study, has been through-the-thickness stitching of carbon-fiber/epoxy composites with Kevlar yarns to provide greater damage tolerance and allow for low-cost manufacturing [1]. Stitched composites have been shown to be a viable material for commercial aircraft wing structures due to their high retention of in-plane properties and increased resistance to delamination growth [2]. This study extends the use of stitching from laminated composites to composite sandwich structures.

A sandwich structure consists of a lightweight core material bonded to two thin face sheets of a stronger and stiffer material such as carbon/epoxy. The major advantage of the sandwich is its high flexural stiffness to weight ratio. The lightweight foam core serves to place the stiffer face sheet material further from the neutral axis where its resistance to flexural loads is amplified. Other advantages of the sandwich structure include electric, acoustic, and thermal insulation. The combination of damage tolerant stitched carbon-epoxy structures with sandwich structures is an attempt to achieve the desirable properties of both types of structures. Stitched sandwich structures may be designed to achieve high damage tolerance from the stitching while maintaining the high stiffness to weight ratio of the sandwich structure. However, significant new challenges must be addressed before this innovative concept of stitched sandwich structures can be considered a viable technology. First, an affordable methodology

must be developed for manufacturing a stitched sandwich structure that maintains the traditional attractive properties of composite sandwich structures, including high flexural stiffness, high flexural strength, and minimal weight. Second, the stitched sandwich structures must show significantly enhanced damage tolerance and interlaminar strength as compared to unstitched sandwich structures.

This investigation focused on assessing the feasibility and potential benefits obtained by uniformly stitching foam-core sandwich panels with Kevlar yarns. To offer low cost manufacturing, stitched sandwich panels were manufactured using low-cost, out-of-autoclave processing. Sandwich panels were stitched in a dry preformed state, vacuum bagged, and infiltrated using Vacuum Assisted Resin Transfer Molding (VARTM) processing. The through-the-thickness stitches provided resin infusion paths to the facesheet adjacent to the tool surface. Evaluation of mechanical properties focused on three-point and four-point bending tests, core shear tests, flatwise tensile tests, edgewise compression tests, as well as compression after impact testing. The objective of this investigation was to demonstrate that stitching of sandwich structures, manufactured using low-cost processing methods, produces significant increases in damage tolerance and interlaminar strength while maintaining the attractive properties of traditional sandwich structures. Following the benefits obtained from the stitching of laminated composite, it is natural to expect similar benefits when such stitching technology is applied to sandwich structures. With these benefits, stitched sandwich structures will be viable for a variety of applications where increased interlaminar strength and damage tolerance as well as low-cost manufacturing are required.

CHAPTER 2

LITERATURE REVIEW

Composite sandwich structures have been used for many years, primarily in applications where high flexural strength and high flexural stiffness are required at a minimal weight. Many applications of sandwich structures have been in the aerospace industry. One of the early uses of sandwich structures in an aerospace application was the 1937 application of balsa wood core and cedar plywood facesheets in the DeHavilland Albatross airplane [3].

Typical sandwich structures consist of a light core material placed between two thin facesheets or skins. Three common types of core materials are balsa wood, honeycomb structures, and rigid foams. Typically the facesheets are made from materials such as aluminum, fiberglass, graphite, and aramid [4]. The advantage of the sandwich construction is gained by placing the stiff facesheets at a greater distance away from the neutral axis in bending, analogous to the flanges of an I -beam. However, the core and facesheets must be designed together as a composite structure. There are two typical techniques used to bond the facesheet to the core. The first is to adhesively bond the completed face sheet using a resin film or paste. The other technique is to use the same infiltration process that infiltrates the fibers of the

facesheet. This is a process that simultaneously bonds the facesheets to the core as the fibers are infiltrated.

In a properly designed sandwich structure, the facesheets carry most of the tensile and compressive stresses due to axial loading and bending whereas the core carries most of the shear stresses. The core and the facesheets must remain bonded at the skin-core interface for the two materials to function effectively as a sandwich structure. This critical interface is susceptible to delaminations and in general has limited strength since there are no reinforcements bridging the interface. Knowing that the skin/core interface is critical to sandwich structures, it follows that improvements to the interlaminar strength of this interface will increase the strength and damage tolerance of the sandwich structure.

The use of stitching as a through-the-thickness reinforcement has been investigated by several researchers for laminated composites. In recent years stitched monolithic composite materials have been evaluated extensively for structural applications. Of particular interest has been the through-the-thickness stitching of carbon-fiber/epoxy composites with Kevlar yarns to provide greater damage tolerance and allow for low-cost manufacturing [1].

Testing and analysis of stitched carbon-epoxy structures was a research topic within the NASA Advanced Subsonic Technology Program (AST) for several years. Through the AST Program, stitched composites have been shown to be a viable material for commercial aircraft wing structures due to their high retention of in-plane properties and increased resistance to delamination growth. In one phase of the AST Program, a Textile Mechanics Working Group was developed to investigate both experimental and

analytical aspects of stitched, braided, and woven composites for commercial aircraft applications [1]. Specialized tests were developed and performed to assess the performance of stitching. Sharma and Sankar [2] developed test methods to assess delamination growth resistance of stitched composites. Adams [5] performed specialized testing to determine the debonding behavior of stitches bridging a delamination and provide "in-situ" compliances of a stitch in a delaminated composite for use in finite element modeling. Additionally, predictive capabilities for damage progression were developed in a later phase of the AST program [6, 7]. Testing of stitched composites in the AST Program progressed from single stitch row specimens to large structural panels to a full wing box validation test. This NASA/Boeing Stitched Wing featured through-the-thickness stitching of carbon fiber preforms followed by resin film infusion. Uniform rows of stitching were used throughout the wing skins to provide increased damage tolerance. Additionally, stiffeners and spars were preformed and stitched to the wing skins prior to resin infiltration. The full-scale wing box validation test was performed successfully during the summer of 2000 at NASA Langley Research Center [8]. Other research involving stitched monolithic composites has addressed a wide range of issues, including assessing mechanical performance and damage tolerance [9-14], developing analysis methodologies for stitched composites [15, 16], and the stitching of lap joints [17].

To date, stitching of sandwich structures has received minimal attention. Currently there is only one published study on the stitching of sandwich composites. This recent investigation was performed to investigate the energy absorption characteristics of stitched sandwich panels [18]. Panels were fabricated from glass fiber

preformed facesheets and a foam core stitched together with Kevlar thread. The dry preforms were injected with resin using an RTM process at room temperature. Several stitched sandwich panels with different stitch densities were produced and tested under an edgewise-compressive load. Static crush tests were performed on panels of various densities of through-the-thickness stitching. Additionally, the instability of the panels just before crushing failure was explored using finite element analysis. Results indicated that higher densities of stitching increased the load the panel could sustain as well as energy absorption.

The current investigation focused on fabrication and testing of uniformly stitched foam-core sandwich panels. Fabrication methods developed for stitched sandwich panels are presented in Chapter 3. Tensile testing of individual Kevlar stitches infiltrated with epoxy resin is presented in Chapter 4. The evaluation of the mechanical properties of the stitched sandwich panels is described in Chapter 5. An investigation into the damage tolerance of stitched sandwich panels is presented in Chapter 6. Conclusions and recommendations are made in Chapter 7.

CHAPTER 3

FABRICATION

3.1 Fabrication procedure

The first step in this study was to develop a fabrication technique for manufacturing stitched composite sandwich structures. The selection of materials and fabrication methods for stitched sandwich structures was guided by past successes in stitching of carbon/epoxy composite laminates. This chapter will discuss the materials selected as well as the fabrication process used to produce stitched sandwich panels.

Material selection was the first step in the fabrication process. Two different types of core material were selected. Both core materials were closed-cell foams. Open-cell foams were not considered because they would be saturated with resin during the infiltration process. Two different vendors were chosen to supply the foam cores. The foam cores chosen were General Plastics LAST-A-FOAM FR-6706 polyurethane six pound per cubic foot density foam and Northern Fiber Glass Rohacell industrial grade 31 polymethacrylimide two pound per cubic foot density foam [19,20]. These foams were selected for their low densities and the ability to stitch through them using a conventional stitching needle and Kevlar yarn.

The facesheets were made from multiaxial warp-knit carbon fiber preforms [21], composed of a $[\pm 45/0/90/0/\pm 45]_T$ layup of dry AS4 carbon fiber knitted together with polyester thread. This carbon fiber preform material, used previously in the NASA

Stitched Wing Program, consisted of 44% 0 degree material 44% +/- 45 degree material and 12% 90 degree material. These dry preforms were relatively easy to stitch through, having a feel similar to that of an extremely coarse and heavy textile. The dry perform facesheets and foam core were then assembled in a dry lay-up (Figure 3.1) already stitched.

Two variations of stitched sandwich panels were investigated in this study, referred to as "Utah" panels and "NASA" panels. The Utah panels, manufactured at the University of Utah, were developed first and used in the initial phase of this study. The NASA panels were produced later in the study at NASA Langley Research Center using knowledge gained during the production of the Utah panels. Although the two types of panels were similar in many respects, there were important differences between them. The NASA panels used two layers of multiaxial warp-knit fabric for each facesheet whereas the Utah panels used one layer for each facesheet. Although both sets of panels used closed cell foams as the core material, the core densities and the core manufacturers differed as previously discussed. Kevlar 29 yarn was used to stitch both sets of panels because of its high strength and its successful performance in previous stitching applications with composite laminates.

Stitching of the Utah panels consisted of a two-part process. Holes were punched in the panels using a needle and a CNC-Milling machine to achieve straight, accurately placed stitches. The stitch holes were placed at half-inch intervals between stitches and at half-inch spacing between stitch rows. The panels were then stitched by hand using a modified lock stitch. The lock stitch is the basic stitch used on a common

Figure 3.1 Top surface of dry panel

sewing machine as shown in Figure 3.2. Note that the intersection between the upper stitch thread and the lower bobbin thread occurs at the middle of the core. The modified lock stitch is produced by pulling the upper stitch yarn completely through the core to the bottom surface of the panel as Figure 3.3 illustrates. This produces a continuous stitch yarn through the entire thickness of the panel. Note that since the upper stitch yarn is looped through the thickness of the panel, each stitch is composed of two yarns.

All Utah panels were stitched using a 1600 denier yarn for the upper stitch yarn. Three bobbin yarns were used: 400,1600, and 3200 denier. The 3200 denier bobbin yarn was obtained by twisting two 1600 denier yarns together. Initially, panels were stitched at 90 degrees normal to the panel surfaces. Later in the investigation, additional panels were stitched at 45 degrees to the surfaces of the panel as shown in Figure 3.4 to investigate the performance of “angled” stitches. Panels with

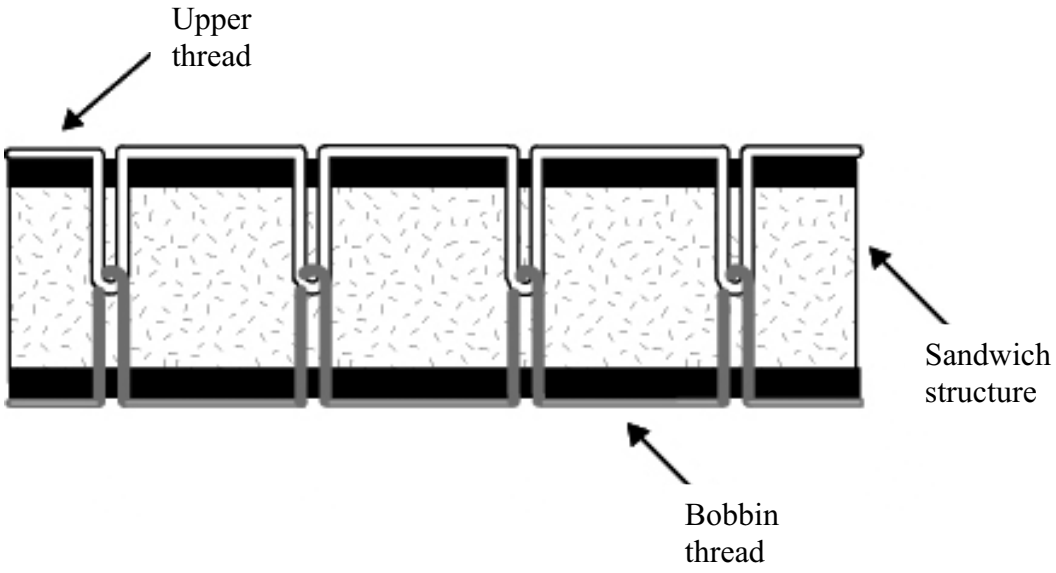

Figure 3.2 Diagram of traditional lock stitch.

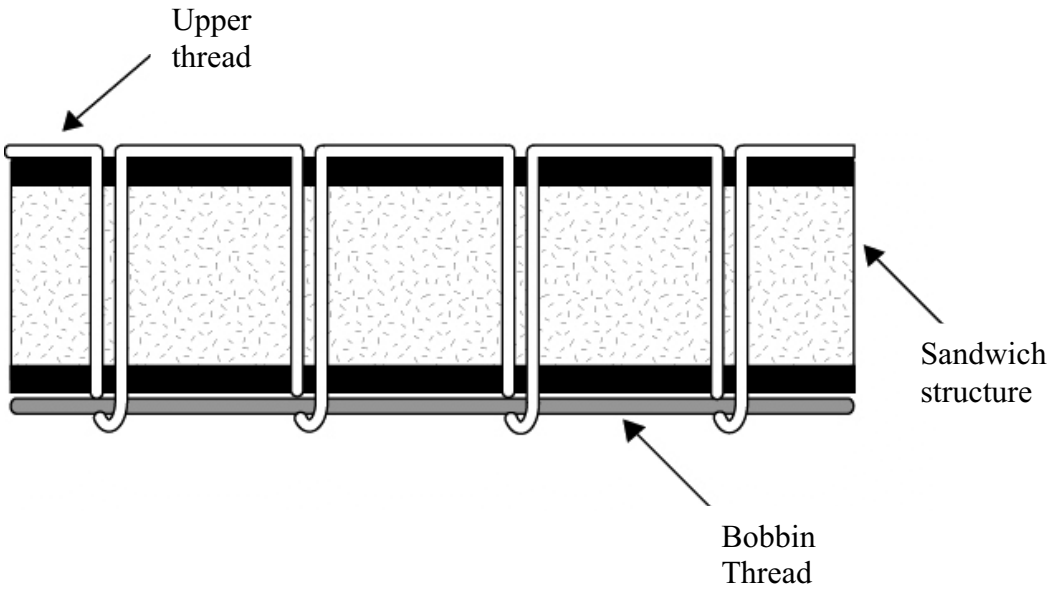

Figure 3.3 Diagram of Modified Lock Stitch.

Figure 3.4 Cross-section of angled stitching.

angles stitching were produced by the same method as the 90 degree stitched panels.

One row of stitches through the panel was stitched at the appropriate angle. The next adjacent row was stitched in the opposite direction. This crossing of stitches, as shown in Figure 3.5, insures an equal number of stitches in each direction and allows for spacing in the panel where cuts can be made without cutting through stitches. Specimens could then be fabricated out of the angled stitched panels that have the same number of stitches as the 90 degree stitched panels.

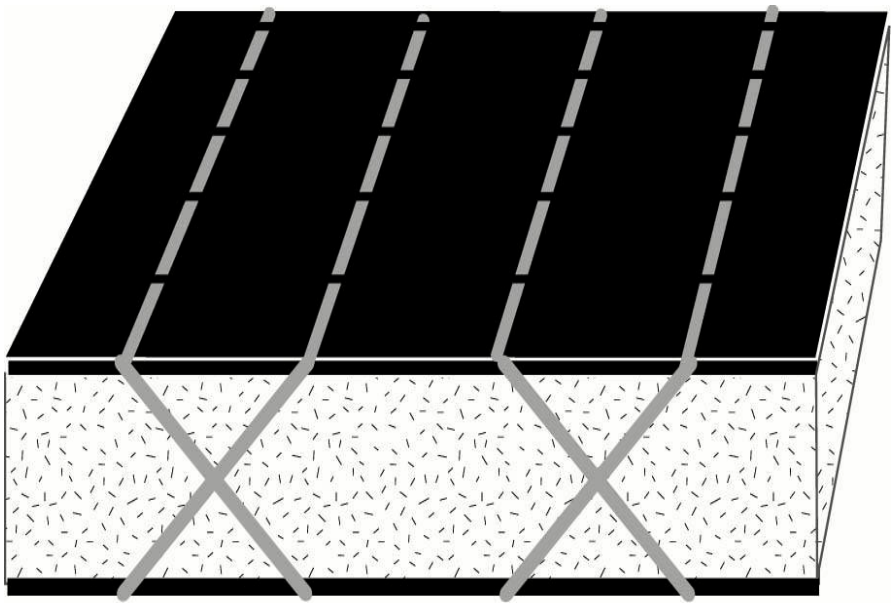

Figure 3.5. Diagram of panel stitched at an angle.

All NASA panels were stitched using the same modified lock stitch. However, the NASA panels were stitched using a Pathe automated stitching machine developed for the Advanced Subsonic Technology (AST) Stitched Wing Program. The NASA panels were stitched with 0.25 in. spacing between stitches and with three different spacing between stitch rows: 0.25 in., 0.5 in., and 1.0 in. All NASA panels were stitched using 1600 denier yarn for both the stitch and bobbin thread and all were stitched at 90 degrees to the surface of the panels.

As the needle is pushed through the foam core, individual cells of the closed cell foam are either pierced or compressed to rupture. These damaged cells fill with resin during the infiltration process, resulting in a column of resin as shown in Figure 3.5. Initial studies performed using several different sizes of stitching needles showed that the diameter of this resin column is proportional to the diameter of the needle used in the stitching process. This extra resin surrounding the stitch is undesirable since it increases the weight of the panel without providing significant additional reinforcement to the foam core. For this reason, the 0.09 in. diameter needle (commonly used with industrial sewing machines) used initially was replaced with a 0.05 in. diameter needle. Figure 3.6 illustrates the resin column produced by these two needle diameters.

The infiltration of the sandwich panel was preformed using a Vacuum Assisted Resin Transfer Molding (VARTM) technique. VARTM infiltration utilizes a vacuum to pull resin at atmospheric pressure into the mold and throughout the preform. Prior to infiltration, the sandwich panels were first wrapped in Teflon coated fiberglass to aid the release of the finished panel. A layer of coarse nylon mesh was placed on each side of the panel to assist the infiltration by distributing the resin over the surface

a. 0.05 in. diameter needle

b. 0.09 in. diameter needle

Figure 3.6 Resin columns produced by stitching needles.

of the panel. The assembly was placed on a flat aluminum plate and sealed inside a vacuum bag with breather cloth to absorb excess resin and allow for the gasses to exit the mold. Small tubes were inserted into the vacuum bag at opposite ends. One tube was connected to a vacuum pump and the other to the resin container. This assembly is illustrated in Figure 3.7.

Two different resin systems were used during the initial development phase. The first resin system used was Dow 600 vinyl ester resin [22]. Since vinyl ester resin cures at room temperature, small practice panels could be infiltrated quickly and without the use of a heating source. Vinyl ester resin was used throughout the preliminary stages of this study while the infiltration process was being refined. After the infiltration process was well developed, an elevated-temperature curing resin was used. Shell 862 resin with 2181 hardener [23], a 150 degree Fahrenheit temperature curing system, was selected because of its low viscosity at room

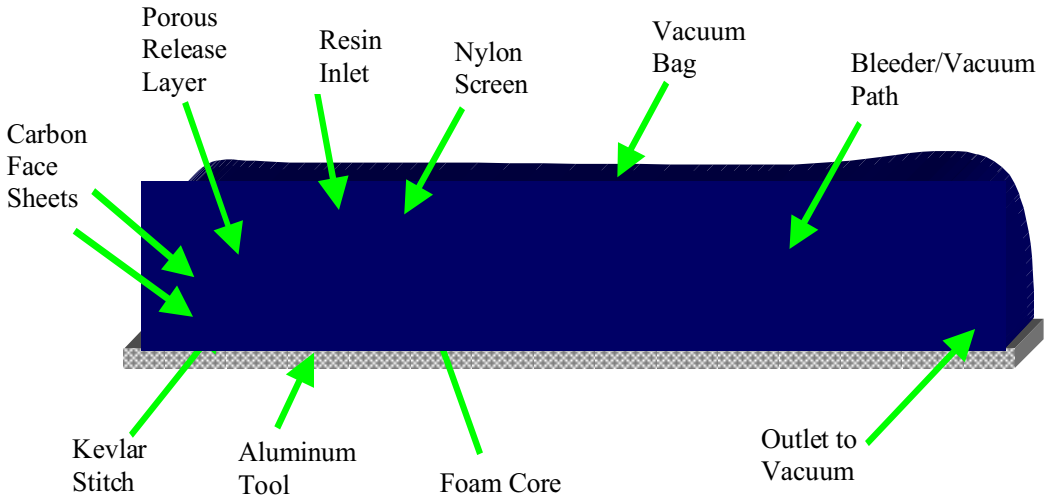

Figure 3.7 Cross section of infiltration assembly.

temperature and its proven use with similar infiltration processes. This resin system is commonly used in sporting good applications where high toughness characteristics are required.

After the resin and hardener were mixed, the resin inlet tube was placed into the resin pot and the vacuum pump was turned on. Resin was pulled through the tube and into the vacuum bagged panel assembly, infiltrating the facesheets as well as the Kevlar stitches as shown in Figures 3.8a through 3.8d. The through-the-thickness stitching produced resin paths that allow resin to flow freely between the top and bottom facesheets of the panel. Thus, the facesheets were infiltrated and bonded to the core in the same processing step.

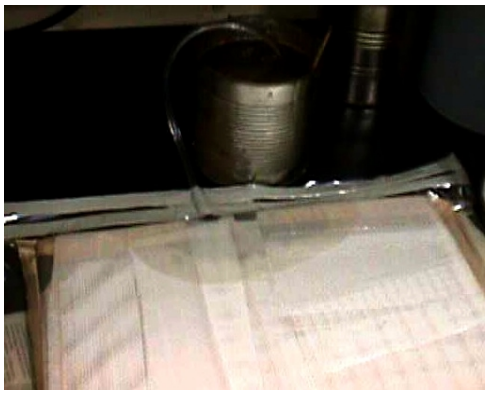

a. Beginning of Infiltration.

b. Midpoint of Infiltration.

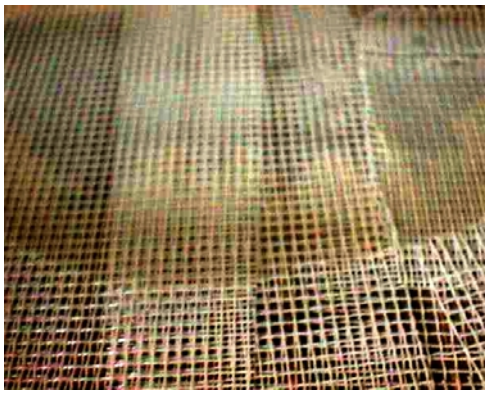

c. Close-up view of Infiltration.

d. Fully Infiltrated.

Figure 3.8 VARTM Infiltration Process

After the panel was fully infiltrated, the resin inlet was sealed and the panel was placed in an oven at 150 degree Fahrenheit for curing. Compaction was obtained by maintaining a vacuum throughout the curing process.

In many of the initial infiltration attempts, air bubbles were trapped in the stitch holes at the bottom and top of the panels. After subsequent infiltrations, it was found that the orientation of the panel contributed greatly to this problem. Consequently, it was found that by placing the panel with the bobbin yarn on the bottom against the tooling and with the addition of a wetting agent, BYK 505[24], this problem was solved.

The finished panels were cut to the appropriate size using a water-cooled diamond saw as shown in Figure 3.9. To avoid damage to the soft foam core, clamping pressure applied to the panel was minimized during the cutting process. Special care was taken to insure that the cuts were made at equal distances from the stitches on each side of the specimen. The Utah panels were cut into specimens with dimensions 2.0 in. x 2.0 in. for flatwise tension, 1.0 in. x 10.0 in. for flexure, 8.0 in. x 2.0 in. for core shear, and 2.0 in. x 2.6 in. for edgewise compression. Because of the different densities of stitching and to minimize waste, the NASA panels were cut to different specimen dimensions than the Utah specimens. Specimens from the NASA panels were 1.93 in. x 1.93 in. for flatwise tension, 1.93 in. x 8.0 in. for core shear, 1.93 in. x 10.0 in. for flexure, and 1.93 in. x 2.5 in. for edgewise compression. A width of 1.93 in. rather than 2.0 in. accounted for the width of the cutting blade and centered the stitch rows within the specimens.

Figure 3.9 Cutting of specimens with water-cooled diamond saw.

3.2 Panel weight measurements

Weight is an important attribute of the sandwich structure. Weight measurements were taken from representative panels prior to mechanical testing. Panel sections approximately 11 in. x 7 in. were used for the weight measurements. After conditioning the panels for several days at 70 degrees Fahrenheit, weight measurements were taken using a weight balance and are included in Tables 3.1 and 3.2. Areal weight is given in weight per area of the panel.

The areal weight measurements of the Utah panels were not what was initially expected. The stitched panels weighted 4% less than the unstitched panel and the angled stitched panel weighed 2% more than the unstitched panels. It was expected that stitching would increase the weight of the panel because of the increase in resin volume

needed to infiltrate the stitches and the stitch columns. Having the same amount of foam core and fiber in the facesheets, the only difference can be the weight of the yarn and resin. The addition of yarns can only increase the weight; thus the difference must be in the amount of resin in the face sheets. The unstitched panels must have a higher resin content in the face sheets for them to weigh more than the stitched panels. During the VARTM infiltration process of and unstitched panel, the compaction pressure is maintained only by the vacuum pressure in the vacuum bag. In the stitched panels there is also the compaction of the stitches holding the facesheets to the core. This results in a higher fiber volume fraction in the facesheets and a lower overall weight of the stitched panels. The panels stitched at an angle have a longer resin column,

Table 3.1 Areal weight of Utah panels

Specimen type:	Areal weight, lb/in^2	Percent of unstitched panel
Unstitched	.00893	100%
Stitched	.00856	96%
Angled Stitched	.00912	102%

Table 3.2 Weight of NASA Panels

Specimen type:	Density (lb/in^2) weight per area of panel	Percent of Unstitched panel of same thickness
.05 in. core unstitched	0.0136	100%
.05 in. core 1.0 in. stitch spacing	0.0141	104%
.05 in. core .05 in. stitch spacing	0.0148	109%
.05 in. core 0.25 in. stitch spacing	0.0163	119%
1.0 in. core unstitched	0.0144	100%
1.0 in. core 1.0 in. stitch spacing	0.0153	106%
1.0 in. core .05 in. stitch spacing	0.0166	116%
1.0 in. core 0.25 in. stitch spacing	0.0188	131%

and thus more resin than the panels stitched at 90 degrees. This would explain why the weight is 2% greater than the unstitched panels.

The results from the areal weight of the NASA panels agreed with what was expected intuitively. The unstitched panels weighed the least, and the panel with the 0.25 in. stitch spacing weighed the most. It can be observed that the areal weight increases with increases in stitch density. The difference between the trends in areal weight of the NASA and Utah panels may be caused in part by the fabrication facilities. The NASA panels were fabricated at a lower altitude and with different vacuum pressure. Other differences could have been caused by the different thicknesses in the facesheets and core material.

Prior to presenting the mechanical testing of the stitched sandwich panels, results obtained from tensile testing of infiltrated Kevlar yarns will be presented in the following chapter.

CHAPTER 4

TENSILE TESTING OF KEVLAR YARNS

Tensile testing was performed to determine the stiffness and strength of the Kevlar 29 yarns used for stitching the composite sandwich structures. Tensile testing was performed on both resin-infiltrated as well as noninfiltrated Kevlar yarns following ASTM standard D 2256 [25]. The stiffness and strength of the Kevlar yarns are of interest for analytical and numerical modeling of stitched sandwich structures.

Tensile testing was performed on Kevlar 29 PVA (400/1X4) yarn thread supplied by NASA Langley Research Center. This yarn was the same 1600 denier yarn used as the stitch thread in both the Utah and NASA panels. Thus, the yarn tested is identical to the needle yarn that extended through the thickness of the stitched sandwich panels. Note that two thicknesses of Kevlar 1600 denier yarn loop through-the-thickness of the sandwich to form a stitch whereas a single yarn was tested here.

To most accurately simulate the actual stitch behavior in an infiltrated sandwich panel, the Kevlar yarns were infiltrated with Hexcel 3501-6 epoxy and cured prior to testing. The work on tensile testing of Kevlar yarns was completed as part for the stitched wing program. This work was completed prior to the development of a fabrication process for stitched sandwich structures. For this reason the epoxy used to test the infiltrated yarns is different from that used to infiltrate the stitched sandwich

panels.

While infiltrating a yarn within a sandwich structure was rather straightforward, infiltrating a separate, independent yarn proved challenging. A VARTM-based infiltration procedure was developed similar to that used to infiltrate the stitched sandwich panels. First, the epoxy resin was melted and degassed in a vacuum oven. The melted epoxy was then poured over the Kevlar yarn pieces to be infiltrated. The threads and epoxy were next sealed in a vacuum bag and placed into a warm convection oven, which kept the epoxy at low viscosity. An external vacuum pump was used to pull a vacuum in the sealed bag for several minutes, forcing the epoxy into the porous Kevlar threads. The vacuum bag was opened while still in the convection oven (to keep the epoxy melted) and the infiltrated threads were straightened, hung in the oven with a small weight attached, and cured at 350 degrees Fahrenheit for 4 hours.

Microscopic evaluation of the infiltrated yarns showed that the epoxy resin had fully infiltrated the Kevlar yarn. A photomicrograph of the cross section of an infiltrated yarn is shown in Figure 4.1.

After the yarns were infiltrated and cured, specimens were cut to the desired lengths. Three specimen lengths were tested, with gage lengths of 5 in., 10 in., and 20 in. Five specimens were prepared for each gage length. An additional length of 3 in. was used for gripping, resulting in total specimen lengths of 8 in., 13 in., and 23 in. Testing was performed in accordance with ASTM D 2256-95a. To prevent slipping or damage to the yarn ends, 220 grit emery paper was placed adjacent to the yarn followed by 0.06 in. thick butyrate sheets.

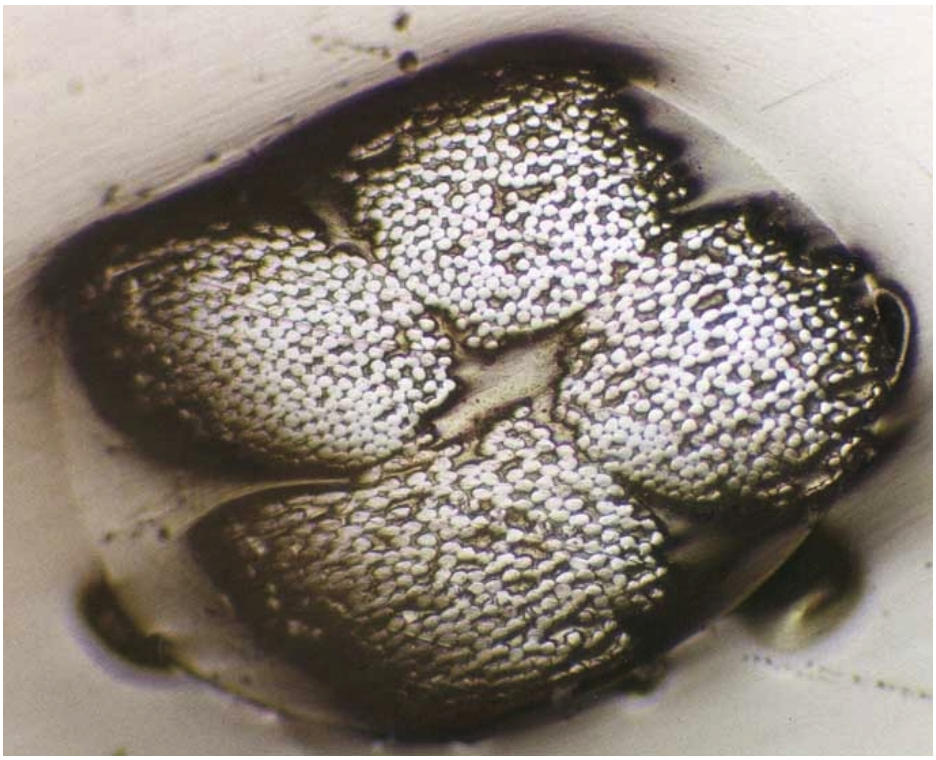

Figure 4.1 Photomicrograph of 1600 denier infiltrated Kevlar yarn cross section

This assembly was gripped using serrated-surface wedge grips. Specimens were tested under constant displacement loading using an Instron electromechanical test machine. As the specimen was elongated, load and crosshead deflection was recorded. Figure 4.2 shows a typical load versus deflection plot obtained from a 10 in. gage length infiltrated yarn specimen. This plot shows that after the initial loading stage, the load versus deflection behavior of the specimen is approximately linear until failure.
The yarn specimen stiffnesses were determined from the slopes of the initial linear portion of the load versus deflection curves.

If there were no compliance in the load train, then the stiffness values obtained from the load versus deflection curves would be due entirely to the yarn specimen. If

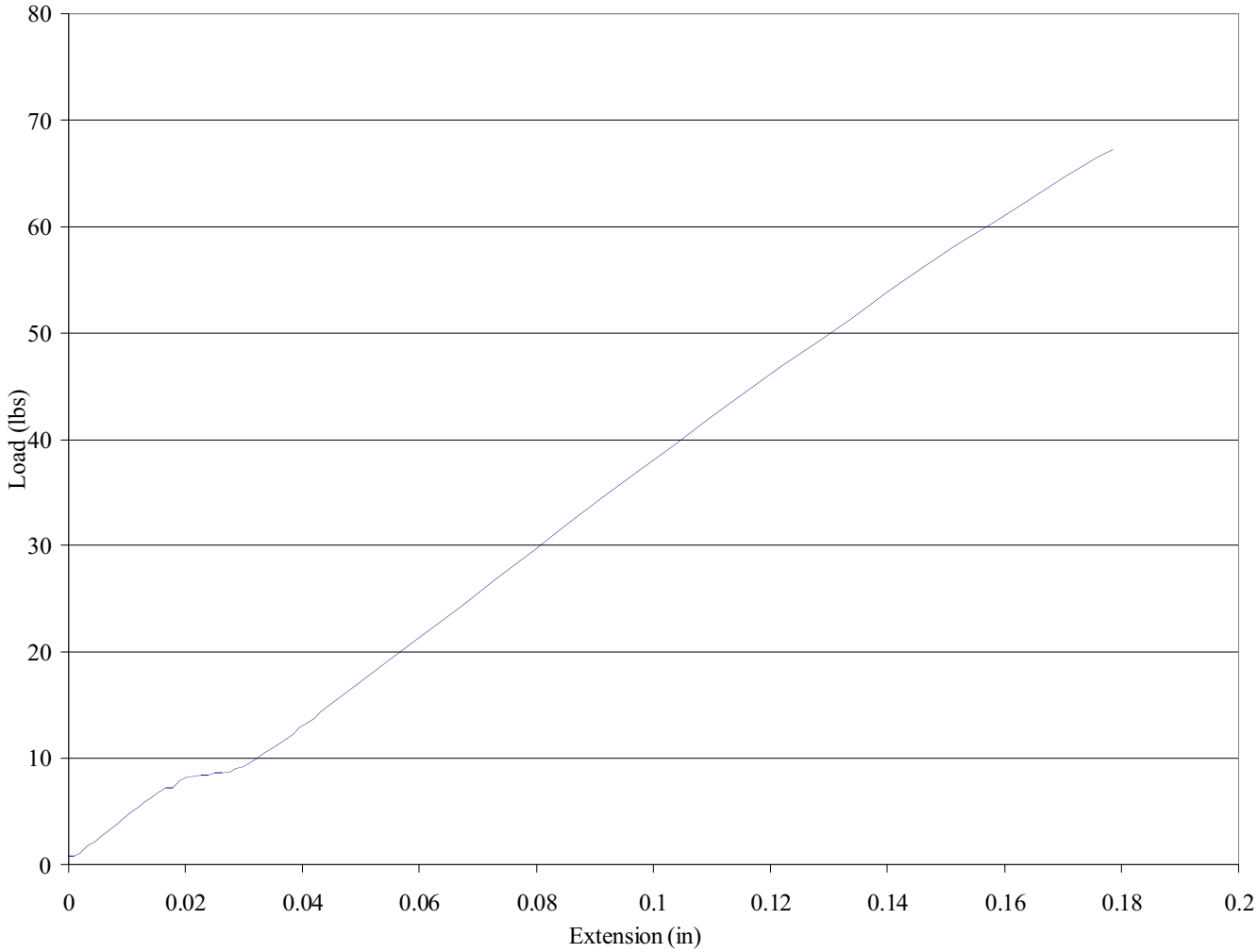

Figure 4.2 Typical load versus deflection plot for Kevlar yarn specimen

this were the case, the yarn specimen stiffnesses would decrease in proportion to the gage length. That is, the stiffness values would decrease by a factor of two from the 5 in. to the 10 in. gage length and from the 10 in. to the 20 in. gage length. Since this trend was not observed in the test results, appreciable load train compliance was suspected. The compliance in the load train was determined by plotting the yarn specimen compliance (inverse of its stiffness) versus gage length as shown in Figure 4.3. These data were fit with a straight line and extrapolated to the zero gage length compliance value. This value, representing an estimate of the load train compliance, was 0.560 in./kip. Thus the load train stiffness, defined as the inverse of the load train compliance, was $K_{loadtrain}$ = 1.79 kip/in. From these determinations, the stiffness of the load train was accounted for by modeling the Kevlar yarn specimen and remaining load train as two springs in series with stiffnesses given by $K_{specimen}$ and $K_{loadtrain}$, respectively. Thus the total stiffness K_{total}, defined as the slope of the load versus deflection curve, may be expressed in terms of the load train stiffness $K_{loadtrain}$ and the specimen stiffness $K_{specimen}$ as

$$\frac{1}{K_{total}} = \frac{1}{K_{loadtrain}} + \frac{1}{K_{specimen}}$$

Solving for the specimen stiffness, $K_{specimen}$

$$K_{specimen} = \frac{K_{loadtrain} K_{total}}{K_{loadtrain} - K_{total}}.$$

Thus, the stiffness of the yarn specimen may be determined from the measured stiffness of the total assembly K_{total} (yarn plus load train) and the stiffness of the load train $K_{loadtrain}$.

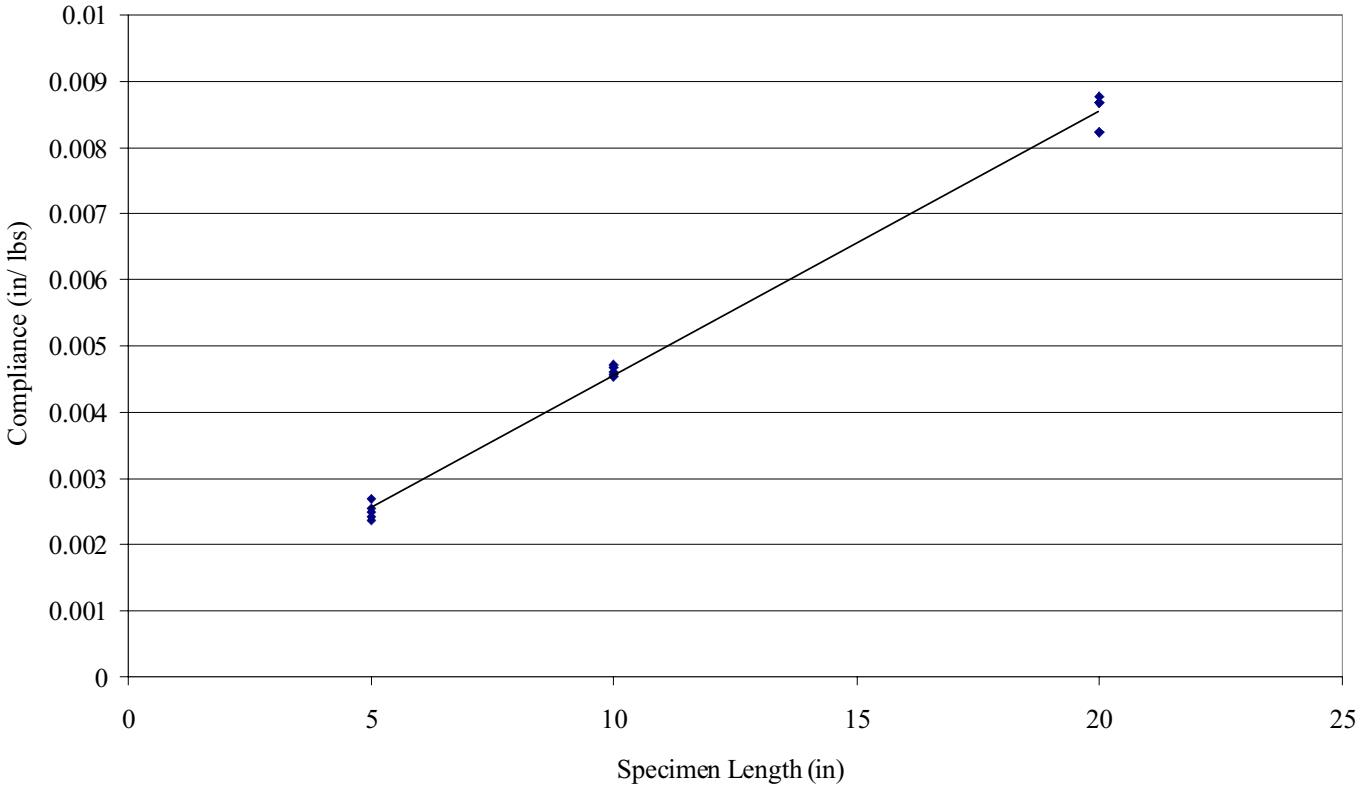

Figure 4.3 Plot of load train compliance trend line

Following this correction for the load train compliance, the resulting specimen stiffness values were divided by the gage length to obtain the yarn stiffness per unit length. These stiffness values are listed in Table 4.1. The average yarn stiffness per unit length from the 15 specimens tested was 2.52 (kip/in.)/in. The average maximum load from the 15 specimens tested was 63.4 lb.

To compare with the infiltrated test results, five yarn tensile tests were performed with noninfiltrated Kevlar yarns using a 10 in. specimen length. Results from the noninfiltrated yarn tests are shown in Table 4.2. Once again, the specimen stiffnesses were adjusted to account for compliance in the load train by modeling the

Table 4.1 Infiltrated yarn stiffness results

Gage Length, in.	Max load, lbs.	Stiffness, kip/in.	Unit Stiffness (kip/in.)/in.
5	67.2	0.400	2.58
5	61.9	0.392	2.51
5	63.1	0.424	2.77
5	60.9	0.373	2.35
5	61.6	0.412	2.67
10	63.5	0.214	2.43
10	68.1	0.212	2.40
10	60.1	0.218	2.49
10	62.1	0.217	2.47
10	59.9	0.221	2.51
20	56.1	0.115	2.46
20	61.3	0.122	2.61
20	71.9	0.114	2.44
20	60.7	0.115	2.46
20	71.9	0.122	2.61

Table 4.2 Uninfiltrated yarn stiffness test results

Gage Length, in.	Max load, lbs.	Specimen Stiffness, kip/in.	Yarn Stiffness (kip/in.)/in.
10	43.5	0.169	1.87
10	41.9	0.168	1.85
10	47.8	0.166	1.83
10	52.1	0.169	1.86
10	43.1	0.172	1.91

specimen and load train as two springs in series. The load train stiffness value of $K_{loadtrain}$ = 1.79 kip/in, obtained using the infiltrated yarn specimens, was used in these determinations. The average yarn stiffness value obtained from the five tests was 1.86 (kip/in.)/in. Comparing these results to those obtained from infiltrated yarn testing shows a 26% decrease in yarn stiffness in the noninfiltrated yarns as compared to the infiltrated yarns. The greater yarn stiffness in the infiltrated yarns is believed to result from the hardened epoxy preventing relative deformation between the fibers of the yarn when loaded in tension. This significant difference in stiffness produced by resin infiltration is important for modeling stitches in a fully infiltrated stitched sandwich structure.

It is important to note that the stiffness values presented in Tables 4.1 and 4.2 are for a single Kevlar yarn, which is equivalent to one-half of a stitch used in the stitched sandwich panels in this investigation. Thus, the effective stiffness of the two-yarn Kevlar stitch is estimated to be 5.04 (kip/in.)/in. when fully infiltrated with resin and 3.72 (kip/in.)/in. when noninfiltrated. The tensile strength of an infiltrated two-yarn stitch is estimated as 127 lb. Additionally it is noted that the epoxy resin used to

infiltrate the stitch yarns (Hexcel 3501-6) was different than the resin used to infiltrate the stitched sandwich panels (Shell 862). However, the difference in yarn stiffness due to the different epoxy resins is expected to be small.

Results from the tensile testing of infiltrated yarns may be used to estimate the flatwise tensile strength of the stitched sandwich structures. A lower bound in flatwise tensile strength may be obtained by neglecting the load carrying capacity of the foam core. Assuming that the tensile strength of a single stitch is 127 lbs, the flatwise tensile strength of a 2 in. by 2 in. specimen may be estimated by multiplying the tensile strength of a single stitch by the number of stitches in the flatwise tension specimen. Using this approach, the predicted maximum load for the flatwise tension specimens tested are presented in Table 4.3.

Table 4.3 Predicted strength of flatwise tensile specimens

Specimen Type	Number of Stitches	Predicted Maximum Load (lbs.)
Utah stitched	16	2032
NASA 1.0 in. stitch spacing	16	2032
NASA 0.5 in. stitch spacing	32	4064
NASA 0.25 in. stitch spacing	64	8128

In summary, tensile testing of the Kevlar yarns yielded two very important results. First, the stiffness of the infiltrated yarns is needed for modeling of stitches in sandwich structures. Second, the tensile strength of the infiltrated yarns is useful for estimating the flatwise tensile strength obtainable in stitched sandwich structures. These predictions will be compared with experimentally determined values in the following chapter.

CHAPTER 5

MECHANICAL TESTING

Mechanical testing was performed to determine the effects of stitching on the mechanical properties of sandwich structures. Specimens with different stitch densities, stitch angles and core thicknesses were tested in flexure, flatwise tension, core shear, and edgewise compression. Where possible, standard test methods were followed. This chapter will discuss the procedures followed in each of the tests as well as the results from the testing.

5.1 Flexural Testing

Flexural testing was carried out according to ASTM standard C393 [26]. Flexural specimens cut from the Utah panels were 1.0 in. in width and 10.0 in. long. Specimens cut from the NASA panels were cut to the same length but were1.93 in. in width. This width, 2.0 in. minus one-half the width of the cutting blade, was used in the NASA specimens to center the stitch rows within the specimens without wasting material. Four-point flexure testing was conducted initially with the Utah specimens to prevent having a maximum moment applied to a single point on the flexure specimens, while three-point loading was conducted using the NASA specimens. After analysis of the failure modes of the Utah specimens, it was determined that three-point testing

would reduce the amount of shear stress in the core of the sandwich panel. Thus three-point loading was conducted using the NASA specimens. The four-point flexure test set-up used quarter-point loading over an 8.0 inch span, as Figure 5.1 illustrates. Figure 5.2 shows the three-point test fixture with the same 8.0 inch span used.

All flexure testing was performed using an electromechanical testing machine at a constant crosshead displacement rate of 0.2 inches/min. Load and crosshead

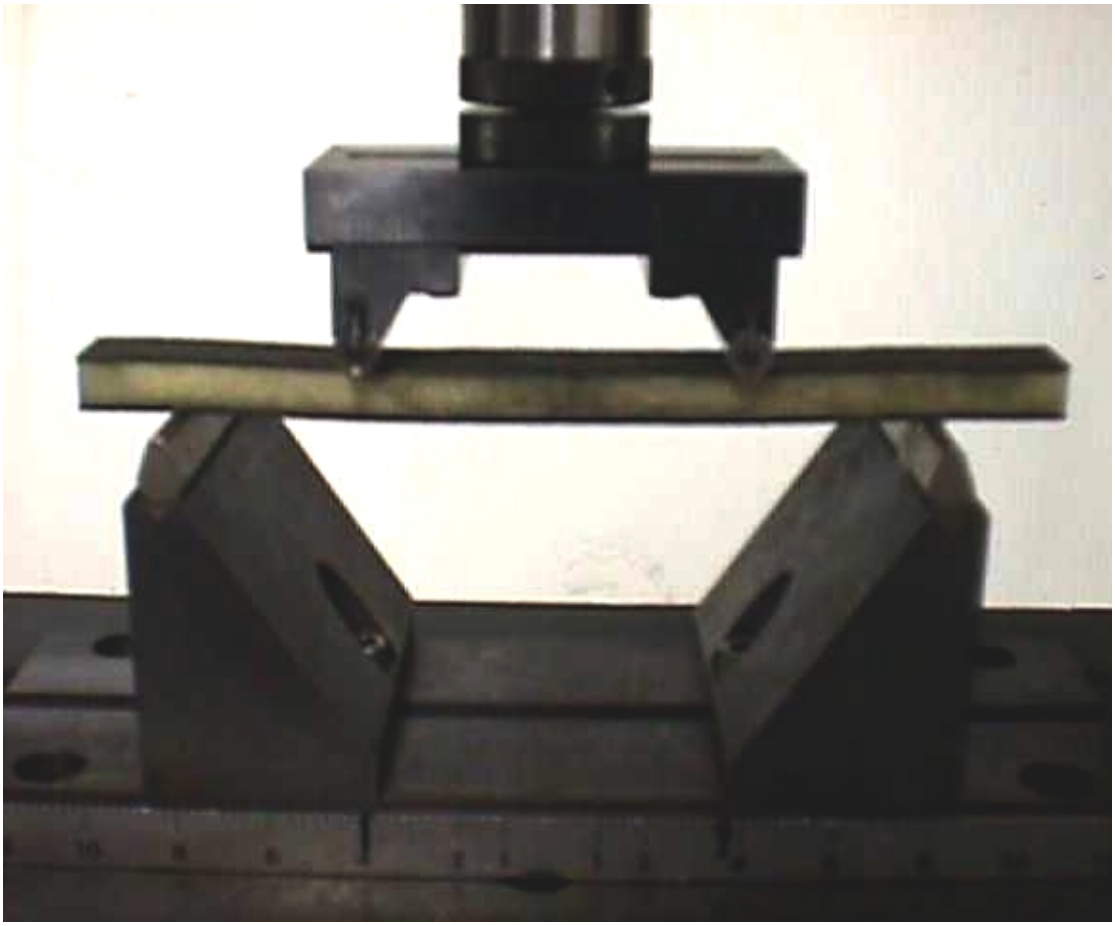

Figure 5.1 Four-point flexure test fixture.

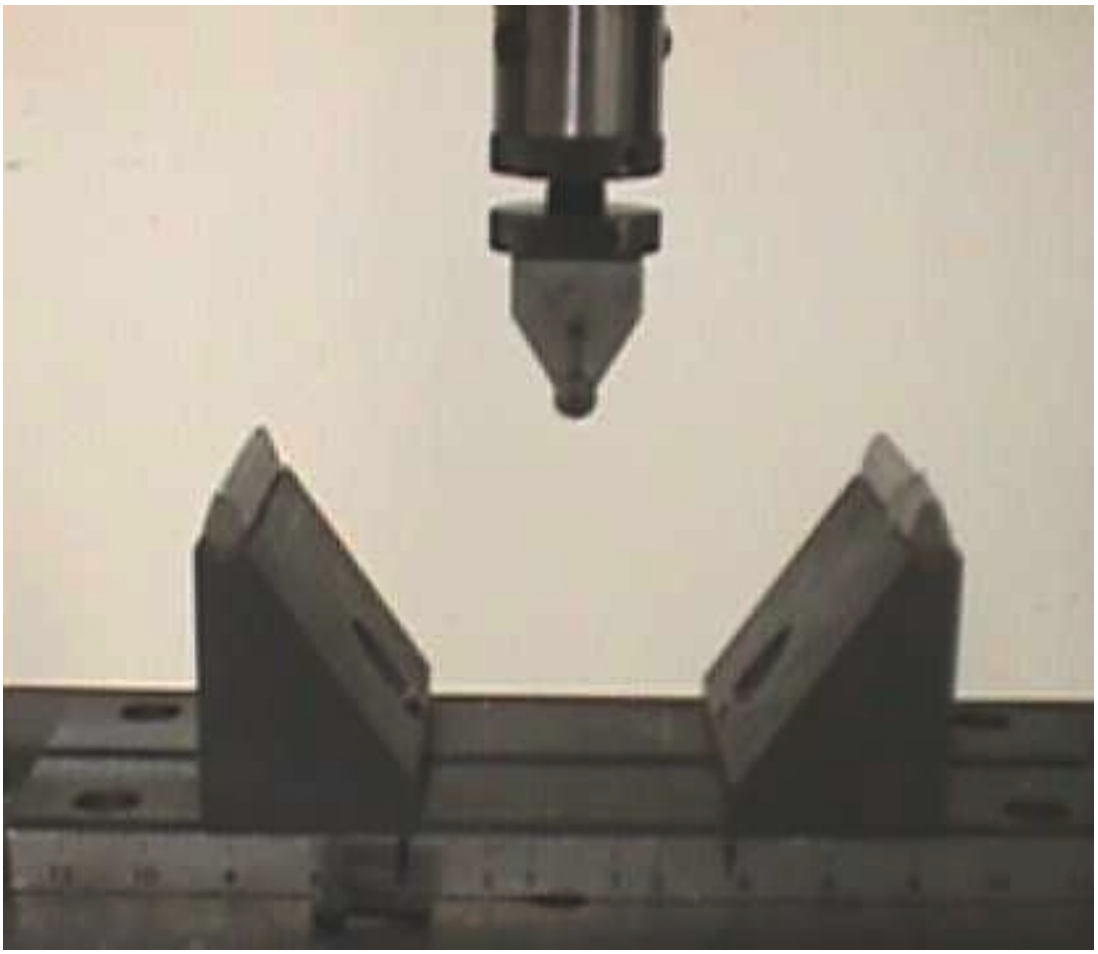

Figure 5.2 Three-point flexure test fixture.

deflection were recorded during testing. From these measurements, the effective flexural rigidity, EI, was calculated using elementary beam theory.

For the four-point bending configuration with quarter-point loading, the midpoint (crosshead) displacement δ is given by the relation:

$$\delta = \frac{11}{768}\frac{PL^3}{EI},$$

where P is the applied load and L is the span length (8 inches). Rearranging to solve for

flexural rigidity, EI, produces the relation:

$$EI = \frac{11\,L^3}{768}\left(\frac{P}{\delta}\right),$$

where the quantity P/δ represents the initial slope of the load versus crosshead displacement curve obtained from the four-point bend test. For three point bending the relation is similar:

$$EI = \frac{L^3}{48}\left(\frac{P}{\delta}\right)$$

In addition to the flexural rigidity, the load corresponding to initial failure and the maximum load were recorded. Finally, the energy absorbed was calculated, defined as the area under the load versus crosshead deflection curve up to the point of final failure. Final failure was defined as the point where the damage propagated to the outer loading points at which time testing was terminated. The energy absorbed was used qualitatively to compare energy absorption in flexure between the stitched and unstitched specimens.

Results from four-point flexure testing of the Utah specimens are presented in

Table 5.1. Representative load versus crosshead displacement plots obtained from unstitched and stitched Utah specimens are shown in Figure 5.3. In the unstitched specimens, loading progressed smoothly up to the maximum failure load, at which point a core failure occurred by cracks forming in the foam core as shown in Figure 5.4a. The cracks propagated unstably along the facesheet to the edge of the specimen as shown in Figure 5.4b. This core failure and crack growth was instantaneous. Thus, the initial failure load was the same as the maximum load.

In the stitched flexural specimens, loading progressed to a level comparable to the maximum load level for the unstitched specimens at which point initial failure occurred in the core. This initial failure, an angled crack through the core, was located between the inner and outer loading points on one side of the specimen as shown in Figure 5.5. This crack extended through the thickness of the core. Unlike the unstitched specimen, however, this crack did not propagate along the facesheet beyond the next row of stitches. This initial failure event produced a small load drop. As the crosshead displacement increased, the load increased to a slightly higher level, at which point a second crack occurred on the opposite side of the specimen as shown in Figure 5.6.

Loading increased past this initial failure level to the maximum load, at which point further core cracking occurred. These additional core cracks did not propagate past adjacent stitch rows.

Table 5.1 Utah panel four-point flexural results

Specimen Type	Flexural Stiffness, EI, kips/in.	Initial Failure Load, lbs.	Max Load, lbs.	Energy Absorbed in.-lbs.
Unstitched	1.18 1.18 1.17 1.18 1.20 average = 1.18	173 189 179 176 163 average = 177	173 188 179 176 163 average = 177	25.4 26.4 22.9 21.5 19.3 average = 22.1
Stitched	1.32 1.08 1.18 1.19 1.24 1.26 average = 1.23 (4.2 % increase)	165 180 176 180 171 137 average = 169 (4.5 % decrease)	210 195 203 207 222 196 average = 206 (16.4 % increase)	159 329 150 239 287 252 average = 236 (967 % increase)
Angled stitched	1.80 1.72 1.70 average = 1.74 (47.4 % increase)	234 235 216 average = 228 (28.8 % increase)	234 235 216 average = 228 (28.8 % increase)	236 245 130 average = 203 (819 % increase)

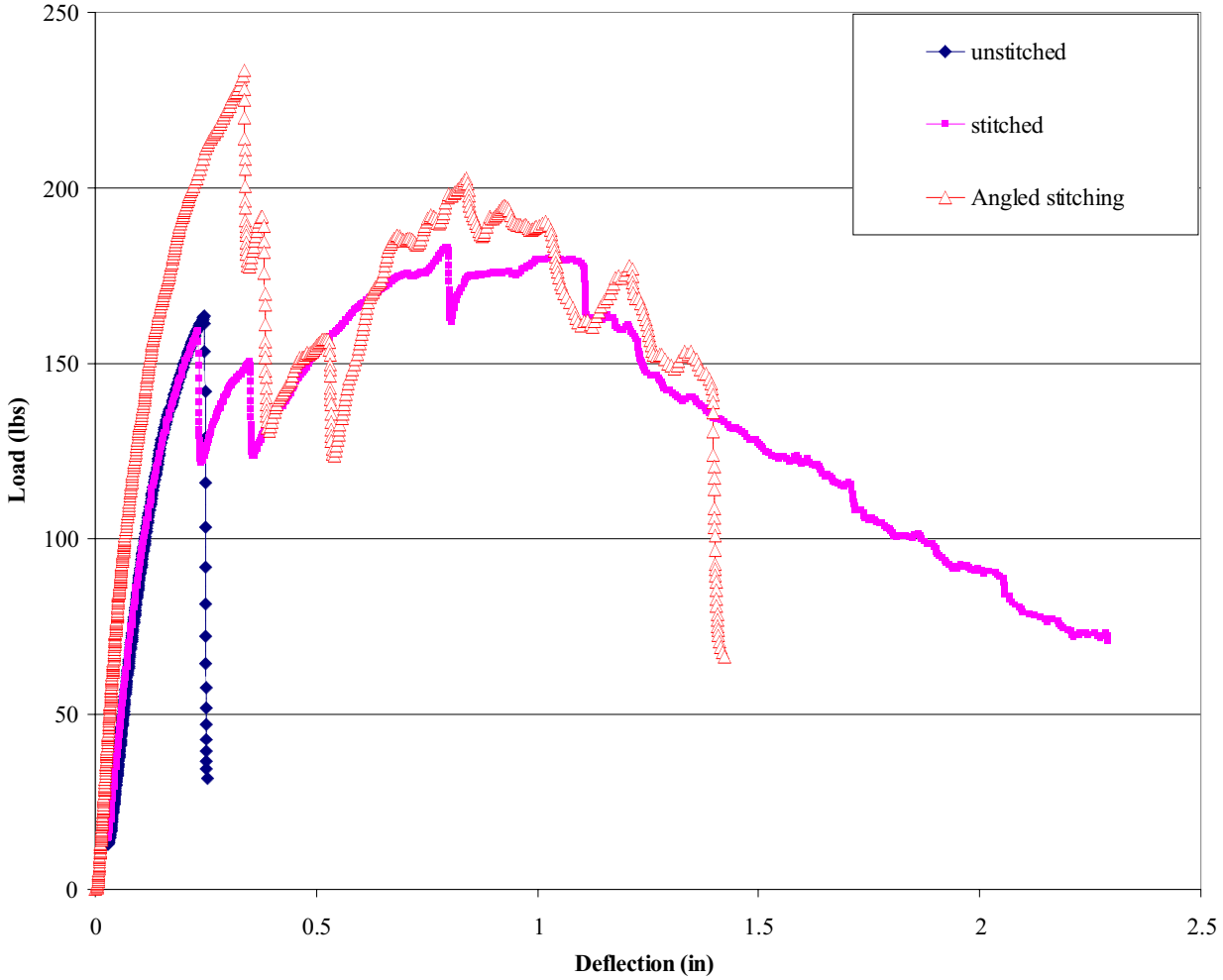

Figure 5.3. Typical four-point flexure results from Utah specimens.

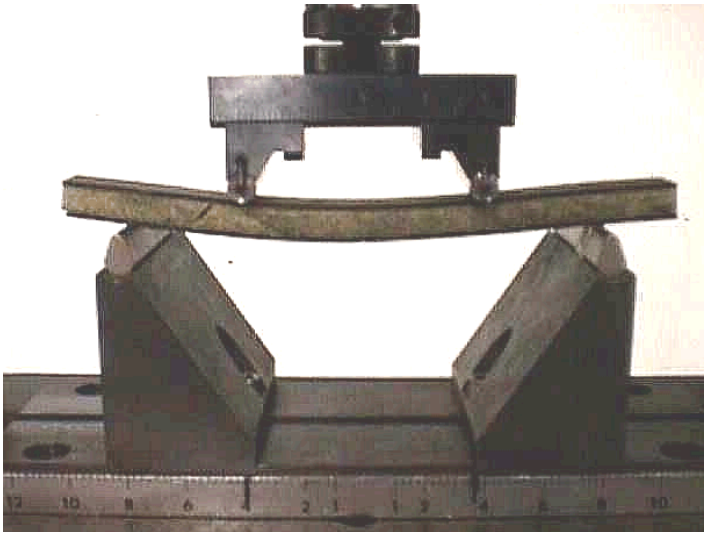

a. Entire unstitched flexural specimen.

b. Close-up of crack extending to specimen end.

Figure 5.4. Unstitched Utah specimen subjected to four-point flexure testing.

Figure 5.5 Initial failure in stitched Utah specimen in four-point flexure loading.

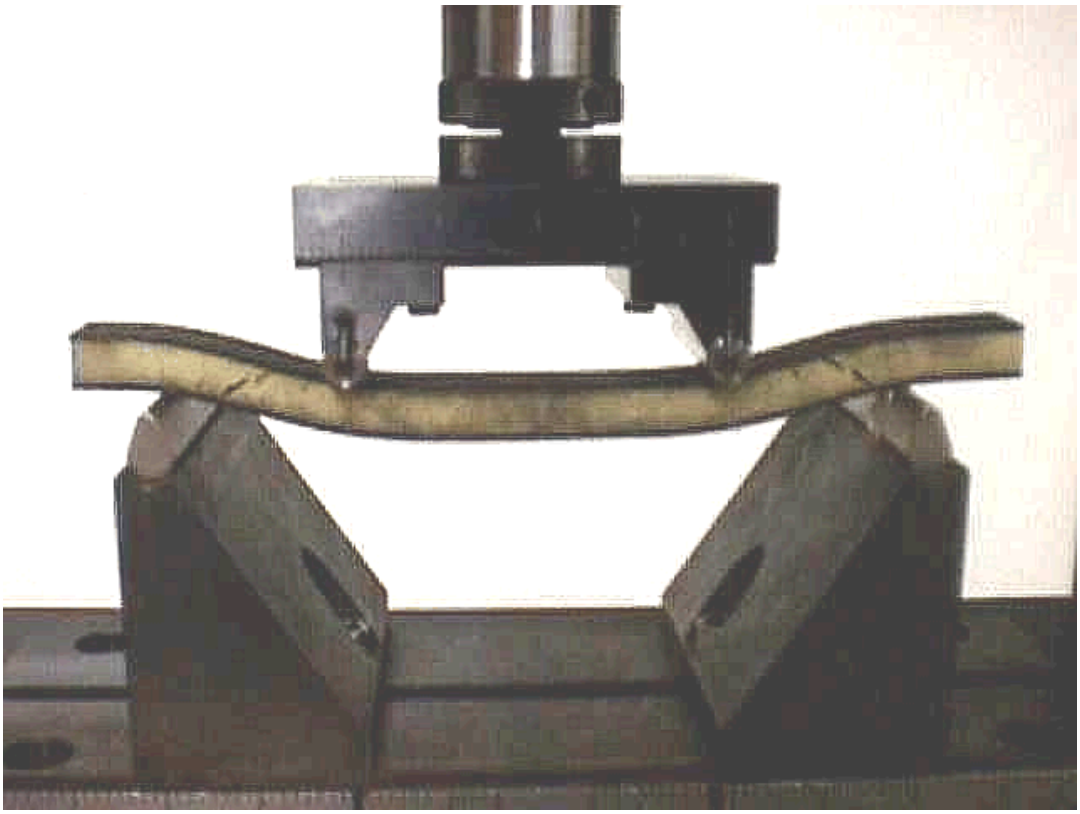

Figure 5.6. Core cracks in both sides of stitched Utah flexure specimen.

As additional core cracks occurred, the applied load did not increase beyond the previous maximum value. Loading was stopped when the load dropped to 80% of the maximum load value. Representative failed unstitched and stitched flexure specimens are shown in Figure 5.7.

While both stitched and unstitched specimens exhibited similar core cracks as their initial failures, these cracks propagated along the facesheets to the ends of the unstitched specimens but were contained within the stitch rows in the stitched specimens. These results suggest that stitching is an effective mechanism for suppressing facesheet delaminations under flexural loading.

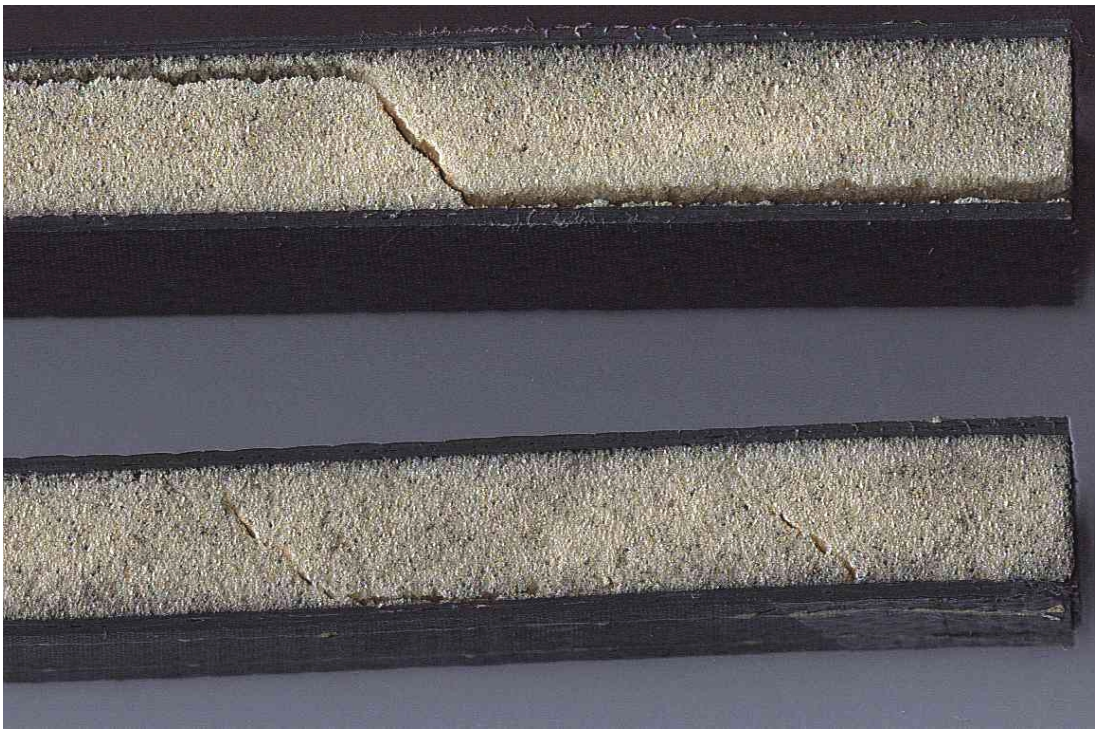

Figure 5.7. Failed unstitched (upper) and stitched (lower) Utah specimens.

Additionally, the area under the load versus displacement curves, referred to as the energy absorbed in Table 5.1, is more than 10 times greater for the stitched specimens than the unstitched specimens from the Utah panels.

The angled stitched specimens produced the largest flexure strength and stiffness out of all the Utah panels. The angled stitched flexure specimens reached initial and maximum failure loads that were on average 29% higher than the unstitched specimens and 11% higher then the normal stitched specimens. The failure of the angled stitched specimens was observed to be very similar to the normal stitched specimens. Similar cracks were observed as in the initial failure as discussed previously. After the initial failure, cracking continued as the specimen continued to

hold load. The difference was that load never reached a value above the initial failure load. The failed specimen as shown in Figure 5.8 appears to be very similar to the normal stitched specimen, having cracks through the thickness but not extending the length of the specimen.

Three-point flexure testing was conducted on specimens from the NASA panels. These tests were performed to determine the effects of stitch spacing and core thickness on flexural stiffness, flexural strength, and flexural toughness. Results from three-point flexure testing of the NASA specimens are presented in Table 5.2. Representative load versus crosshead displacement plots for specimens with 0.5 in. core thickness are shown in Figure 5.9. Many similarities were noted between the results from the NASA specimens and the Utah specimens. The initial failure mode in all specimens tested was angled core cracking. These core cracks propagated unstably along the face sheet to the edge of the specimen in the unstitched specimen but were contained within adjacent

Figure 5.8 Failed angled stitched specimen.

Table 5.2 Three-point flexure test results for NASA panels

Specimen Type	Flexural Stiffness (kips/in.)	Initial Failure Load (lbs)	Max Load (lbs)	Energy Absorbed (in.-lbs.)
0.5 in.core unstitched	2.29 2.30 2.24 ave. = 2.28	257 237 247 ave. = 247	257 237 247 ave. = 247	22.9 19.6 21.2 ave. = 21.2
0.5 in. core 1.0 in. stitch spacing	2.75 2.73 2.73 ave. = 2.74	246 275 278 ave. = 266	471 549 509 ave. = 510	466 693 570 ave. = 576
0.5 in. core 0.5 in. stitch spacing	3.15 2.93 2.90 ave. = 2.99	250 269 246 ave. = 255	563 521 504 ave. = 529	668 638 574 ave. = 626
0.5 in.core 0.25 in. stitch spacing	3.86 3.80 3.40 ave. = 3.69	278 282 278 ave. = 280	700 670 663 ave. = 678	800 841 786 ave. = 809
1.0 in. core unstitched	3.51 3.34 3.42 ave. = 3.44	375 373 404 ave. = 384	375 373 404 ave. = 384	39.9 38.6 52.2 ave. = 43.6
1.0 in. core 1.0 in. stitch spacing	3.77 3.82 3.84 ave. = 3.81	433 404 433 ave. = 423	536 560 563 ave. = 553	604 693 779 ave. = 692
1.0 in. core 0.5 in. stitch spacing	4.05 4.00 3.90 ave. = 3.98	449 471 447 ave. = 456	715 635 723 ave. = 691	995 762 916 ave. = 891
1.0 in. core 0.25 in. stitch spacing	4.46 4.19 3.81 ave. = 4.15	345 380 323 ave. = 349	726 713 691 ave. = 710	852 712 761 ave. = 775

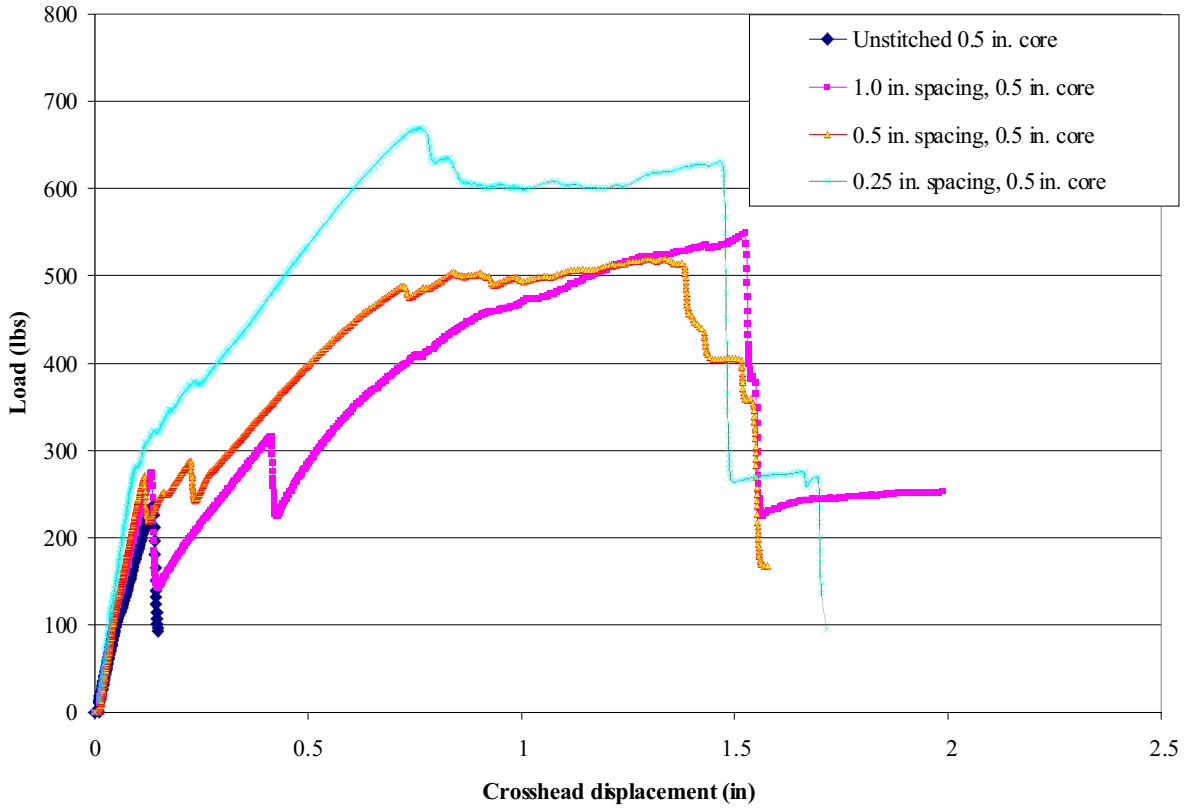

Figure 5.9 Typical three-point flexure results from NASA specimens.

stitch rows in the stitched specimens.

Table 5.3 presents the average flexural stiffness, initial failure load, maximum load, and flexural toughness for each condition tested as well as the percentage difference for each stitched condition relative to the unstitched configuration. For all cases tested, flexural stiffness increased with increasing stitch density. The greatest increases were observed with the thinner 0.5 in. core.

The resin-infiltrated stitches and surrounding resin columns are believed to provide these observed stiffness increases by reducing the shear deformation in the core during flexure loading. The load at which failure initiated did not improve significantly with the addition of stitches. In fact, a 9% decrease in initial failure load was observed for the 1.0 in. core thickness with 0.25 in. stitch spacing. For all other stitch configurations, a small increase in initial failure load was measured in comparison to the unstitched configurations. Although the initial failure load did not increase significantly with the addition of stitching, the maximum load obtained showed significant improvement for all stitched configurations.

The greatest percentage increases were measured in the thinner 0.5 in. core configurations, where all three stitch spacings produced greater than 100% improvement in comparison to the unstitched condition. Tremendous improvements in flexural toughness, defined as the area under the load versus deflection curve, were measured for all stitched configurations. In the 1.0 in. core specimens, the flexural toughness increased by factors of 15 to 20 whereas in the 0.5 in. core specimens, factors of 26 to 37 improvement were obtained.

Table 5.3 Summary and comparison of flexure test results for NASA panels.

Specimen Type	Ave. Flexural Stiffness kips/in. (% diff.)	Ave. Initial Failure Load Lbs. (% diff.)	Ave. Max. Load Lbs. (% diff.)	Ave. Flexural Toughness in.-lbs . (% diff.)
0.5 in.core unstitched	2.28	247	247	21
0.5 in. core 1.0 in. stitch spacing	2.74 (20-21%)	266 (0-13%)	510 (91-122%)	576 (2198-3269%)
0.5 in. core 0.5 in. stitch spacing	2.99 (27-38%)	255 (0-9%)	529 (104-128%)	626 (2707-3151%)
0.5 in.core 0.25 in. stitch spacing	3.69 (49-69%)	280 (13-14%)	678 (168-183%)	809 (3707-3967%)
1.0 in.core unstitched	3.44	384	384	44
1.0 in. core 1.0 in. stitch spacing	3.81 (10-12%)	423 (5-13%)	553 (44-47%)	692 (1385-1787%)
1.0 in. core 0.6 in. stitch spacing	3.98 (13-18%)	456 (16-23%)	691 (65-88%)	891 (1748-2282%)
1.0 in. core 0.25 in. stitch spacing	4.15 (11-30%)	349 (-16-(-1)%)	710 (80-86%)	775 (1633-1954%)

In summary, results from flexure testing show that stitching leads to significant improvements in the flexural strength and energy absorption of sandwich beams. Although stitching has little effect on the initial formation of core cracks under flexure loading, the core cracks do not propagate past adjacent stitch rows in the stitched sandwich specimens. Flexural stiffness increases with increasing stitch density, with the largest increases occurring for the thinner 0.5 in. core. Additionally it was learned that the use of angled stitching produce the highest flexural strength and stiffness.

5.2 Flatwise Tensile Testing

The next set of tests performed on the sandwich panels were flatwise tensile tests. Quasi-static flatwise tensile testing was performed according to ASTM C297 [28] on square specimens, measuring 2.0 in. square for the Utah specimens and 1.93 in. square for the NASA specimens. Specimens were adhesively bonded to 2.0 in. x 2.0 in. steel loading blocks, machined to be pin loaded as shown in Figure 5.10. A close up of the attached specimen is shown in Figure 5.11. The specimens were connected to the test machine through the load train shown in Figure 5.12. A total of three specimens were tested from each panel type. Testing was performed in an electromechanical testing machine at a constant crosshead displacement rate of 0.15 in./min. Load and crosshead deflection were recorded during testing. The initial failure load, defined as the first drop in the load-deflection curve, was determined from the load-deflection plot. The maximum load obtained during testing was also recorded.

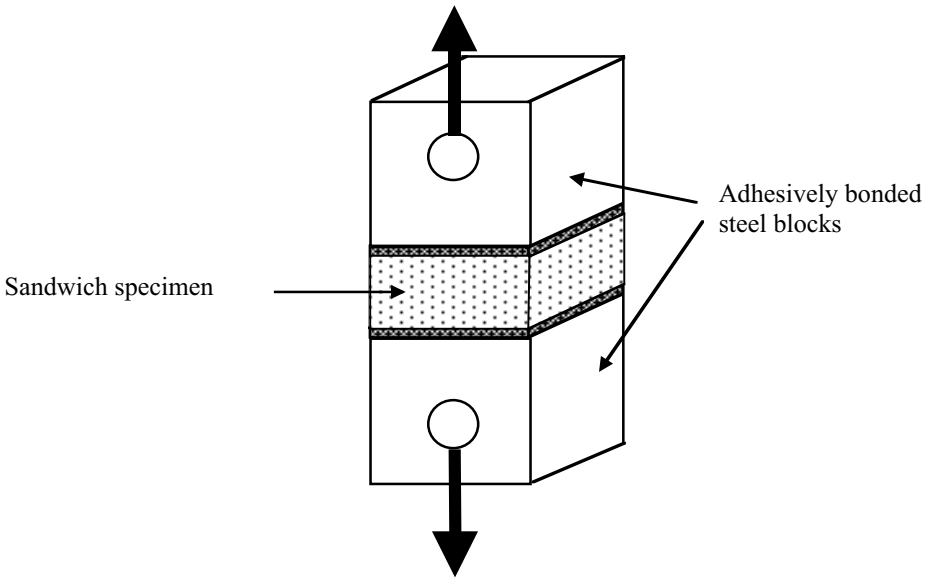

Figure 5.10 Flatwise tensile test configuration.

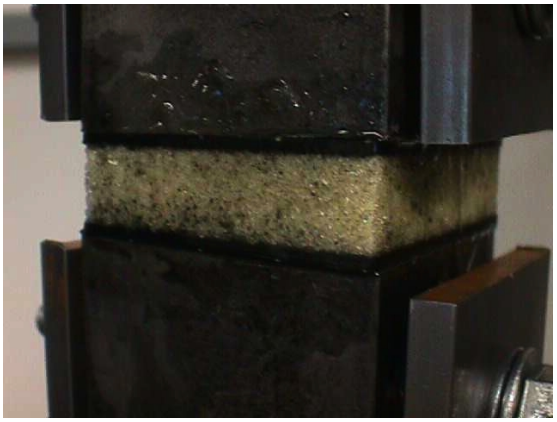

Figure 5.11 Flatwise tensile specimen ready for testing.

Figure 5.12 Flatwise tensile test load train.

Flatwise tensile testing was performed on specimens cut from both the Utah panels and the NASA panels. The objective of flatwise tensile testing was to determine the improvement in the out-of-plane strength of sandwich panels due to stitching.

Results from flatwise tensile testing of specimens from the Utah panels are presented in Table 5.4. Representative load versus crosshead displacement plots obtained from unstitched and stitched Utah specimens are shown in Figure 5.13. Summarized test results and comparisons between stitched and unstitched performance are presented in Table 5.5.

Table 5.4. Utah panel flatwise tensile test results

Specimen type	Initial failure load, lbs.	Maximum load, lbs.
Unstitched	715 804 713 average = 744	715 804 713 average = 744
Stitched with 400 denier bobbin thread	732 782 747 average = 754	749 829 747 average = 775
Stitched with 1600 denier bobbin thread	823 761 879 average = 821	960 942 879 average = 927
Stitched with 3200 denier bobbin thread	847 897 948 average = 898	1080 1055 1166 average = 1101
Angled Stitching	702 647 653 average = 667	904 678 988 average = 857

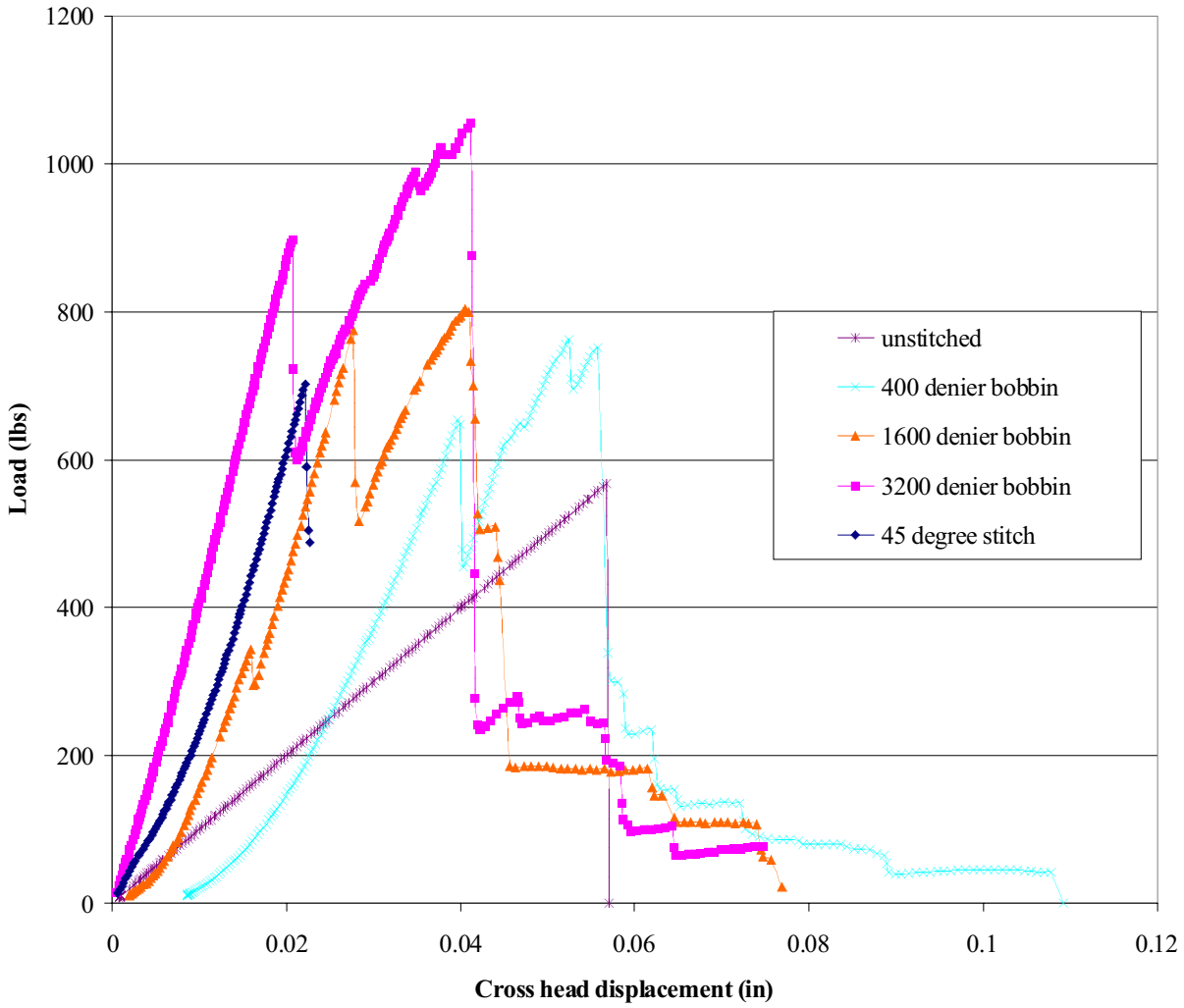

Figure 5.13 Typical flatwise tensile results from Utah specimens.

Table 5.5 Summary and comparison of Utah flatwise tensile test results

Specimen type	Initial failure load, lbs.	Max. load, lbs.	Max. stress, psi	% of unstitched
Unstitched	744	744	186	100%
Stitched with 400 denier bobbin thread	754	775	194	100-111%
Stitched with 1600 denier bobbin thread	821	927	238	118-129%
Stitched with 3200 denier bobbin thread	898	1101	275	142-157%
Angled Stitching	667	857	214	91-133%

In the unstitched specimens, loading progressed smoothly up to the maximum failure load, at which point the specimens failed catastrophically through the core as shown in Figure 5.14. The average failure load for the unstitched Utah specimens was 744 lbs, corresponding to a failure stress of 186 psi. This failure stress was considered as the baseline to which the results from the stitched specimens were compared.

The initial set of stitched Utah specimens tested with the smaller 400 denier bobbin thread exhibited a relatively linear load versus deflection response until an initial failure occurred, at which point a significant load drop was recorded as shown in Figure 5.13.

Figure 5.14 Failed unstitched Utah specimen from flatwise tensile loading.

Visible damage in the form of cracking of the foam core perpendicular to the applied loading was clearly visible as shown in Figure 5.15. The average load level at which initial failure occurred was only 1.3% higher than the failure load for the unstitched specimens. It was not known whether there was any damage in the stitch or bobbin threads associated with this initial load drop. Following the initial failure, loading progressed to a slightly higher level at which point further core cracking occurred and another load drop was recorded. This procedure was repeated a small number of times, each with an increasing maximum load, until a large load drop occurred that was not recovered as the crosshead displacement increased.

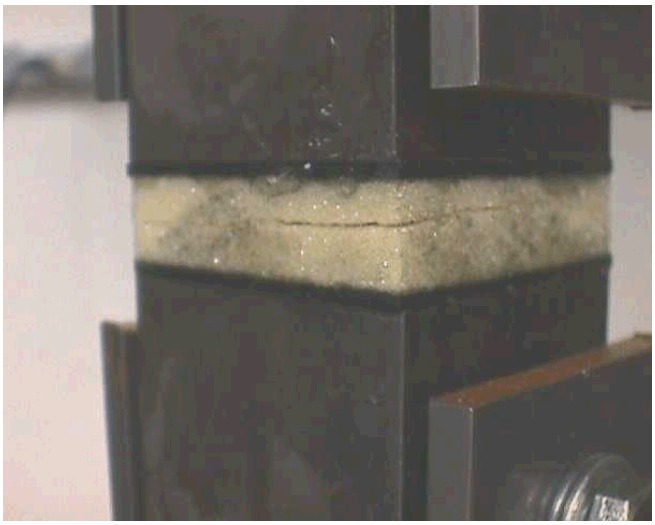

Figure 5.15 Initial failure in stitched Utah specimen during flatwise tensile testing.

The average value of the maximum load recorded was 775 lbs, corresponding to a maximum tensile stress of 194 psi. Thus, only a 4% increase in tensile strength was obtained by stitching when the smaller bobbin thread was used. Based on the tensile strength of infiltrated yarns reported in Chapter 4, a flatwise tensile strength of 2032 lbs. was predicted for these specimens. Thus, only 38% of the predicted flatwise tensile strength was obtained in these specimens. As shown in Table 5.5, the difference between the initial failure load and the maximum load was only 3% for these specimens. Upon inspection of the failed specimens, it was determined that the smaller bobbin thread failed at the intersection with the thicker stitch thread, leaving the stitch loop intact. Following failure of the bobbin thread, the resin-infiltrated stitched pulled out of the surrounding foam core, leaving the stitch column intact as shown in Figure 5.16.

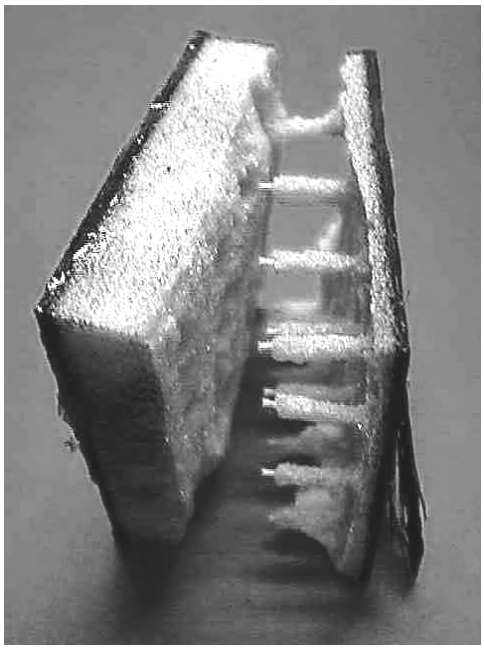

Figure 5.16. Failed Utah specimen stitched with 400 denier bobbin thread.

Based on this observed failure, another stitched Utah panel was fabricated with the same stitch configuration but with a larger 1600 denier bobbin thread. This bobbin thread was the same size as the stitch thread. Once again, the initial failure mode during flatwise tensile testing was cracking of the foam core, which resulted in a significant load drop. Further loading was possible to higher load levels at which point further core cracking occurred, each producing another load drop as shown in Figure 5.13. The average value of the maximum load recorded was 927 lbs, corresponding to a maximum tensile stress of 232 psi. Thus, the use of the larger 1600 denier bobbin thread yielded a 36% increase in tensile strength as compared to the unstitched specimens. However, this failure load was only 38% of the predicted flatwise tensile strength based on the tensile strength of infiltrated yarns. An inspection of the failed specimens showed that

although the larger 1600 denier bobbin thread produced a significantly higher flatwise tensile strength than the smaller 400 denier bobbin thread, the bobbin threads in both sets of specimens failed in the same manner. Figure 5.17 shows a typical failed specimen with the larger 1600 denier bobbin thread, showing the through-the-thickness stitches intact following testing. In most of the stitches, the bobbin thread failed at the intersection with the stitch, leaving the stitch loop intact.

Based on the observed failure mode in the specimens with the 1600 denier bobbin thread, an even larger 3200 denier bobbin thread was then used to stitch another panel. This 3200 denier bobbin thread was obtained by twisting two 1600 denier threads together prior to stitching. The stitch thread was kept at the same 1600 denier size as in previous panels. During flatwise tensile testing, initial core cracking associated with the initial load drop occurred at an average load of 898 lb. Loading progressed to a maximum applied load that averaged 1101 lbs corresponding to a

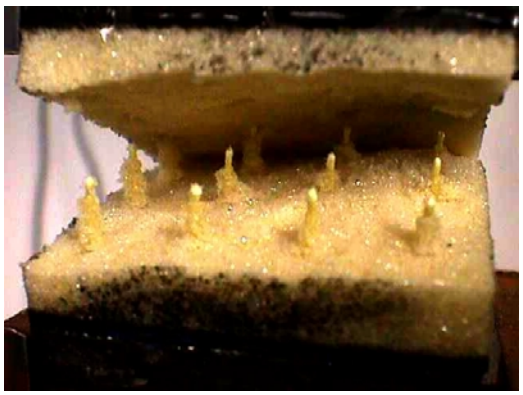

Figure 5.17 Failed Utah specimen stitched with 1600 denier bobbin thread.

maximum stress of 275 psi. Thus, the use of a 3200 denier bobbin thread yielded a 44% increase in tensile strength as compared to the unstitched specimens. However, this failure load was still only 54% of the predicted flatwise tensile strength based on the tensile strength of infiltrated yarns. The difference between the initial failure load and the maximum load increased to 29% for these specimens. Inspection of the failed specimens showed that although the 3200 denier bobbin thread did not fail, the majority of the 1600 denier stitches failed at the stitch loop where the stitch and bobbin threads intersect as shown in Figure 5.18. A few stitches were observed to fail at the opposite stitch-facesheet interface and in the middle of the core.

In summary, flatwise tensile test results of the Utah panels showed significantly lower strengths than predicted based on the tensile strength of infiltrated yarns. Failure of the stitches commonly occurred at the intersection with the bobbin threads. For the

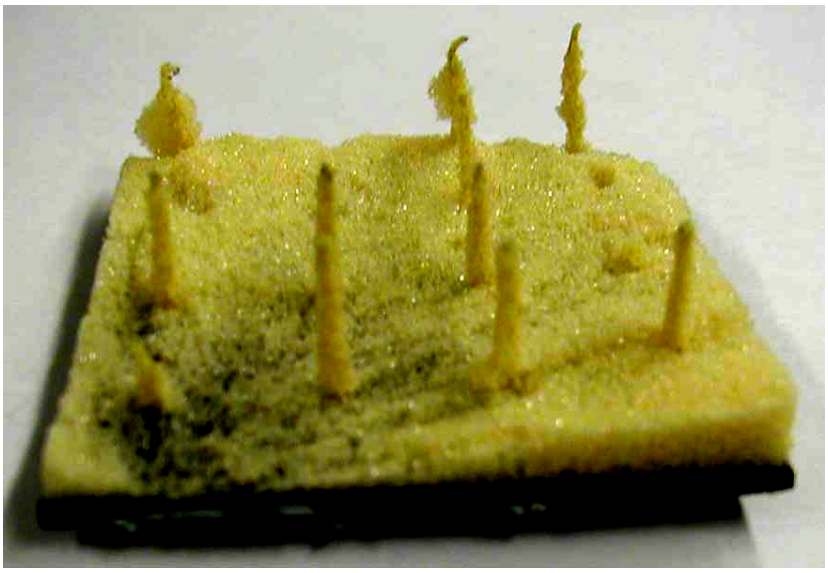

Figure 5.18 Failed Utah specimen stitched with 3200 denier bobbin thread.

cases where the bobbin thread was smaller than or equal to the size of stitch thread, failure of the bobbin thread occurred. For the case where the bobbin thread was twice the size of the stitch thread, the smaller stitch thread failed. These results suggest that the stitch threads are highly loaded as they reach the outer surfaces of the panel and connect with the bobbin threads, possibly delaminating from the facesheets prior to maximum load. Additionally, these results suggest that there is a significant stress concentration at the stitch thread/bobbin thread connection, resulting in failures at this location well below the predicted tensile strength of infiltrated straight stitches.

Based on the results obtained from flatwise tensile testing of the Utah panels, the NASA panels were all stitched using a 1600 denier bobbin thread. The facesheet thickness was also doubled in comparison to the Utah panels, although not in direct response to these test results.

Average results from tension specimens stitched at an angle are also shown in Tables 5.5. The angled stitched specimens had the lowest initial failure load although the maximum failure of the angled stitched specimens was still greater than the unstitched specimens. The failure of the angled stitched specimens was very similar to the normal stitched specimens. After the initial failure, cracks were observed in the foam as occurred in the normal stitched specimens. From the initial failure, load continued to rise until the maximum failure load was reached. The angled stitches failed at either the top of bottom interface between the face sheet and core as seen in Figure 5.19.

The maximum failure load of the angled stitched specimens was still higher than the unstitched maximum load and higher then the normal stitched specimens stitched

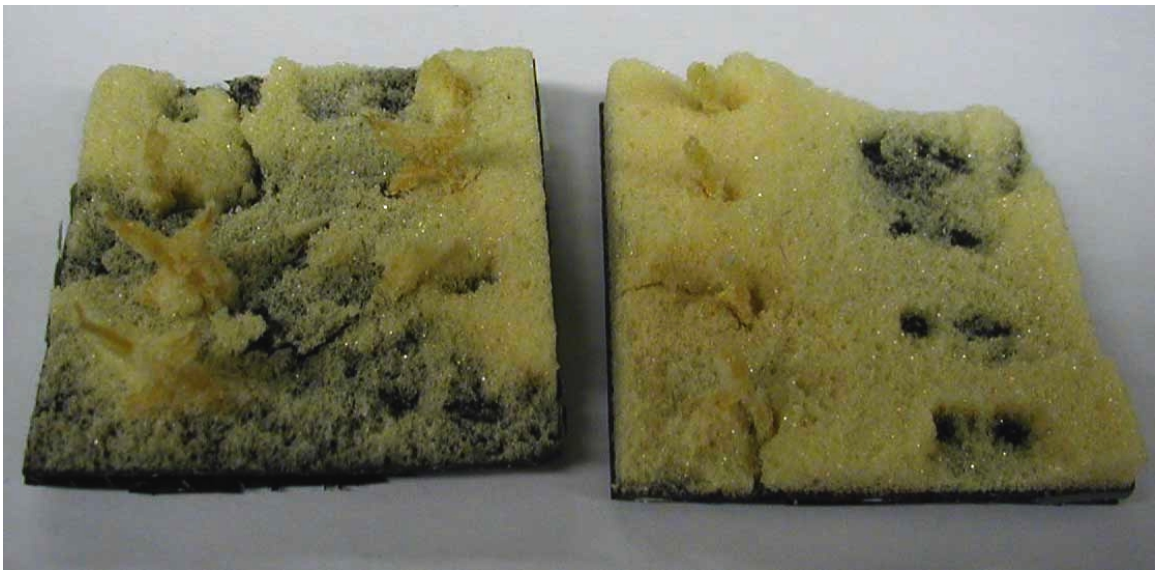

Figure 5.19 Failed angled stitched tension specimens

with the 400 denier bobbin thread. The initial failure load of the angled stitched specimens was lower than all of the tension specimens tested. The angled stitched specimens had the most core damage due to stitching because of the longer length of yarn within the specimens. There is also a complex state of stress set up by the crossing of the stitches and the direction in which it is loaded. This is possibly the cause of the low initial failure.

Flatwise tensile testing was also conducted on specimens from the NASA panels. These tests were performed to determine the effects of stitch spacing and core thickness on the out-of-plane tensile strength. The NASA panels differed from the Utah panels in that the facesheet thickness was doubled, the density of the foam core was decreased to 2 lb/ft^3 from 6 lb/ft^3, and 1600 denier stitch and bobbin threads were used for all panels. Flatwise tensile test results from the NASA specimens are presented in Table 5.6. Representative load versus crosshead displacement plots for specimens with

Table 5.6. Flatwise tensile test results for NASA panels

Specimen type	Initial failure load, lbs.	Max load, lbs.
0.5 in.core unstitched	318 466 237 average =340	318 466 237 average = 340
0.5 in. core 1.0 in. stitch spacing	992 888 889 average = 923	1174 1292 984 average = 1150
0.5 in. core 0.5 in. stitch spacing	1453 1408 1418 average = 1426	2815 2649 2554 average = 2672
0.5 in.core 0.25 in. stitch spacing	6185 5360 5214 average = 5586.6	6185 5360 5214 average = 5587
1.0 in. core unstitched	495 546 427 average =490	495 546 427 average = 490
1.0 in. core 1.0 in. stitch spacing	1048 936 906 average = 963	1427 1608 1474 average = 1503
1.0 in. core 0.5 in. stitch spacing	3285 3060 2974 average = 3107	3285 3060 2974 average = 3107
1.0 in. core 0.25 in. stitch spacing	5003 5639 5142 average = 5261	5003 5639 5142 average = 5261

0.5 in. core thickness are shown in Figure 5.20. As was the case with the Utah specimens, the addition of stitching to the NASA specimens produced a significant increase in maximum load. For both core thicknesses tested, the initial failure load and the maximum failure load increased tremendously with increasing stitch density. Table 5.7 summarizes and compares the results of the flatwise tensile tests of the NASA panels.

Although the general trend of increasing strength with the addition of stitching was common to both the Utah and NASA specimens tested, there were some significant differences. First, the load versus deflection curves were considerably different for some stitched NASA specimens. The unstitched specimens exhibited the same linear-to-failure response for both core thicknesses such that the initial failure was the final failure. Specimens from the unstitched panel with the 1.0 in. thick core exhibited a 44% strength increase over the unstitched panel with the 0.5 in. core. For all specimens tested with a stitch spacing less than the core thickness (0.5 in. core with 0.25 in. stitch spacing, 1.0 in. core with 0.5 in. stitch spacing, and 1.0 in. core with 0.25 in. stitch spacing), the load versus deflection plots were linear to failure and the initial failure was the final failure. The load versus deflection plots for the remaining stitched configurations with a stitch spacing greater than or equal to the core thickness were similar to those from the Utah stitched specimens. The load versus deflection plots for these specimens exhibited an initial failure associated with visible cracking of the foam core and a small load drop. The load continued to rise until the maximum failure occurred and the load dropped significantly. This behavior is shown in the 0.5 in. core specimens in Figure 5.20.

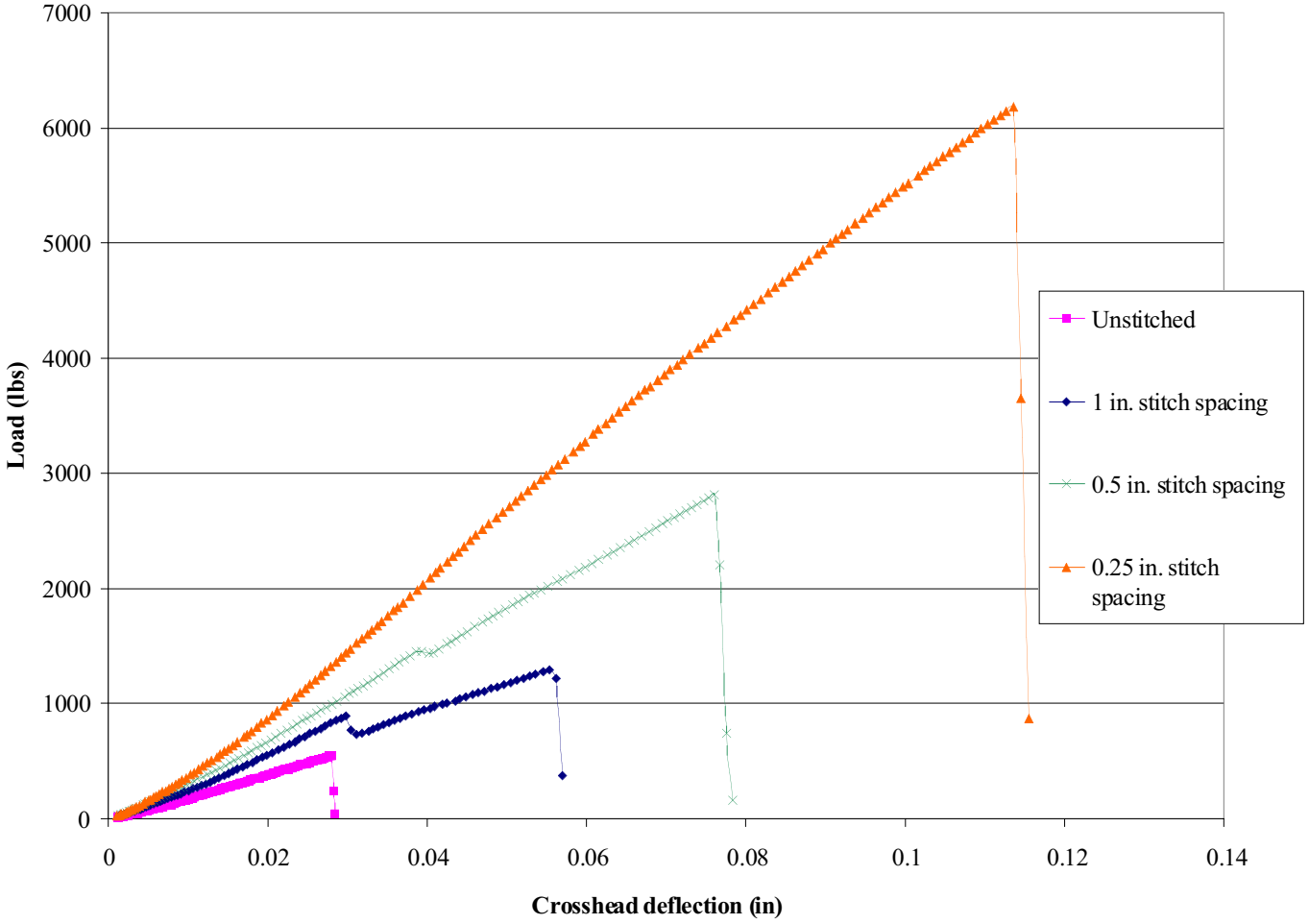

Figure 5.20 Typical flatwise tensile results from 0.5 in. core NASA specimens.

Table 5.7 Summary and comparison of NASA flatwise tensile test results

Specimen type	Initial failure load, lbs.	Max. load, lbs.	Max. stress, psi	% of unstitched
0.5 in.core unstitched	340	340	90	100%
0.5 in. core 1.0 in. stitch spacing	923	1150	310	289-380%
0.5 in. core 0.5 in. stitch spacing	1426	2673	711	751-828%
0.5 in.core 0.25 in. stitch spacing	5587	5587	1492	1533-1819%
1.0 in. core unstitched	490	490	135	100%
1.0 in. core 1.0 in. stitch spacing	963	1503	408	291-328%
1.0 in. core 0.5 in. stitch spacing	3107	3107	848	607-670%
1.0 in. core 0.25 in. stitch spacing	5261	5261	1463	1021-1151%

Further differences between the Utah and NASA panels were observed when inspecting the failed flatwise tensile specimens. In the Utah specimens, which had a single layer of warp-knit fabric in each face sheet, the stitches nearly always failed at the intersection between the stitch loop and the bobbin thread as discussed previously. In the NASA specimens, the stitches rarely failed at this location. As shown in Figure 5.21, approximately one-half the stitches failed at the interface between the face sheet and core. A majority of the remaining stitches failed at other locations within the core. A small number of stitches, usually at the edges of the specimen, still failed at the stitch loop/bobbin connection as shown in Figure 5.22.

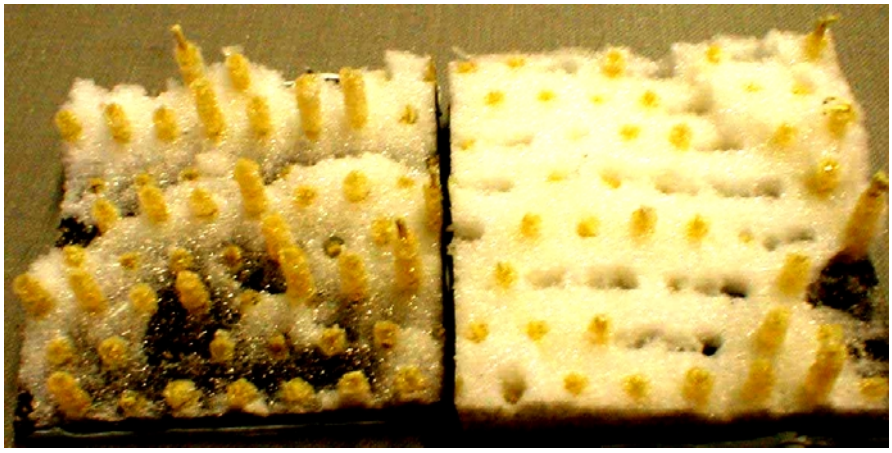

Figure 5.21 Failed NASA specimen with 0.5 in. core and 0.25 in. stitch spacing.

Figure 5.22 Failed NASA specimen with 1.0 in. core and 0.25 in. stitch spacing.

In summary, the results from flatwise tensile testing have shown that stitching of sandwich composites significantly increases the out-of-plane tensile strength. In contrast to stitching of traditional laminated composites, the size of the bobbin thread used for stitched sandwich structures has been shown to influence the flatwise tensile strength. The influence of bobbin thread size increases as the thickness of the facesheets decreases. Angled stitching was also shown to increase the maximum tensile strength by an average of 15% over unstitched although the average maximum was 8% less then the average of 1600 denier normal stitched specimens.

5.3. Core Shear Testing

Core shear testing was performed on 8.0 inch long specimens cut from both the Utah panels and the NASA panels. The Utah panels were cut to 2.0 inches in width and the NASA panels were cut to as width of 1.93 inches. The objective of the core shear testing was to determine the improvement in the interlaminar shear strength of sandwich panels due to stitching.

Core shear testing was performed according to ASTM C273 [28]. This test method does not produce pure shear, but with the proper length (as selected for this testing) the secondary stresses have a minimum effect on the results of core shear testing [28]. The core shear test is similar to a simple lap shear test; however the load is applied such that the specimen is loaded at a slight angle to the plane of the facesheets. Specimens were adhesively bonded between steel plates and fastened to fixtures machined to enabled a tensile load to be applied through a line connecting opposite corners of the sandwich specimen as shown in Figures 5.23 and 5.24. Load

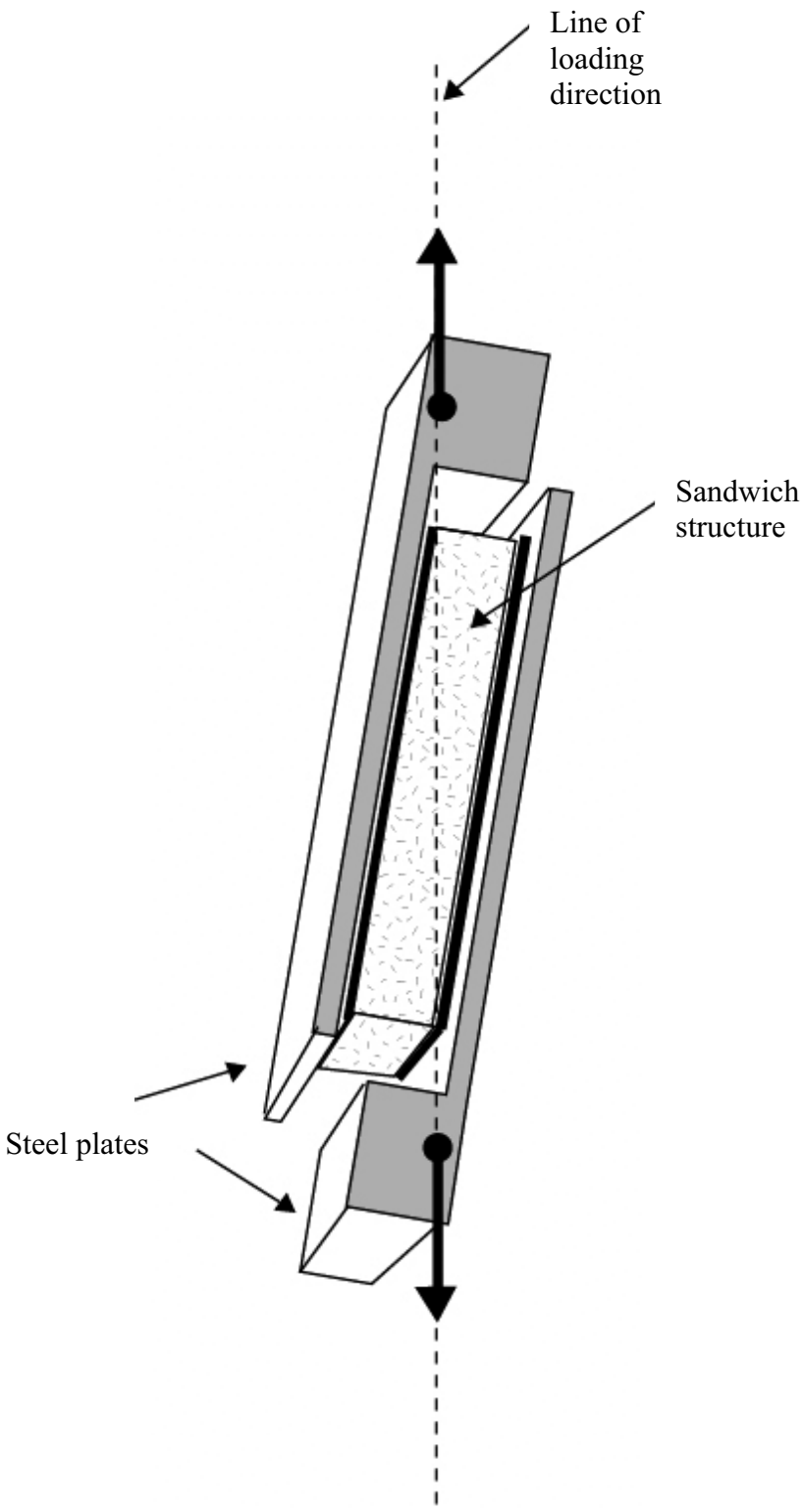

Figure 5.23 Diagram of core shear loading fixture.

Figure 5.24 Load train for core shear testing.

was applied at a constant rate of 0.02 in./min. Load versus deflection plots were recorded during the test. The initial failure load, maximum failure load, and the energy absorption to failure were also recorded.

Results from core shear testing of specimens from the Utah panels are presented in Table 5.8. Representative load versus crosshead displacement plots obtained from unstitched and stitched Utah specimens are shown in Figure 5.25. In the unstitched specimens, loading progressed smoothly up to the maximum failure load, at which point the specimens failed suddenly and catastrophically at the interface between the core and facesheet. The average failure load for the unstitched Utah specimens was 1044 lbs.

Table 5.8. Utah panel core shear test results

Specimen type	Initial failure load, lbs.	Max load, lbs.	Max shear stress, psi	Energy absorbed, in.-lbs.
Unstitched	1106 941 848 average = 1024	1106 941 847 average = 1024	69 59 53 average = 64.0	34 27 21 average = 30.4
Stitched with 400 denier bobbin thread	1000 933 1357 average = 967 91-133% of unstitched	1159 1180 1362 average = 1234 113-133% of unstitched	72 74 85 average = 73.1 113-133% of unstitched	278 248 324 average = 283 816-1066 % of unstitched
Stitched with 1600 denier bobbin thread	1459 1385 1571 average = 1472 135-153% of unstitched	1554 1685 1573 average = 1604 152-165% of unstitched	97 105 98 average = 101 152-165% of unstitched	376 379 400 average = 385 1237-1316% of unstitched
Angled stitched	2304 2565 2268 average = 2379 221-250% of unstitched	2304 2565 2268 average = 2379 221-250% of unstitched	144 160 142 average = 152 221-250% of unstitched	140 138 197 average = 158 454-648% of unstitched

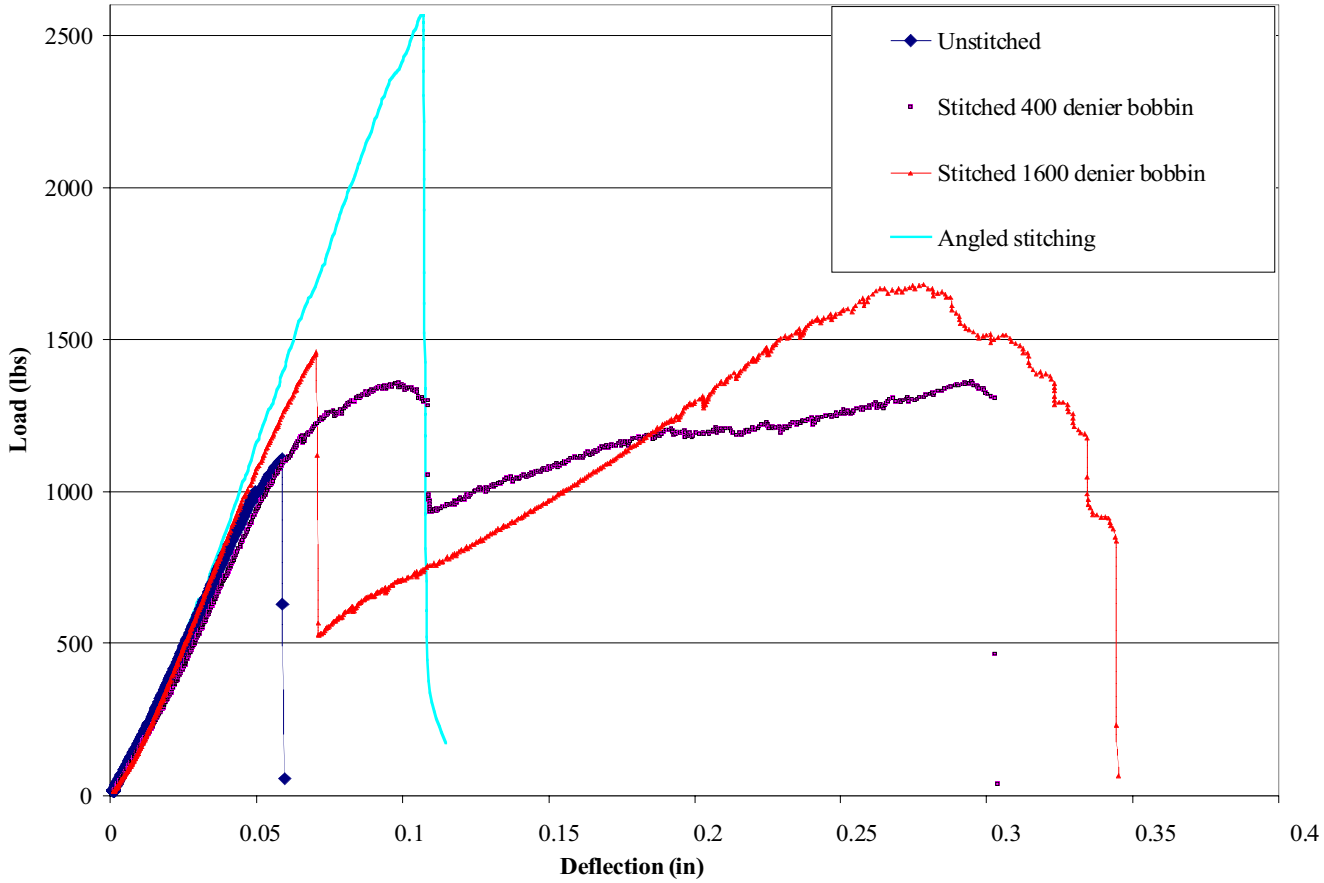

Figure 5.25 Typical core shear test results from Utah specimens.

The initial set of stitched Utah specimens with the smaller 400 denier bobbin thread exhibited appreciable nonlinearity in the load versus defection curve up to the point of initial failure, at which point a significant load drop was measured. This initial failure corresponded with the occurrence of angled cracks through the foam core as shown in Figures 5.26 and 5.27. As the load began to rise again, a series of tiny "pops" could be heard, and the load fluctuated while generally increasing until the panel reached the maximum load level and failed catastrophically. The maximum load was an average of 21% greater than for the unstitched specimens. Additionally, the energy absorbed, or area under the load versus deflection curve, increased by an average of 830% compared to the unstitched specimens. Observation of the failed specimens showed that about half the stitches failed at the interface between the face sheets and core and the other half failed in the bobbin thread.

Figure 2.26 Initial failure of stitched specimen during core shear testing.

Figure 5.27 Widening of core crack under increasing loading for stitched specimen

The stitched Utah specimens with the larger 1600 denier bobbin thread had a maximum load of 1604 lbs, a 57% average improvement over the unstitched case and a 30% average improvement over the stitched specimens with the smaller 400 denier bobbin thread. Further improvement was also measured in the energy absorbed to failure, over 12 times that of the unstitched specimens. Once again, angled cracks through the foam core occurred at the point of initial failure, at which point there was a significant drop in load. An inspection of the failed specimens showed the failure occurred in the stitch thread at the core-facesheet interface in all of the stitches.

Angled stitching produced the highest maximum core shear load for the Utah specimens, over two times greater than the unstitched specimens and an average of 50%

greater than the normal stitched specimens, without a lower initial failure. Initial cracking of the foam core, observed in the normal stitched specimens, were not observed in the angled stitched specimens prior to the maximum load. There was no visible or audible indication of failure until the maximum load was reached. When the maximum failure load was reached, the load dropped below 80% of the maximum load. Observation of these failed specimens revealed that only half of the stitches had failed at the core-facesheet interface. The failed stitches were those stitched toward the angle of the loading direction. The stitches in the opposite direction were still intact, although the core material was almost completely destroyed. Energy absorbed during the test was also improved in the angled stitched specimens. This improvement was not as great as in the normal stitched specimens with a 1600 denier bobbin thread but was still over five times greater than the unstitched specimen.

Results from core shear testing of specimens from the NASA panels are presented in Table 5.9. Representative load versus crosshead displacement plots obtained from unstitched and stitched NASA specimens are shown in Figure 5.28. A summary of the results for core shear testing of specimens from the NASA panels is shown in Table 5.10. In the unstitched specimens both with 0.5 in. and 1.0 in. core thickness, loading progressed smoothly up to the maximum failure load, at which point the specimens failed suddenly and catastrophically at the interface between the core and facesheet. This was the same loading behavior as occurred in the Utah specimens. The average failure load for the unstitched NASA specimens was 467 lbs. and 434 lbs. for the 0.5 in. and 1.0 in. cores respectively.

Table 5.9 Core shear test results for NASA panels

Specimen type	Initial failure load, lbs.	Max load, lbs.	Energy absorbed in.-lbs
0.5 in. core unstitched	495 396 510 average =467	495 396 510 average = 467	8.44 5.66 7.76 average = 7.3
0.5 in. core 1.0 in. stitch spacing	992 956 1006 average = 984	992 956 1006 average = 984	134 151 137 average = 140
0.5 in. core 0.5 in. stitch spacing	1094 1269 1167 average = 1177	1186 1342 1274 average = 1267	201 246 219 average = 222
0.5 in. core 0.25 in. stitch spacing	1455 1463 1284 average = 1400	1986 2209 2042 average = 2079	380 423 390 average = 398
1.0 in. core unstitched	440 506 355 average =434	440 506 355 average =434	6.82 7.94 5.8 average = 6.9
1.0 in. core 1.0 in. stitch spacing	802 877 851 average = 843	881 895 851 average = 876	238 313 239 average=263
1.0 in. core 0.5 in. stitch spacing	1170 1126 1251 average = 1182	1170 1126 1251 average = 1182	394 453 398 average = 415
1.0 in. core 0.25 in. stitch spacing	1101 1212 1111 average = 1141	1531 1297 1490 average = 1439	692 675 655 average = 674

Table 5.10 Summary of NASA panel core shear results.

Specimen type	Initial Failure load (lbs)	Max Failure Load (lbs)	Max Shear Stress (psi)	Energy absorbed (in-lbs)	Percent of unstitched Max load
0.5 in. core unstitched	466.7	466.7	30.2	7.3	100%
0.5 in. core 1.0 in. stitch spacing	984.4	984.4	64.3	140.3	205-215%
0.5 in. core 0.5 in. stitch spacing	1176.7	1267.0	82.1	221.8	254-287%
0.5 in. core 0.25 in. stitch spacing	1400.4	2078.9	134.2	398.1	425-473%
1.0 in. core unstitched	433.6	433.6	28.2	6.9	100%
1.0 in. core 1.0 in. stitch spacing	843.4	875.9	56.7	263.3	196-206%
1.0 in. core 0.5 in. stitch spacing	1182.4	1182.4	77.3	414.9	241-288%
1.0 in. core 0.25 in. stitch spacing	1141.5	1439.4	346.6	674.2	299-353%

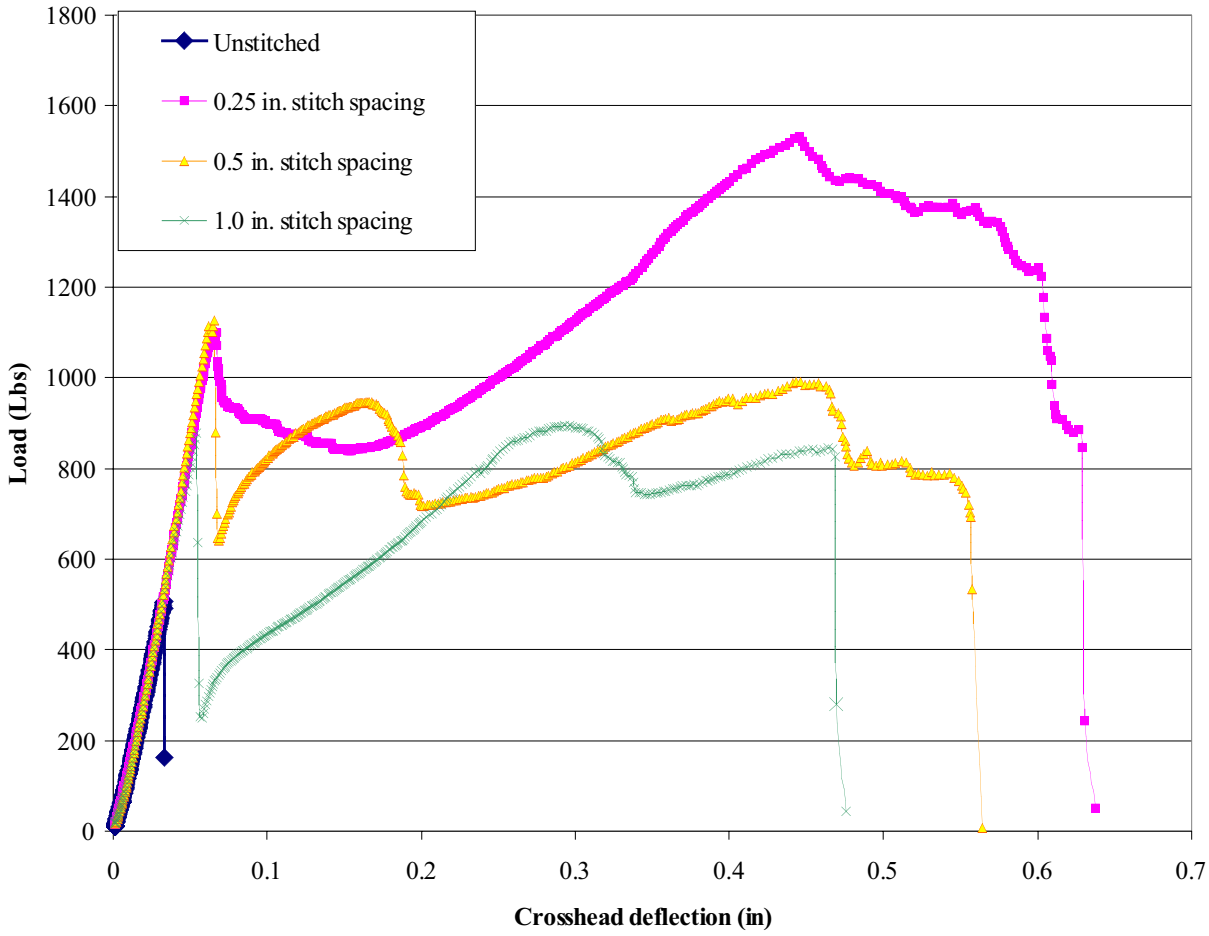

Figure 5.28 Typical core shear test results from NASA specimens.

Results from the NASA core shear specimens showed the same characteristics as the results from the Utah specimens. As Figure 5.28 shows, all of the stitched NASA specimens exhibited a linear load versus deflection behavior initially. After the initial failure load was reached, the load dropped slightly and then continued to rise. This initial failure corresponded with the occurrence of cracks through the foam core as was seen in the Utah specimens. As the load began to increase again, a series of tiny "pops" could be heard. The load fluctuated while generally increasing until the panel reached the maximum load level and failed catastrophically, consistent with what occurred in the normal stitched Utah panels.

The initial and maximum failure loads for the stitched specimens increase as the stitch density increases. NASA specimens with the highest density of stitching experienced the greatest increase in maximum failure load, with an increase of over four times greater than the unstitched specimens. The initial failure was also greatest for the highest stitch density, over three times higher than the initial failure of the unstitched specimens. The energy absorbed is also greater for the stitched specimens, up to nearly 100 times greater for the NASA specimens with the highest stitch density.

The failure of the unstitched specimens was the same for both the Utah and NASA specimens. Figure 5.29 show a typical unstitched core shear specimen failure between the facesheet and core. Failed stitched NASA specimens showed the same results as the 1600 denier normal stitched Utah specimens. All of the stitches failed in the stitch thread at the core-facesheet interface as can be observed in Figure 5.30. This type of failure was consistent for all stitch densities as can be seen in Figures 5.30 and 5.31.

Figure 5.29 Failed Utah unstitched core shear specimen

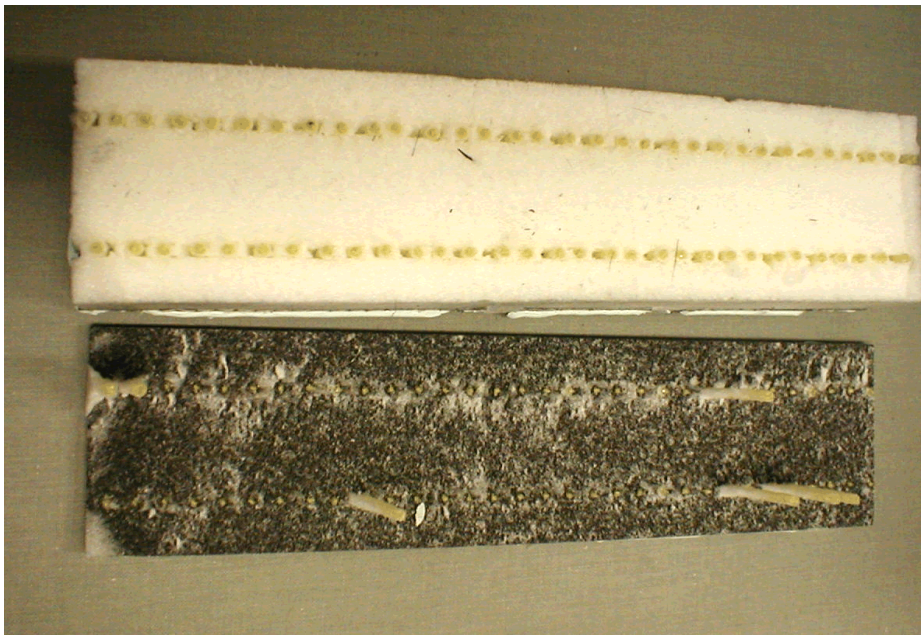

Figure 5.30 Failed NASA core shear specimen with 1.0 in. core and 1.0 in. stitch spacing.

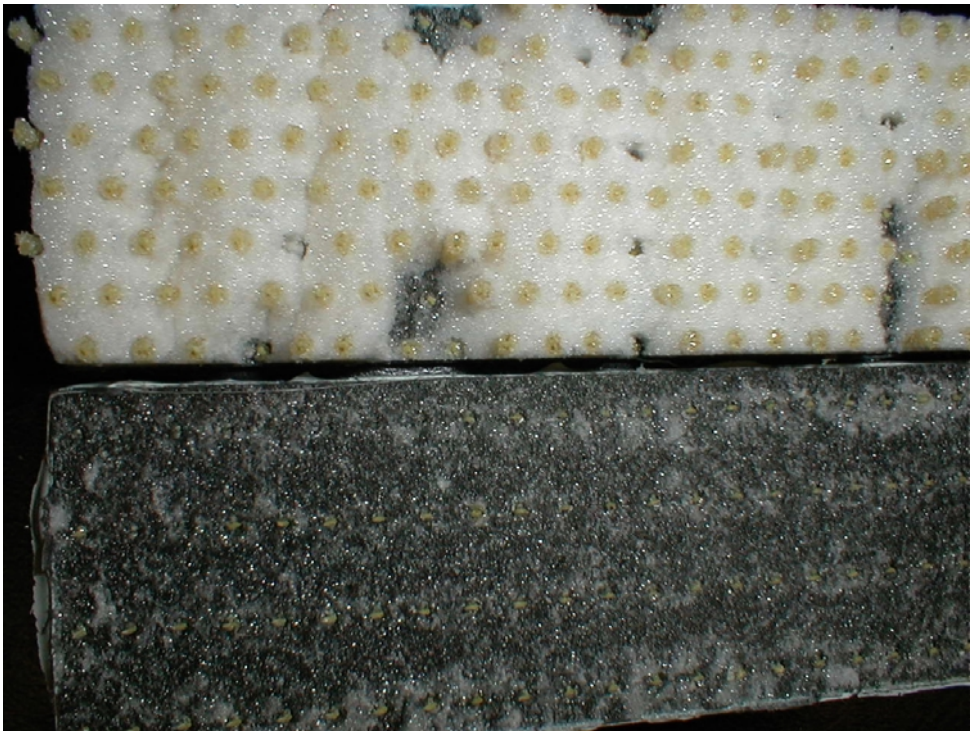

Figure 5.31 Failed NASA core shear specimen with 0.5 in. core and 0.25 in. stitch spacing.

From the testing of the core shear specimens it was concluded that stitching greatly increases the shear properties of sandwich structures. This is consistent with the results from the flexure testing and flatwise tensile testing where the properties of maximum load and energy absorbed during loading were shown to increase with increasing stitch densities. It was also shown in core shear testing, as with flexure testing, that angled stitching increases the maximum shear loading the panel can withstand.

5.5 Edgewise Compression Testing

Edgewise compression testing was performed on specimens cut from both the Utah panels and the NASA panels. The objective of the edgewise compression testing was to determine whether stitching improves the in-plane load carrying capacity of sandwich structures and to quantify the improvements in energy absorption prior to ultimate failure due to different stitching conditions.

Edgewise compression testing was carried out according to ASTM C364 [29]. End loading fixtures, as shown in Figure 5.32, were machined to clamp and hold the top and bottom edges of the specimens. These fixtures were designed to prevent localized damage at the ends of the carbon facesheets often referred to as "brooming." Figure 5.33 shows the fixture that may be adjusted for the different sizes of specimens tested. Figure 5.34 shows a close up of the channel where the top and bottom of the specimen is seated during testing.

Edgewise compression specimens were cut to a length of 2.8 in. This length allowed for a 2.5 in. unsupported gage length when the specimens were clamped in the test fixture. Specimens from the Utah panels were 2.0 in. wide and those from the NASA panels were 1.93 in. wide. The 1.93 in. width was selected to center the stitch rows across the width of the specimens while minimizing waste as previously discussed.

To ensure uniform loading of the specimens, an adjustable hemispherical ball stage was placed below the bottom fixture during testing. This tiltable stage had four screws around the perimeter to hold the desired stage position during the compression

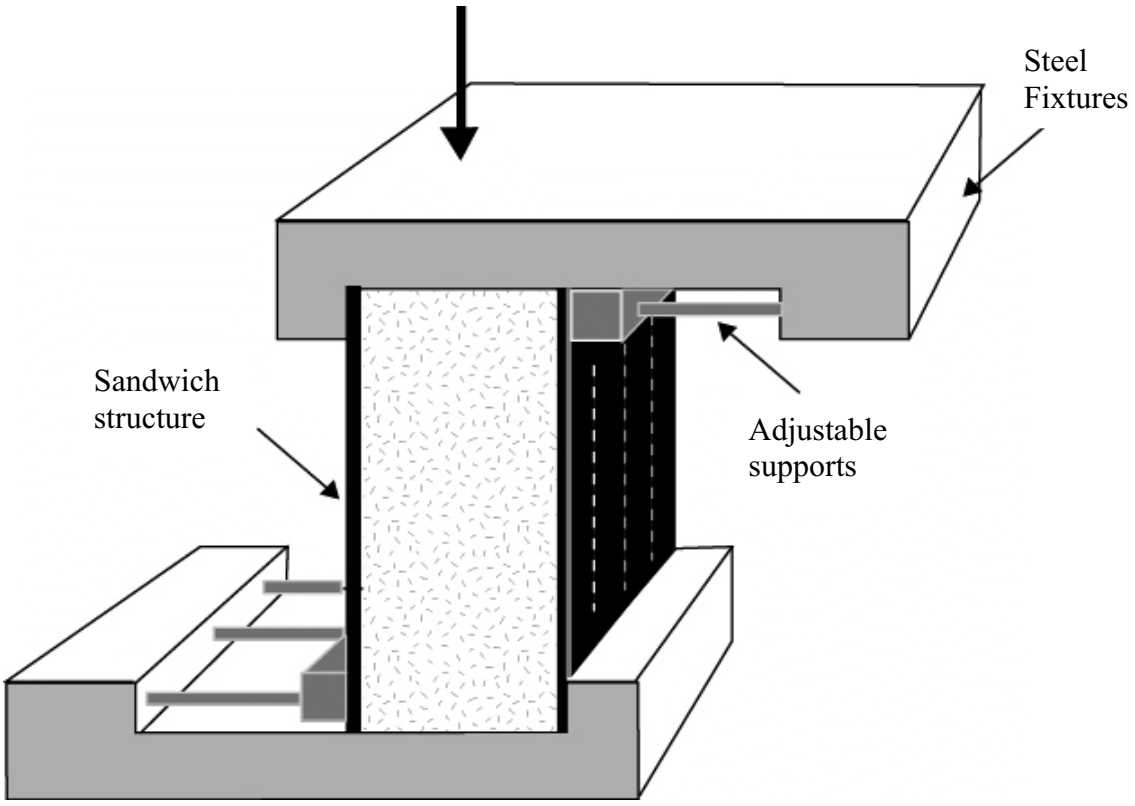

Figure 5.32 Diagram of edgewise compression fixture

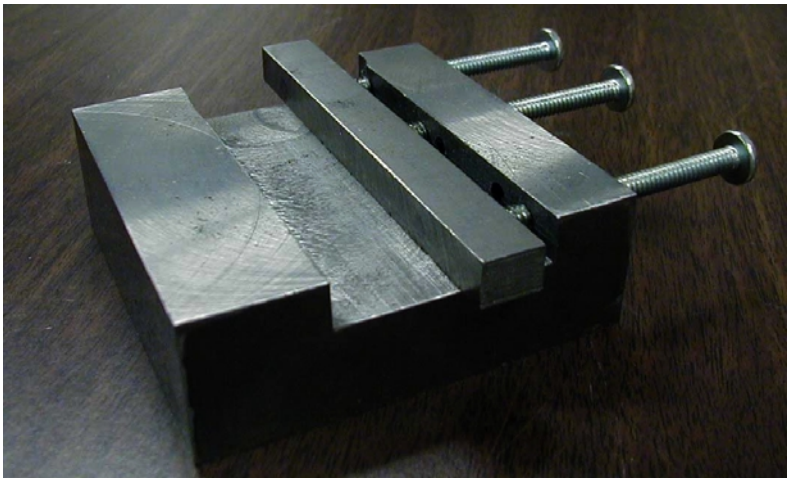

Figures 5.33 Edgewise compression base fixture

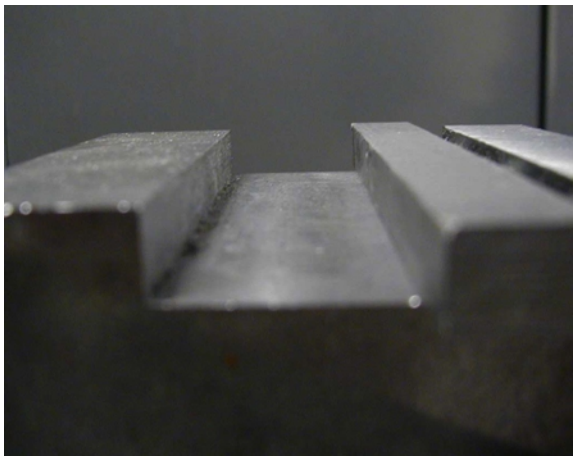

Figure 5.34 Machined channel to prevent “brooming”

test. Two back-to-back extensometers were used to measure strain and insure uniform loading during the initial stages of compression loading. These extensometers along with the hemispherical ball are shown in Figure 5.35. At low load levels, about 20-30% of the failure load, the four strain readings from the extensometers were used to adjust the hemispherical ball stage under the bottom test fixture to produce uniform compressive strains in the specimen. These extensometers were removed prior to loading to failure. The specimens were loaded at a constant displacement rate of 0.02 in./min. Load and crosshead deflection were recorded throughout the test.

Results from flatwise tensile testing of specimens from the Utah panels are presented in Table 5.11. Following the results from previous tests, only stitched specimens with the larger 1600 denier bobbin thread were tested. Representative load versus crosshead displacement plots obtained from unstitched and stitched Utah specimens are shown in Figure 5.36. For both the stitched and unstitched specimens, loading progressed smoothly up to the maximum failure load, at which point

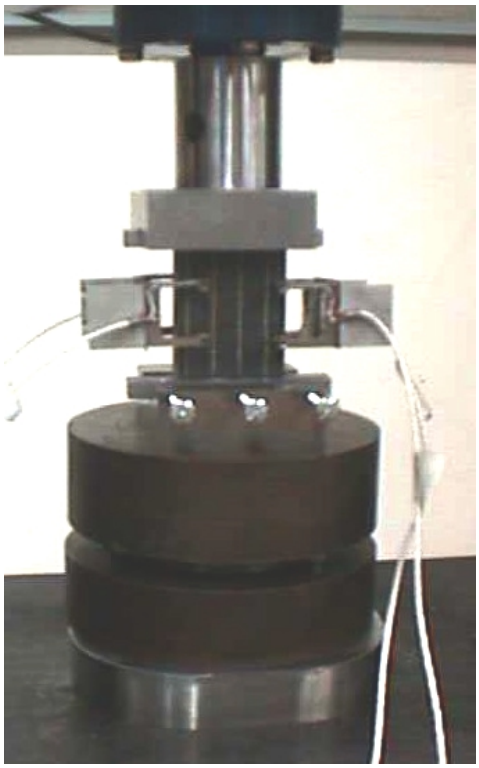

Figure 5.35 Hemispherical ball and extensometers used for specimen alignment.

the load began dropping abruptly and the test was stopped. A 27% improvement in the maximum load was measured as a result of stitching. The energy absorption to failure, or area under the load versus deflection curve, increased by 209% compared to the unstitched specimens.

Observation of the specimens during testing as well as inspection of the failed specimens showed that the unstitched specimens failed as a result of the facesheets delaminating from the foam core and buckling outward. The stitched specimens failed as a result of one of the facesheets buckling inward and pushing into the foam core. From these observations it is concluded that the stitching prevents outward buckling of the face sheets, resulting in an inward buckling occurring at a higher applied load.

Table 5.11. Utah panel edgewise compression test results

Specimen type	Max. Load, lbs.	Percent of Unstitched	Energy Absorbed, in.-lbs.	Percent of Unstitched
Unstitched	3401 3336 3212 average = 3316	100%	26.8 47.3 26.1 average = 33.4	100%
Stitched, 1600 denier bobbin thread	4063 4188 4401 average = 4217	123-133%	79.7 53.7 75.6 average = 69.7	161-239%

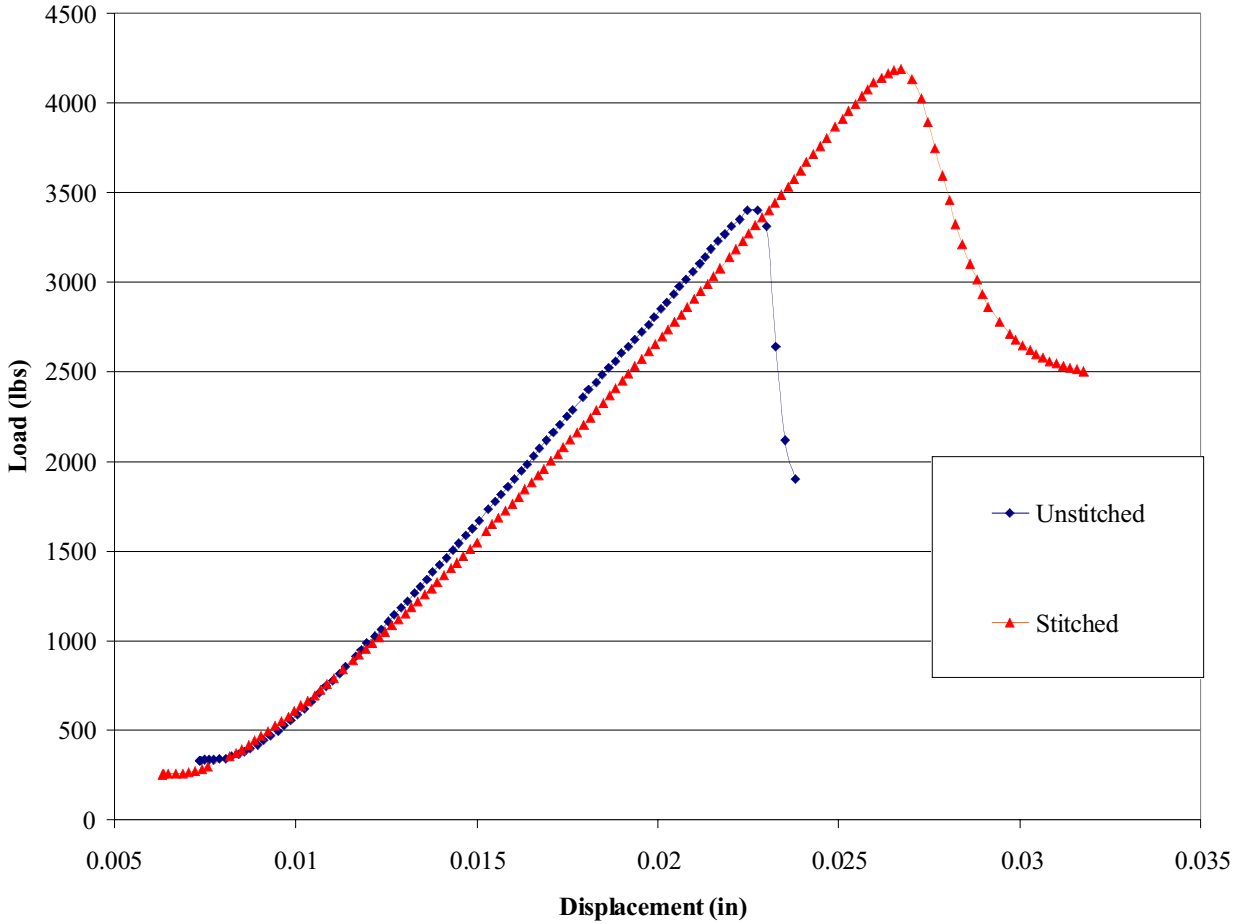

Figure 5.36 Typical edgewise compression results from Utah specimens.

Results from edgewise compression testing of specimens from the NASA panels are presented in Table 5.12. Representative load versus crosshead displacement plots obtained from unstitched and stitched specimens with the 1.0 in. core thickness are shown in Figure 5.37. Following the initial loading phase, the load versus deflection curves for all specimens were linear to the point of maximum load, at which point the load began dropping abruptly and testing was terminated. Improvements in maximum load as a result of stitching ranged from a low average of 13% (1.0 in. core with 1.0 in. stitch spacing) to a high of 50% (0.5 in. core with 0.25 in. stitch spacing). For a given core thickness, the maximum load increased as the stitch spacing decreased. For a given stitch spacing, the maximum load increased as the thickness of the core increased from 0.5 in. to 1.0 in. The energy absorption to failure, or area under the load versus deflection curve, also increased as a result of stitching. Improvements in energy absorption as a result of stitching ranged from a low average of 117% (1.0 in. core with 1.0 in. stitch spacing) to a high of 262% (1.0 in. core with 0.25 in. stitch spacing).

Examination of the failed specimens identified similar trends as were noted for the Utah specimens. For both core thicknesses, the unstitched specimens and the 1.0 in. stitch spacing specimens failed as a result of the facesheets delaminating from the foam core and buckling outward as in the unstitched Utah specimens. Figure 5.38 shows an unstitched specimen with a delaminated face sheet.

The stitched specimens with 0.5 and 0.25 in. stitch spacing all failed as a result of inward buckling of the facesheets as with the stitched Utah specimens. Figure 5.39 shows a failed specimen with 0.25 in. stitch spacing. A subtle inward curvature from the inward buckling failure mode can be see on the side view of the left facesheet and

Table 5.12 NASA panel edgewise compression test results

Specimen type	Max. Load, lbs.	Percent of Unstitched	Energy Absorbed, in.-lbs.	Percent of Unstitched
0.5 in. core unstitched	11,744 11,731 average = 11,740	100%	399 375 average = 387	100%
0.5 in. core 1.0 in. stitch spacing	16352 11896 average = 14,124	101-139%	644 515 average = 580	133-166%
0.5 in. core 0.5 in. stitch spacing	14,829 14,770 15,157 average = 14,919	126-129%	731 865 989 average = 861	189-256%
0.5 in. core 0.25 in. stitch spacing	17,300 16,897 18,576 average = 17,591	144-158%	664 614 810 average = 696	159-209%
1.0 in. core unstitched	14,542 14,292 average = 14,459	100%	214 234 average = 224	100%
1.0 in. core 1.0 in. stitch spacing	14,763 16,627 17,499 average = 16,296	102-121%	118 288 382 average = 263	53-171%
1.0 in. core 0.5 in. stitch spacing	17,922 16,494 average = 17,208	114-124%	484 415 567 average = 489	185-253%
1.0 in. core 0.25 in. stitch spacing	18,246 18,271 17,640 average = 18,052	122-126%	626 480 655 average = 587	214-292%

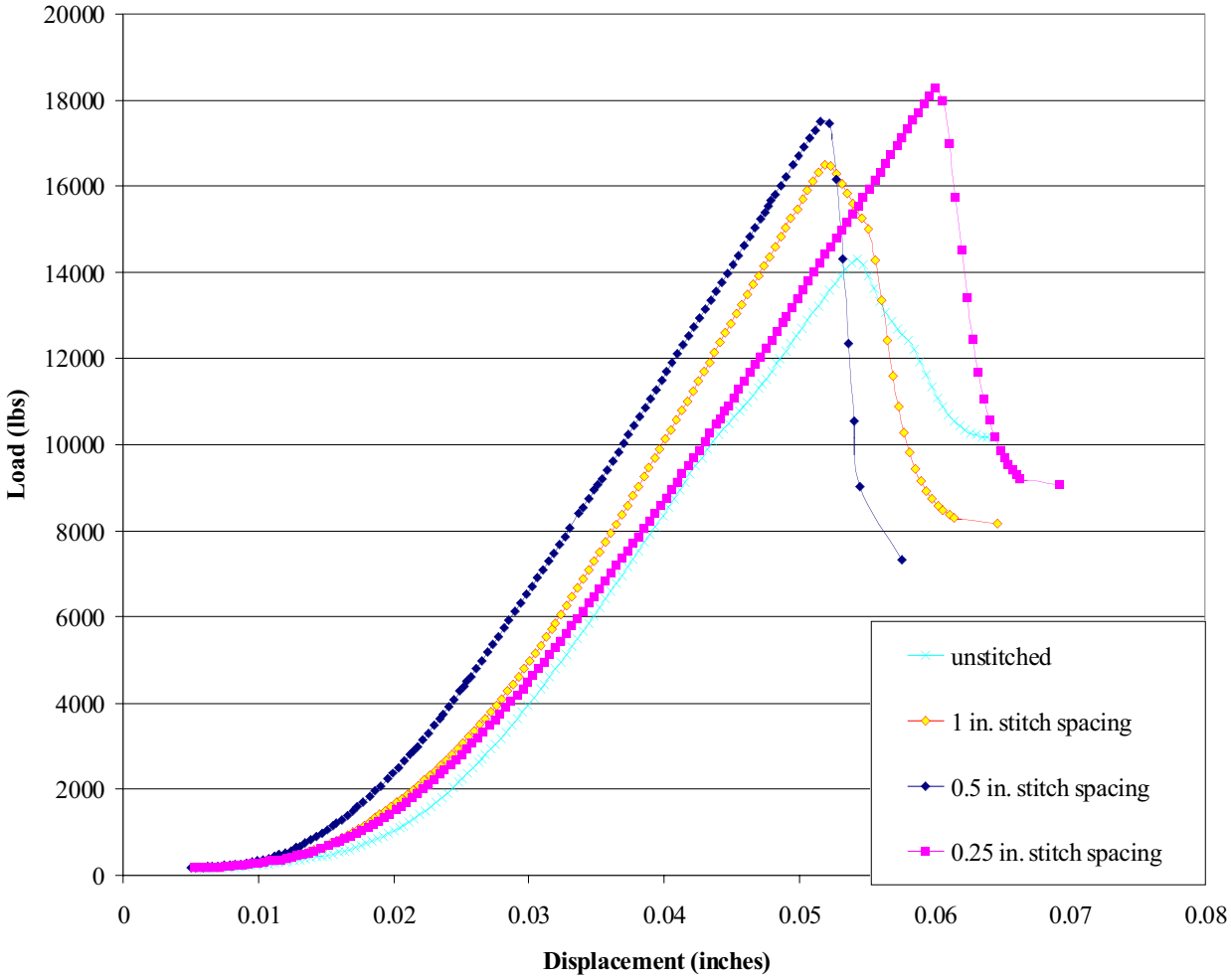

Figure 5.37 Typical edgewise compression results from NASA specimen

Figure 5.38 Failed unstitched NASA edgewise compression specimen

damage can be observed across the surface of the same facesheet. There were no apparent differences in the failure modes of the 0.5 and 1.0 in. core thicknesses.

In summary, results have shown that stitching produces increases in both the maximum load as well as the energy absorbed in edgewise compression testing. Maximum load increased up to a 133 % increase in the Utah specimens and up to 158% in the NASA specimens. Energy absorbed increased by as much as 239% in the Utah specimens and up to 292% in the NASA specimens. Stitching was also shown to change the failure mode from facesheet delamination to inward buckling. However, the improvements in maximum load and energy absorption are rather modest compared to similar improvements measured in flatwise tensile testing and core shear testing.

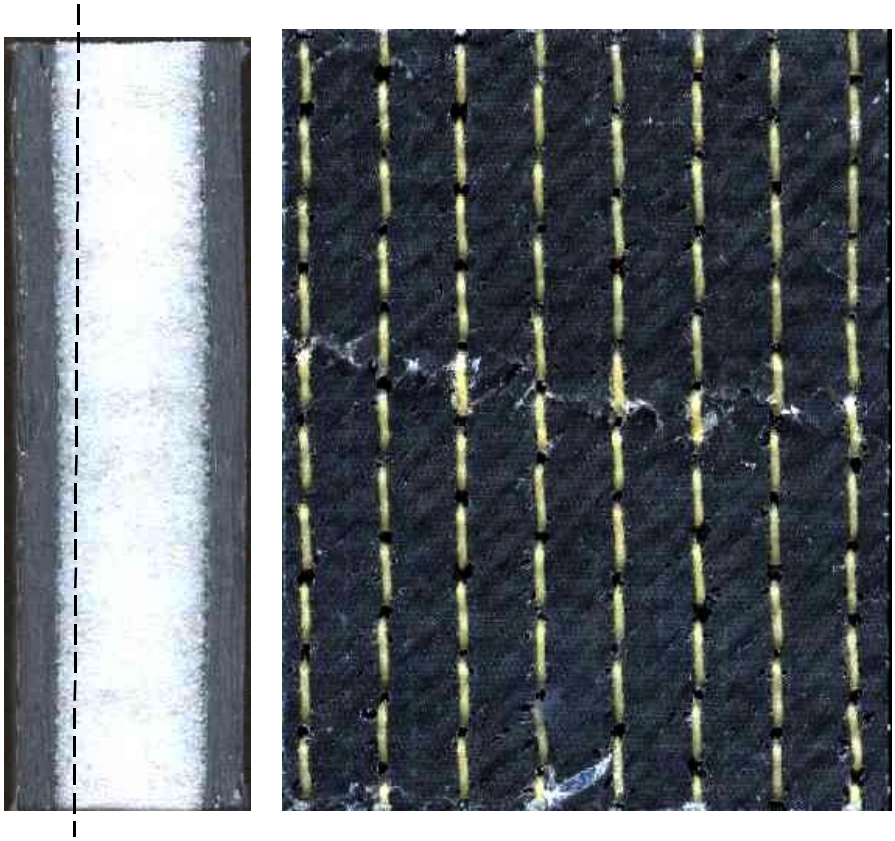

Figure 5.39 Side (left) and surface (right) of failed NASA edgewise compression specimen with inward buckling and 0.25 in. stitch spacing

Thus it appears that although stitching offers tremendous improvements in strength and energy absorption under interlaminar loading (normal and shear), the improvements under in-plane compression loading are more modest.

CHAPTER 6

EVALUATION OF DAMAGE TOLERANCE

Instrumented impacting followed by damage evaluation was performed on the eight different types of NASA panels. Compression after impact testing was also performed to assess the damage resistance and damage tolerance of stitched sandwich specimens.

6.1 Drop-Weight Impact Testing Procedure

Drop-weight impact testing was performed to investigate the effects of stitching on damage resistance of sandwich panels. Compression After Impact (CAI) testing was also performed on some impacted specimens as will be discussed in section 6.2. Impact testing was performed using only the NASA panels. Specimens 5.0 in. x 10.0 in. were cut from the NASA panels, with the 10.0 in. dimension in the 0° fiber direction. The dimensions of these panels were chosen to allow compression after impact testing to be performed. In total, eight different panel types were investigated. There were two different core thickness used, 0.5 in. and 1.0 in. For each thickness there were four different stitching densities, unstitched, 1.0 in., 0.5 in. and 0.25 in.

Impact testing was performed using an instrumented drop weight impact system as shown in Figures 6.1-6.3. The impact tester consisted of a 10,000 lb. capacity load

Figure 6.1 Impact frame

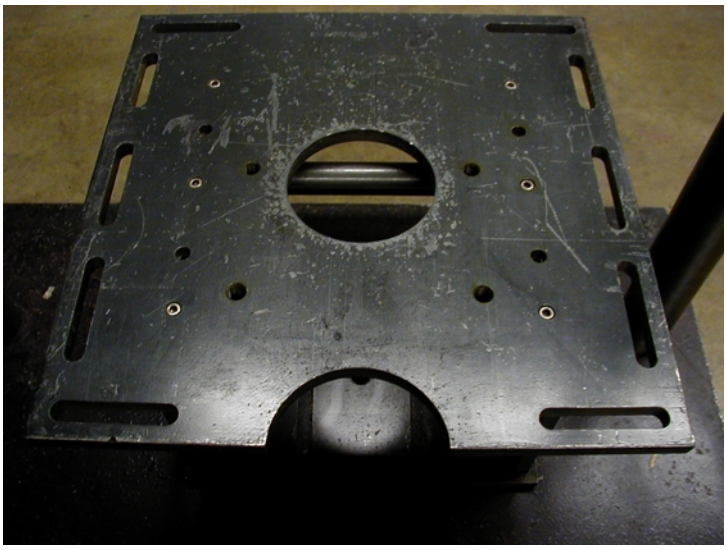

Figure 6.2 Base plate of impact tester.

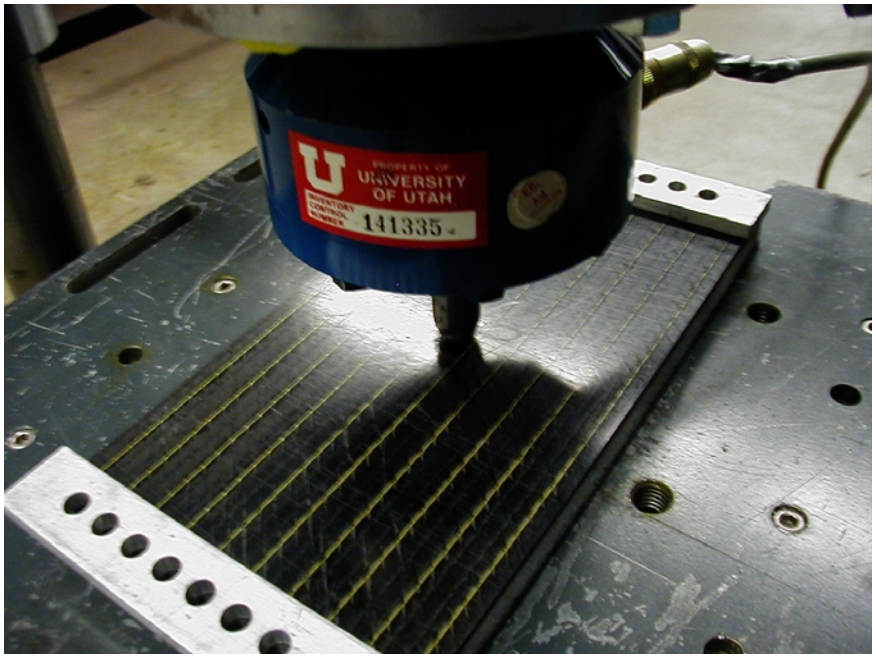

Figure 6.3 Impactor in contact with clamped specimen.

cell mounted onto a crossbeam. The crossbeam was attached to two vertical guide columns with linear bearings as shown in Figure 6.1. The indenter head was threaded into the loadcell and the crossbeam was raised to the height that produced the desired input energy for impact testing. The weight of the indenter head, loadcell, and crossbeam was approximately 35 lbs. The impact force produced during the impact event was recorded as a function of time using a PC-based data acquisition system. Prior to impacting, specimens were centered and clamped on both ends onto the base plate of the impactor which contained a 4.0 in. diameter hole centered directly beneath the impact head as shown in Figure 6.2. Figure 6.3 show a panel clamped to the impactor base plate.

Impacting was performed using two different sizes of hemispherical impactors and two different impact energies. The two different impact energies were 35 ft-lbs and 70 ft-lbs. The two hemispherical impactor diameters were 0.5 in. and 1.88 in. Panels were impacted at 35 ft-lbs using the 0.5 in. impactor. Panels were impacted at both 35ft-lbs and 70 ft-lbs using the 1.88 in. impactor.

Nondestructive evaluation methods were evaluated for characterizing the damage state produced by impact testing. Preliminary evaluations of ultrasonic C-scanning using a 5 MHz transducer with a 2 in. focal length indicated that damage within the foam core could not be detected and facesheet debonding was difficult to detect. Later evaluations performed by Dr. David Hsu at the Center for Nondestructive Evaluation at Iowa State University were successful in identifying simulated facesheet delaminations produced using Teflon inserts.

These later investigations used a 3.5 MHz frequency transucer with a 1.0 in. diameter and a 2.0 in. focal length in water. The C-scan image of the delaminations was based on the amplitude of the first backwall echo. Cracks within the foam core could not be detected.

Following the preliminary evaluation of ultrasonic scanning, x-ray evaluation with a dye penetrant was investigated. To ensure that the dye penetrant was able to reach cracks in the foam core of the sandwich specimens, a small hole, 0.040 in. diameter, was drilled through the top facesheet at the center of impact. Holes were drilled in both the damaged and undamaged panels to insure an equal comparison. The x-ray dye penetrant, made from 30 % zinc iodide, 30% isopropyl alcohol, 20% water and 20% Kodak Photoflo, was injected into the hole. When x-rayed, the dye penetrant served to highlight the damaged area due to the impact. This method proved to be an incomplete method of determining the damage area. Cracks within the damaged panels were not all connected, and the dye penetrant could not spread to all of the damaged regions. Thus only a small amount of damage was visible using the x-ray imaging.

Since neither ultrasonic scanning nor x-ray imaging of the impacted sandwich panels was determined to be suitable for characterizing the damage state, destructive evaluation was investigated. Sectioning of the impacted panels was performed in an attempt to characterize the damage state within the panels. Impacted specimens, identical to those evaluated nondestructively using x-ray imaging, were sectioned using a water-cooled diamond saw. A dye solution specially designed for this purpose was applied to the sectioned surfaces allowing cracks within the damaged sandwich panels to become more visible. This dye was made from 5 % black fountain pen ink, 75%

isopropyl alcohol and 20% Kodak Photoflo. While the section was still wet with the dye solution, it was placed onto a digital scanner and imaged. This technique was found to be very useful for identifying both facesheet damage and core damage following impacting. One limitation to this method is that damage is characterized at only one plane through the impacted panel. However, several parallel and perpendicular sections may be cut in the damage zone to gain a more complete understanding of the damage state. Results of the sectioning will be presented in section 6.2.

6.2 Compression After Impact Testing Procedure

To assess the damage tolerance of stitched sandwich panels, compression after impact testing was performed on several specimens cut from the NASA panels following impacting. As described previously, eight specimen configurations were investigated: two core thicknesses, each with three stitch densities as well as unstitched. Three impact conditions were considered: 35 ft.-lb. impact using a 0.5 in. diameter indenter, 35 ft.-lb. impact using a 1.88 in. indenter, and a 70 ft.-lb. impact using a 1.88 in. indenter. Thus, a total of 24 CAI tests were performed.

Compression after impact testing was performed using the NASA CAI test fixture [30]. This test fixture consists of four separate assemblies, each to support one side of the 5.0 in. wide and 10.0 in. long specimen. The top and bottom plate assemblies provided load transfer to the ends of the specimen and restrained end brooming by clamping 0.375 in. of the ends of the test panel. The remaining two

assemblies were clamped to the sides of the test specimen to stabilize the specimen against buckling. Figure 6.4 shows the fixture with a specimen secured for testing.

An adjustable hemispherical ball stage and dual back-to-back extensometers were used to insure uniform loading similar to the procedure followed for edgewise compression testing. Specimens were mounted into the top and bottom segments of the test fixture and placed into the test machine for compression loading. With the side support assemblies left off the specimens, the two back-to-back extensometers were mounted on either side of the test specimen to obtain a total of four axial strain readings.

At low load levels, the four strain readings from the extensometers were used to adjust the hemispherical ball stage under the bottom test fixture to produce uniform compressive strains in the specimen. These extensometers were removed and the side supports clamped to the specimen prior to loading to failure.

Load and crosshead deflection were recorded throughout the test. All CAI testing was performed using a 50,000 lb. capacity electromechanical test machine at a constant displacement rate of 0.02 in./min.

6.3 Drop Weight Impact Testing Results

Drop-weight impact testing was performed on specimens from the NASA panels to investigate the effects of stitching on the damage resistance of sandwich panels as discussed previously. For each impact condition, eight specimens were tested, one from each of the stitching conditions investigated with the NASA panels: two core

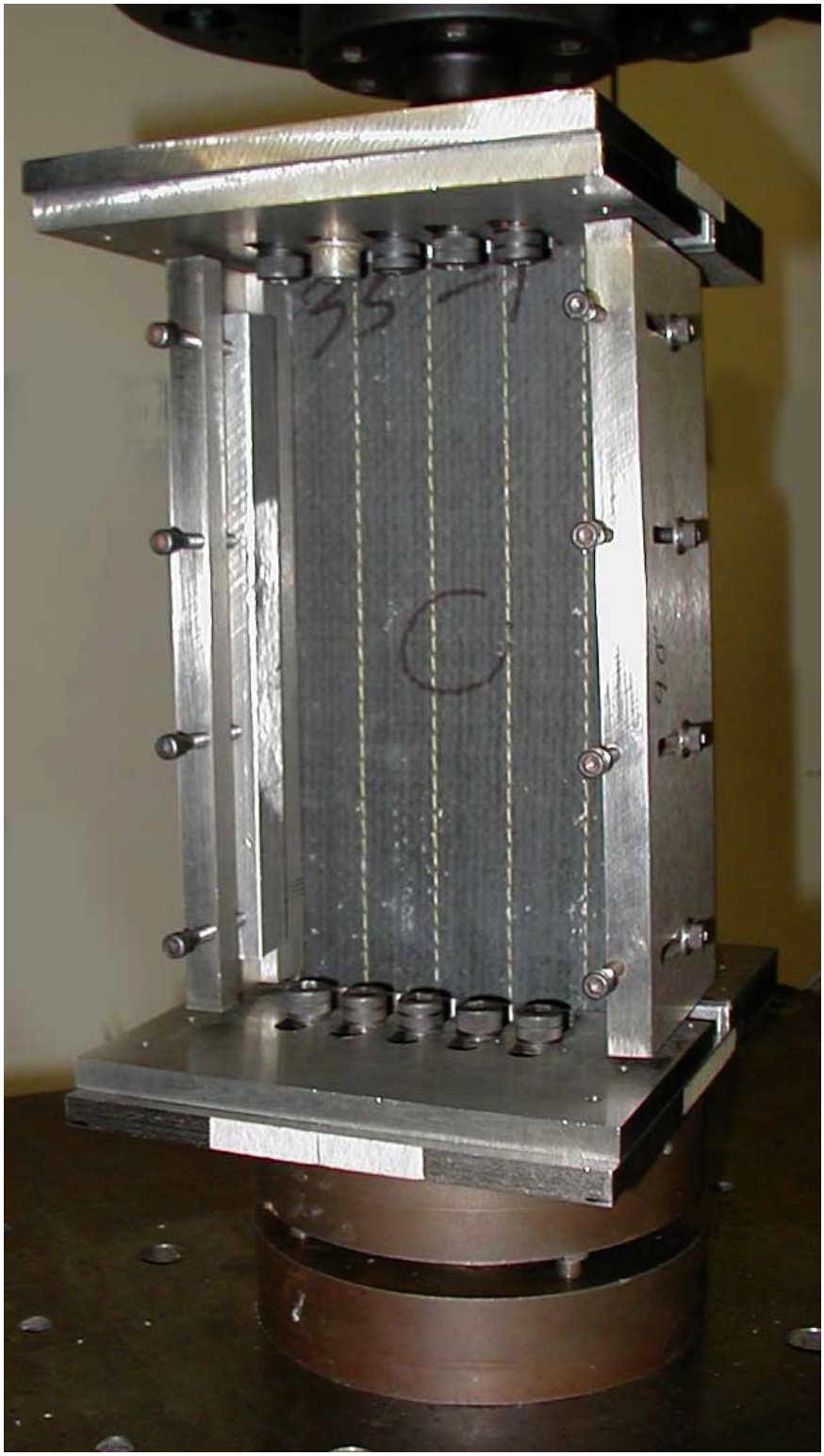

Figure 6.4 CAI specimen and fixture sitting on the hemispherical ball.

thicknesses, each with an unstitched condition and three stitch spacings.

Impact force was recorded as a function of time during each impact event. Figure 6.6 displays a typical impact event for the four types of specimens with a 1.0 in. core thickness. As shown in the figure, the duration of the impact event was between 10 and 12 milliseconds. The unstitched specimens had the longest duration of impact. Specimens with 0.5 in. and 0.25 in. stitch spacing had almost identical impact events with the shortest impact durations. The 1.0 in. stitch spacing specimens typically had an impact duration longer than the specimens with 0.5 in. and 0.25 in. stitch spacing but shorter than the unstitched specimens. These trends were observed for all the specimens impacted.

Tabulated values for the maximum impact force during the impact event are presented in Table 6.1. These results show that a constant input energy level does not produce a constant maximum force. The maximum impact force is shown to increase with increasing stitch density. This trend is believed to be in agreement with results from flexure testing, where stitching was found to increase bending stiffness. Stitched specimens with an increased bending stiffness are expected to produce an increased maximum impact force during impacting with constant impact energy. Table 6.1 also shows that the maximum impact forces from the larger 1.88 in. diameter impactor are greater than the smaller 0.5 in. diameter impactor at the same impact energy. Following impacting, the impacted area within the specimens were nondestructively examined using X-ray inspection. X-ray dye penetrant was injected into the damaged specimens through a small hole drilled through the upper face sheet at the center of the

at the center of the impact. The zinc iodide based dye penetrant was designed to spread throughout the damaged area and be opaque to the X-ray. The damage area was thus visible during X-ray inspection.

X-ray photographs of the specimens with a 0.5 in. core thickness subjected to a 35 ft-lb impact with the 0.5 in. impactor are presented in Figures 6.7-6.10. For comparision purposes, each type of specimen was also X-rayed in the undamaged state. From each impacted specimen, the total damaged area was determined from the X-ray photographs and is presented in Table 6.2.

The damaged area determined from the X-ray photographs is a two-dimensional projection of the three-dimensional damage state within the specimen. To assess the accuracy of nondestructive X-ray determination of the damage area, some of the impacted specimens were sectioned and photographed. Specimens were sectioned through the center of the impact area using a water-cooled diamond saw. An ink-based dye penetrant was applied to the cut surfaces to enhance the crack surfaces within the foam core. Comparisons between the X-ray photographs and the sectioned specimen photographs are presented in Figure 6.11 for a specimen with a 1.0 in. core and 0.25 in. stitch spacing. The specimen was impacted at 35 ft-lb using a 0.5 in. diameter impactor. A large difference was observed between the relatively small damage area detected by X-ray and the large damage area visible following sectioning. Although there are many core cracks produced by the impact, these cracks did not extend to the central damage area underneath the impact.

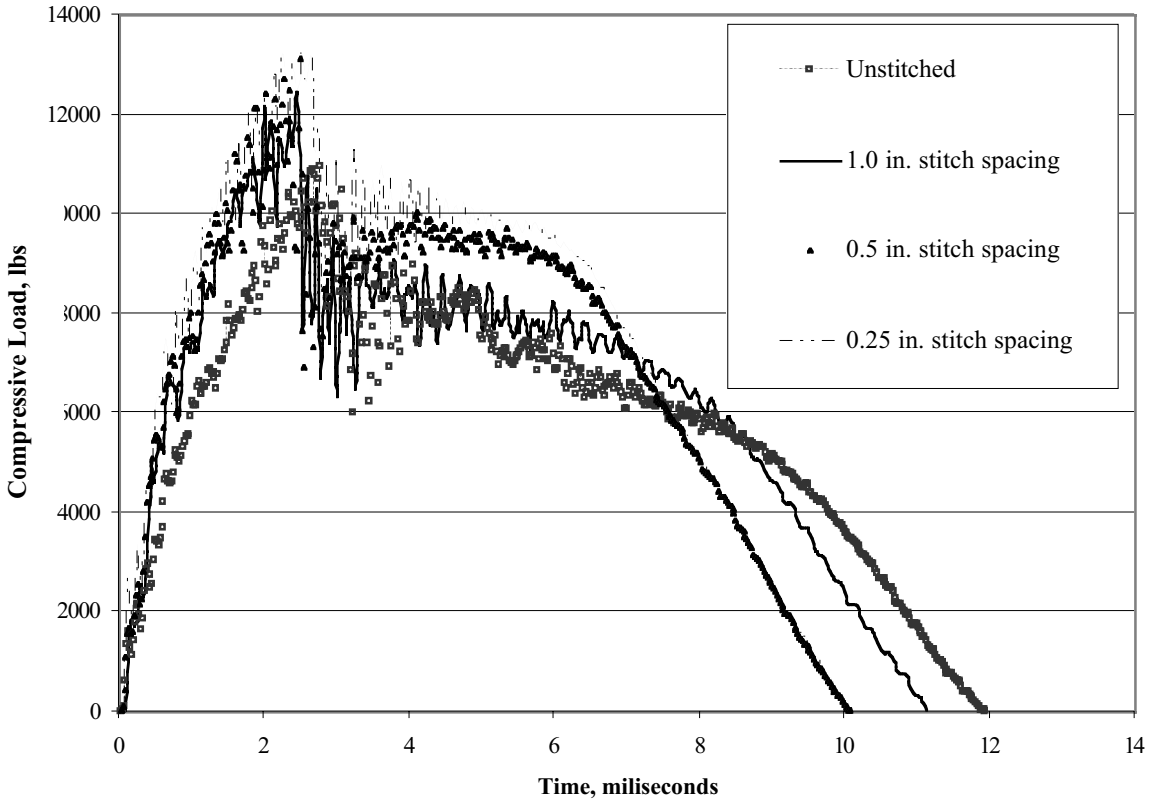

Figure 6.6 Impact force versus time for NASA specimens with 1.0 in. core thickness, 35 ft-lb impact energy.

Table6.1 Maximum impact force recorded during drop weight impacting

Specimen type:	Maximum force, 0.5 in. impactor 35 ft-lb impact (lbs)	Maximum force, 1.88 in. impactor 35 ft-lb impact (lbs)	Maximum force, 1.88 in. impactor 70 ft-lb impact (lbs)
0.5 in.core unstitched	11,589	17,005	19,231
0.5 in. core 1.0 in. stitch spacing	11,796	20448	24,900
0.5 in. core 0.5 in. stitch spacing	11,841	22,467	28,319
0.5 in.core 0.25 in. stitch spacing	13,540	21,205	28,732
1.0 in. core unstitched	10,970	16,890	20,310
1.0 in. core 1.0 in. stitch spacing	12,461	21,618	25,267
1.0 in. core 0.5 in. stitch spacing	12,714	24,509	34,400
1.0 in. core 0.25 in. stitch spacing	13,219	26,185	34,148

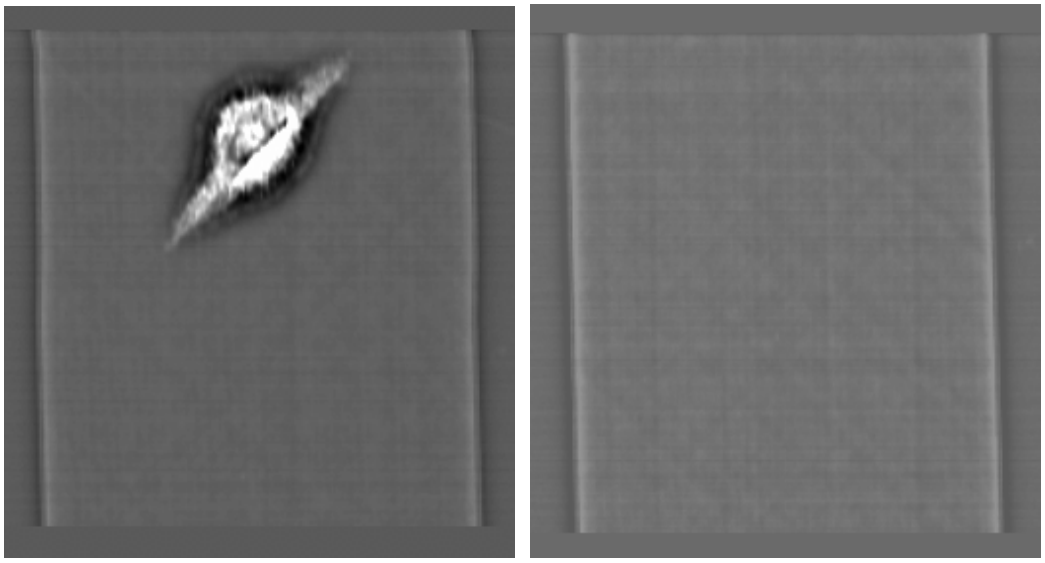

a. 35 ft-lb impact, 0.5 in. impactor. b. No impact.

Figure 6.7 X-ray results of unstitched specimens with 0.5 in. core.

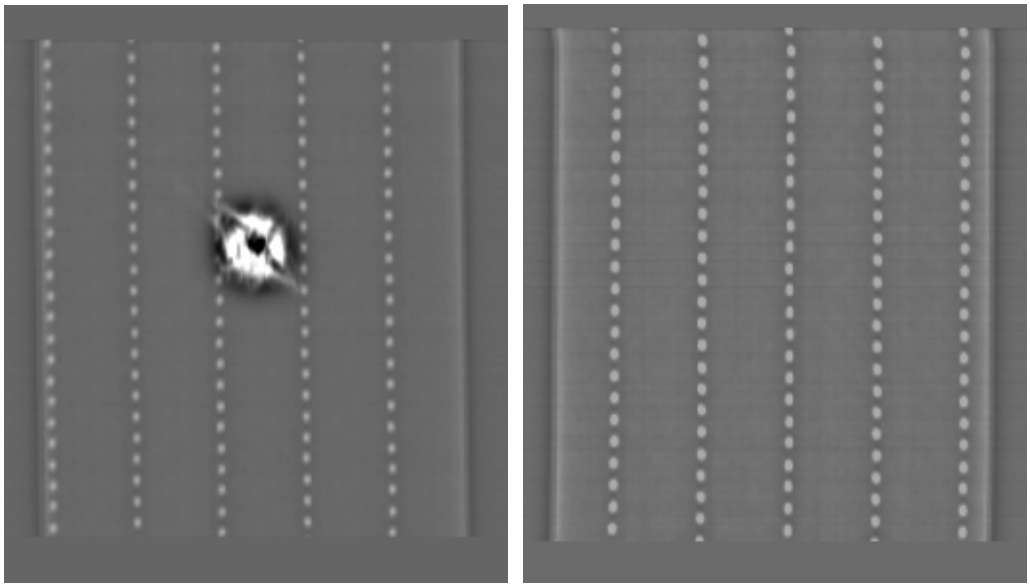

a. 35 ft-lb impact, 0.5 in. impactor. b. No impact.

Figure 6.8 X-ray results of stitched specimens with 1.0 in. stitch spacing and 0.5 in. core.

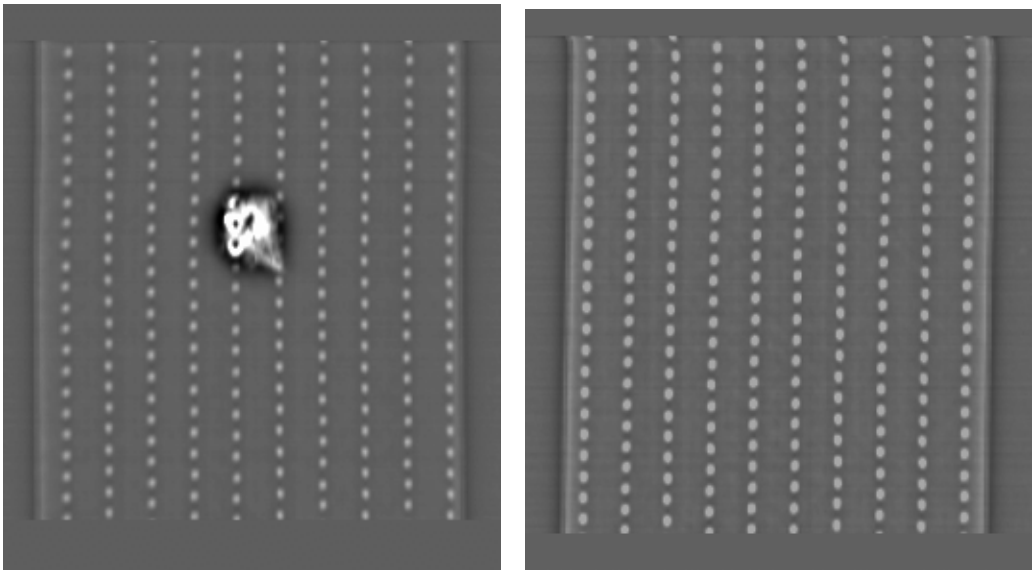

a. 35 ft-lb impact, 0.5 in. impactor. b. No impact.

Figure 6.9 X-ray results of stitched specimens with 0.5 in. stitch spacing and 0.5 in. core.

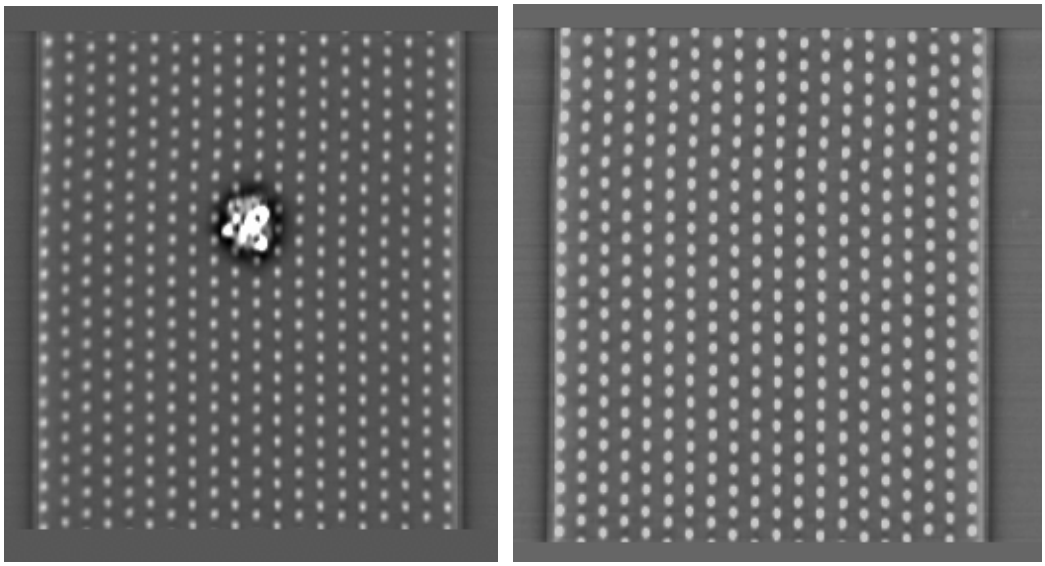

a. 35 ft-lb impact, 0.5 in. impactor. b. No impact

Figure 6.10 X-ray results of stitched specimens with 0.25 in. stitch spacing and 0.5 in. core.

.

Table 6.2 Damaged area from X-ray, 35 ft-lb impact with 0.5 in. diameter impactor

Specimen type:	Damage area, in^2
0.5 in.core unstitched	1.68
0.5 in. core 1.0 in. stitch spacing	0.46
0.5 in. core 0.5 in. stitch spacing	0.41
0.5 in.core 0.25 in. stitch spacing	0.33
1.0 in. core unstitched	0.77
1.0 in. core 1.0 in. stitch spacing	0.50
1.0 in. core 0.5 in. stitch spacing	0.33
1.0 in. core 0.25 in. stitch spacing	0.33

As a result, the dye penetrant injected at the center of the impact area did not seep into these cracks, and thus they were not detected during X-ray photography. Based on these observations, X-ray photography of the impacted specimens was replaced with specimen sectioning. Although sectioning is a destructive evaluation method that eliminates the possibility of postimpact testing of the specimen, this method was deemed necessary to characterize the damage state in the specimens following impacting. Thus, two identical specimens were impacted for each of the impact conditions investigated: one for sectioning and damage evaluation and the second for compression after impact testing.

Selected sectioned specimens are presented in Figures 6.12 – 6.14 to provide an overview of the types of damage observed in the specimens following impact. The complete set of sectioned specimen photographs is presented in the Appendix.

Figure 6.12 shows the damage state in an unstitched specimen with a 1.0 in core following a 35 ft-lb impact with a 0.5 in. diameter impactor. The top facesheet is damaged under the center of impact and a large delamination approximately 3 in. in diameter is present between the top facesheet and core.

The deformation of the top facesheet during the impact crushed a region of the foam core underneath the impact. This region of crushed core absorbed the ink-based dye penetrant and remained darker than the surrounding uncrushed core when photographed. This region of crushed core was sponge-like to the touch, noticeably more compliant than the surrounding uncrushed core.

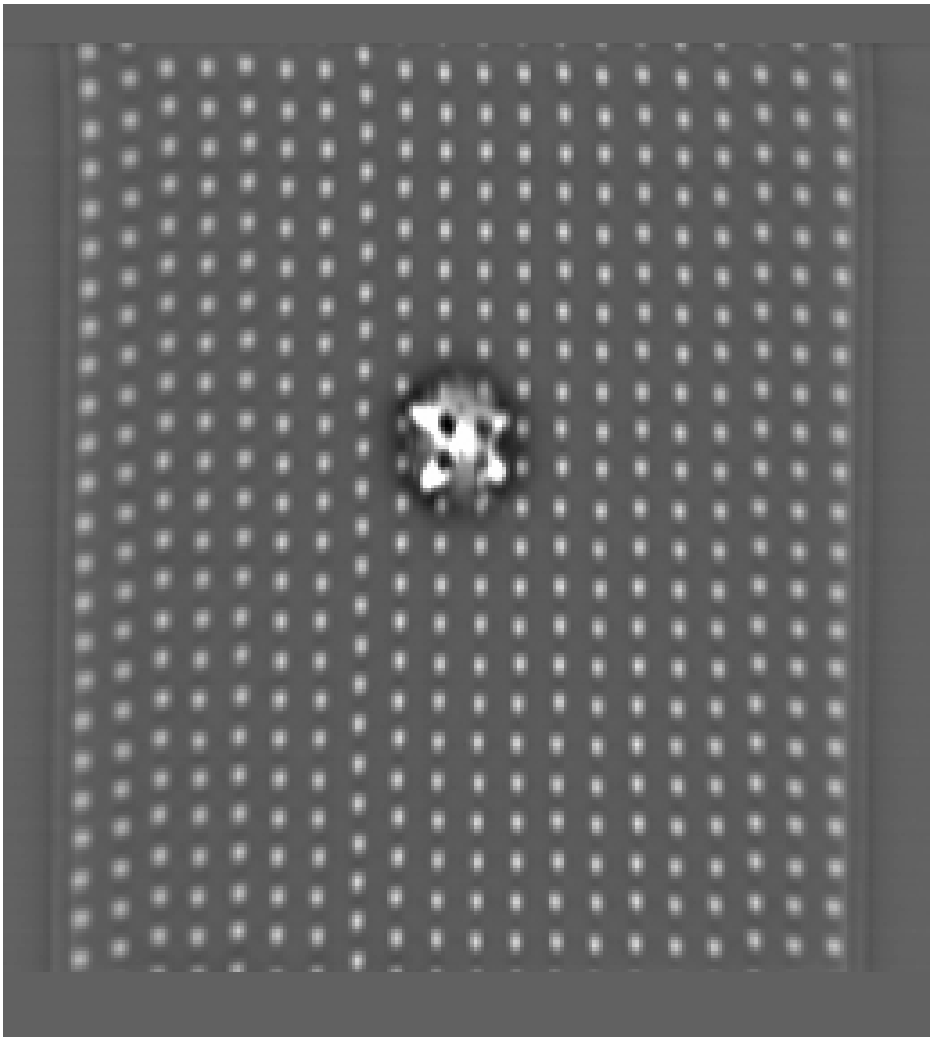

a. X-ray photograph following impact.

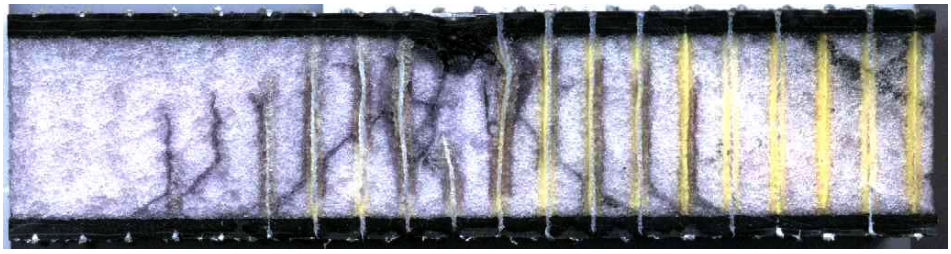

b. Photograph of impacted specimen following sectioning through impact.

Figure 6.11. Comparison between X-ray and sectioned specimen with 1.0 in. core and 0.25 in. stitch spacing following a 35 ft-lb impact with a 0.5 in. diameter impactor.

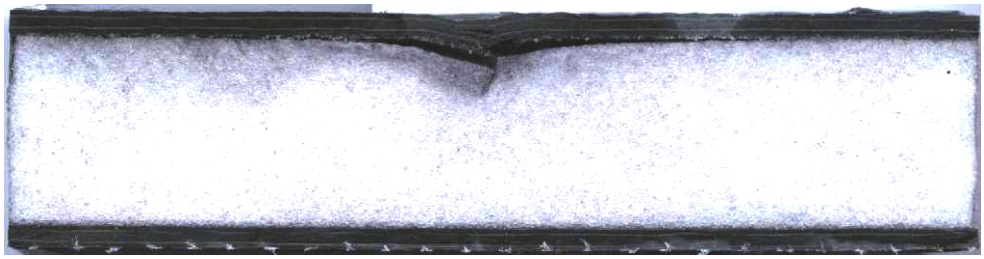

Figure 6.12 Unstitched specimen with 1.0 in core following 35 ft-lb impact with 0.5 in. impactor.

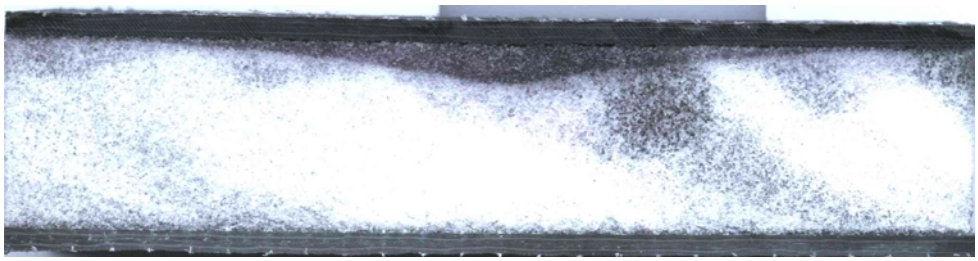

Figure 6.13 Unstitched specimen with 1.0 in core following 35 ft-lb impact with 1.88 in. impactor.

Figure 6.14 Stitched specimen with 1.0 in core and 0.5 in. stitch spacing following 70 ft-lb impact with 1.88 in. impactor.

The thickness of the crushed core region was largest directly underneath the impact, becoming progressively thinner away from the center of impact. The crushed region was permanently deformed such that a cavity was produced between the delaminated facesheet and the core.

A similar damage state was observed in an identical unstitched specimen with a 1.0 in. core following a 35 ft-lb impact with the 1.88 in. impactor as shown in Figure 6.13. Once again, a region of crushed core is clearly visible following application of the ink-based dye penetrant. This crushed core region tapered in thickness away from the center of impact. The crushed core region was approximately 5 in. in diameter. Unlike the impact with the smaller 0.5 in. impactor, the crushed core was not permanently deformed and there was no clearly visible delamination between the top facesheet and the core. Additionally, there was no visible impact damage to the top facesheet of the specimen. Thus the larger impactor produced significant damage to the foam core without producing any externally visible damage to the facesheets.

Figure 6.14 shows the damage state in a stitched specimen with a 1.0 in. core and 0.5 in. stitch spacing following a 70 ft-lb impact with the larger 1.88 in. diameter impactor. As in the previous photograph, there is no externally visible indication of damage to the facesheets yet there is extensive cracking of the foam core. The crushed core region is significantly reduced due to the presence of the stitches. However, a large number of core cracks are produced in the vicinity of the stitches that were not observed in the unstitched specimens. The core cracks appear to be along the outer edges of the stitches, away from the center of impact. These cracks do not extend along the stitches to the facesheets, but rather either terminate a short distance from the

core/facesheet interface or propagate away from the stitch through the core in a diagonal direction. Thus the addition of stitches changes the damage in the foam core from a central crushed region immediately below the impact to a distributed array of core cracks.

After careful examination of these and all other sectioned pictures provided in the Appendix, two quantitative measures were developed to assess the level and types of damage that occurred as a result of impact. These quantitative measures followed from the two common types of damage that was observed in the foam cores of the sandwich specimens: crushing and cracking. The crushed region of the foam core was clearly visible as ink-stained dark regions in the photographs. The crushed regions were generally in the shape of a bell curve, with the center located directly underneath the center of impact. The maximum length of the crushed region in the sectioned photograph through the center of impact was taken as the average diameter of an assumed circular crushed region. This diameter of the crushed core region was used as the first quantitative measure of damage. The other primary form of damage, core cracking, occurred both along the stitch columns as well as in the foam between stitches. The frequency and number of the cracks and the size of the crushed foam region was found to be dependent on the core thickness, the stitch spacing, and the impact conditions. The extent of core cracking was determined by measuring the distance between the outermost cracks in the sectioned photograph through the center of impact. This diameter of cracking was calculated for each specimen sectioned and used as the second quantitative measure of damage. These two damage measures are

presented for the impacted and sectioned specimens in Figures 6.15-6.18.

Figure 6.15 and 6.16 compare the crushed core diameters for the specimens with the 0.5 in. thick core and 1.0 in. thick core, respectively. For all three impact conditions, the crushed core diameter decreases as the stitch spacing decreases. While the crushed core diameter increases for the unstitched specimens as the impactor diameter increases and as the impact energy increases, the crushed core diameter for the stitched specimens is not affected greatly by the impact conditions. A comparison of Figures 6.15 and 6.16 shows that the greatest crushed core diameters generally occurred for specimens with the thinner 0.5 in. core. Since the sectioned photographs indicated that the stitched specimens exhibited more core cracking and less core crushing than the unstitched specimens, the crush core diameter is less useful as a measure of the damage state in the stitched specimens. In fact, measurement of the crushed core diameter was difficult in many of the stitched specimens due to the minimal thickness of the crush region. These results clearly indicate that stitching reduces the amount of core crushing due to impact.

While stitching was effective in reducing core crushing, it produced a greater region of core cracking as shown in Figures 6.17 and 6.18 for the 0.5 in. and 1.0 in. core thicknesses, respectively. For both core thicknesses, a large increase in the diameter of cracking occurred as a result of stitching. As the stitch spacing decreased, the diameter of the cracked area increased. Although the diameter of cracking increased in the stitched specimens as the impactor diameter and impact energy increased, it remained

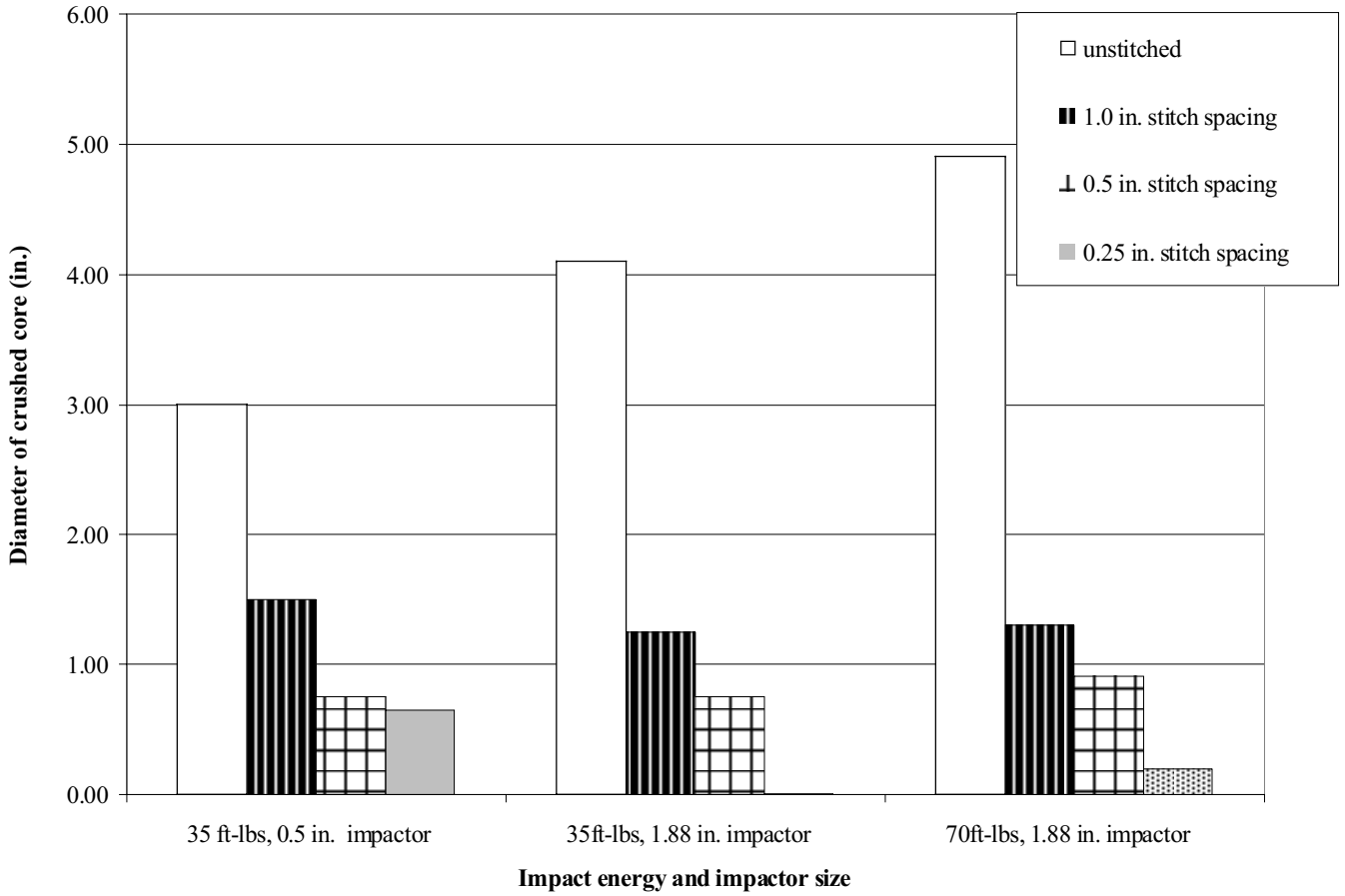

Figure 6.15 Comparison of crushed core diameters for 0.5 in. core panels

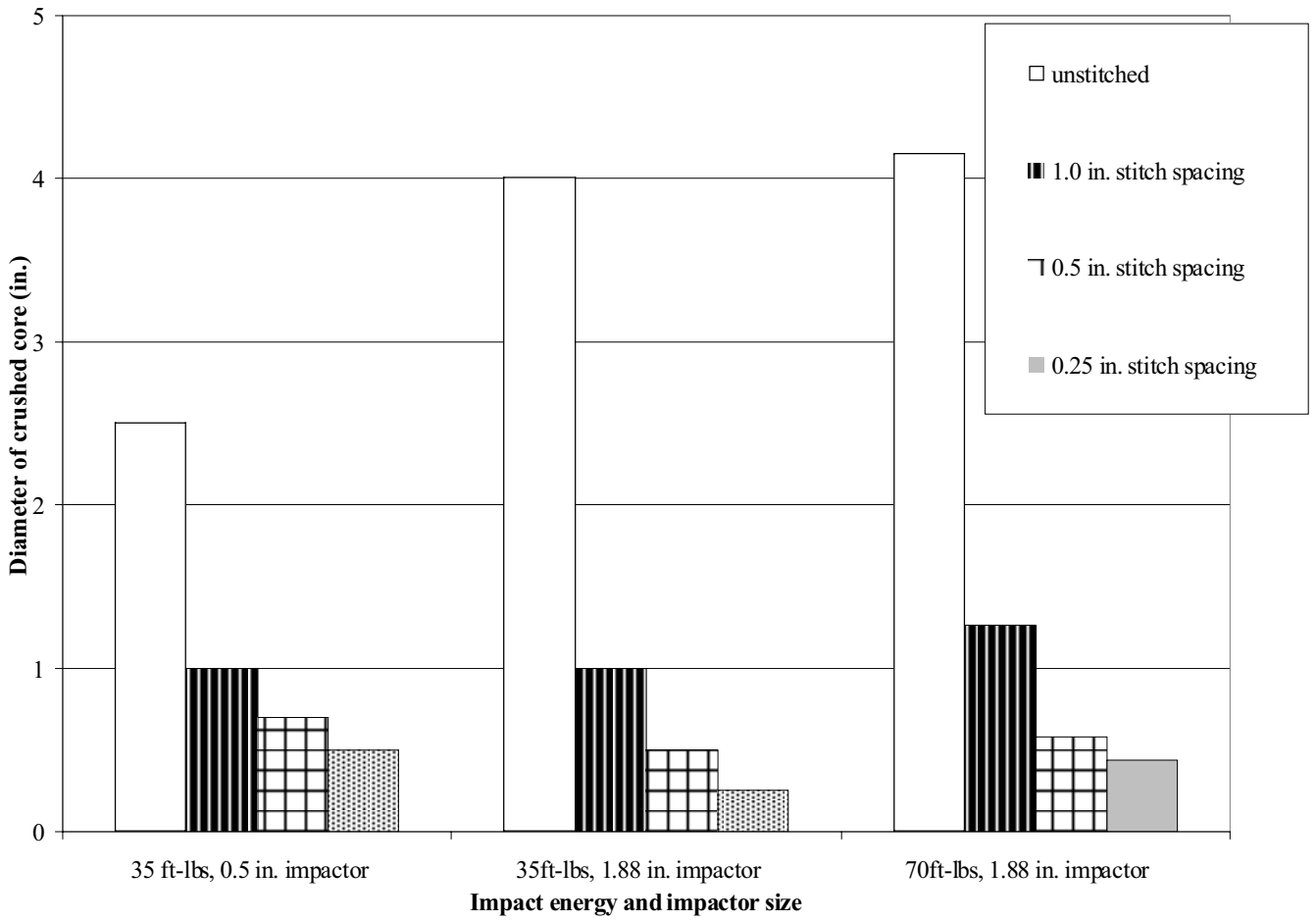

Figure 6.16 Comparison of crushed core diameters for 1.0 in. core panels

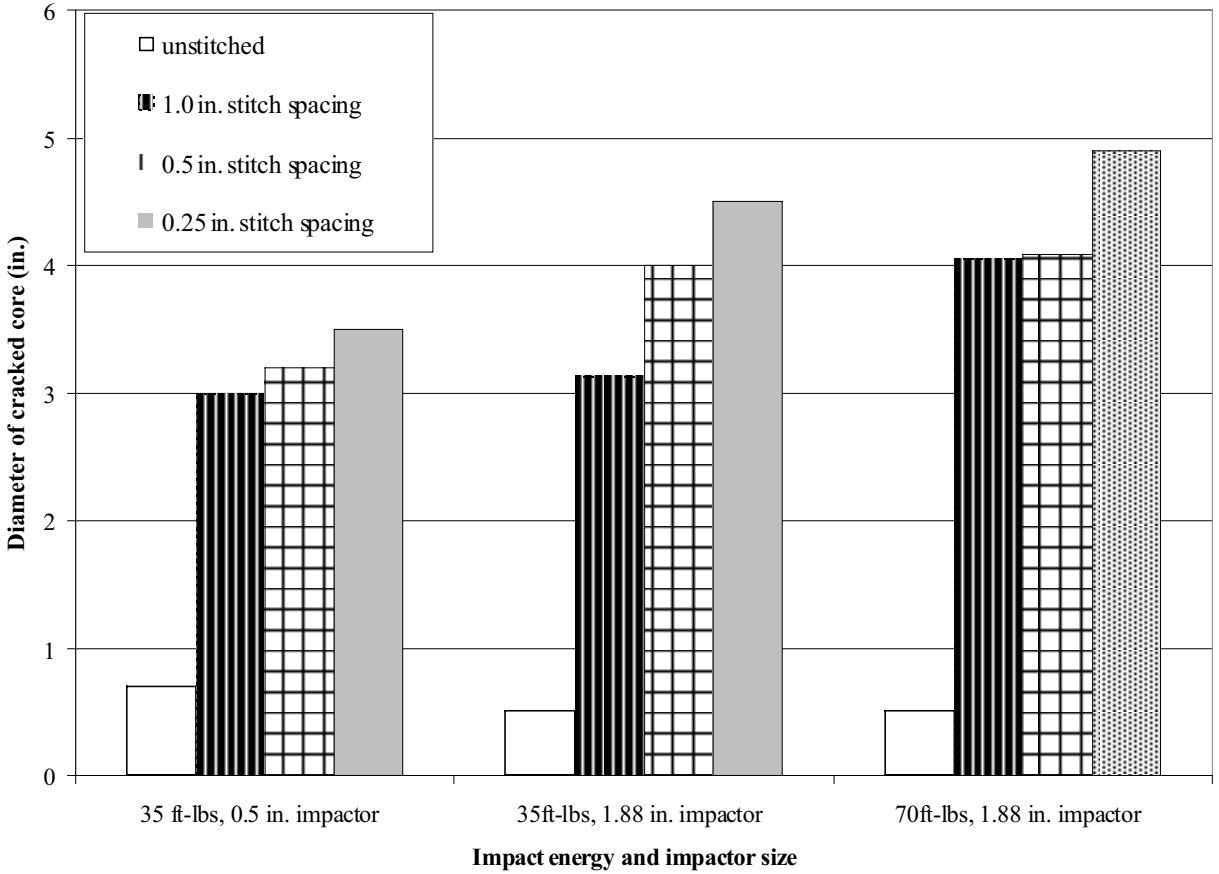

Figure 6.17 Comparison of diameters of crack extent in 0.5 in. core panels.

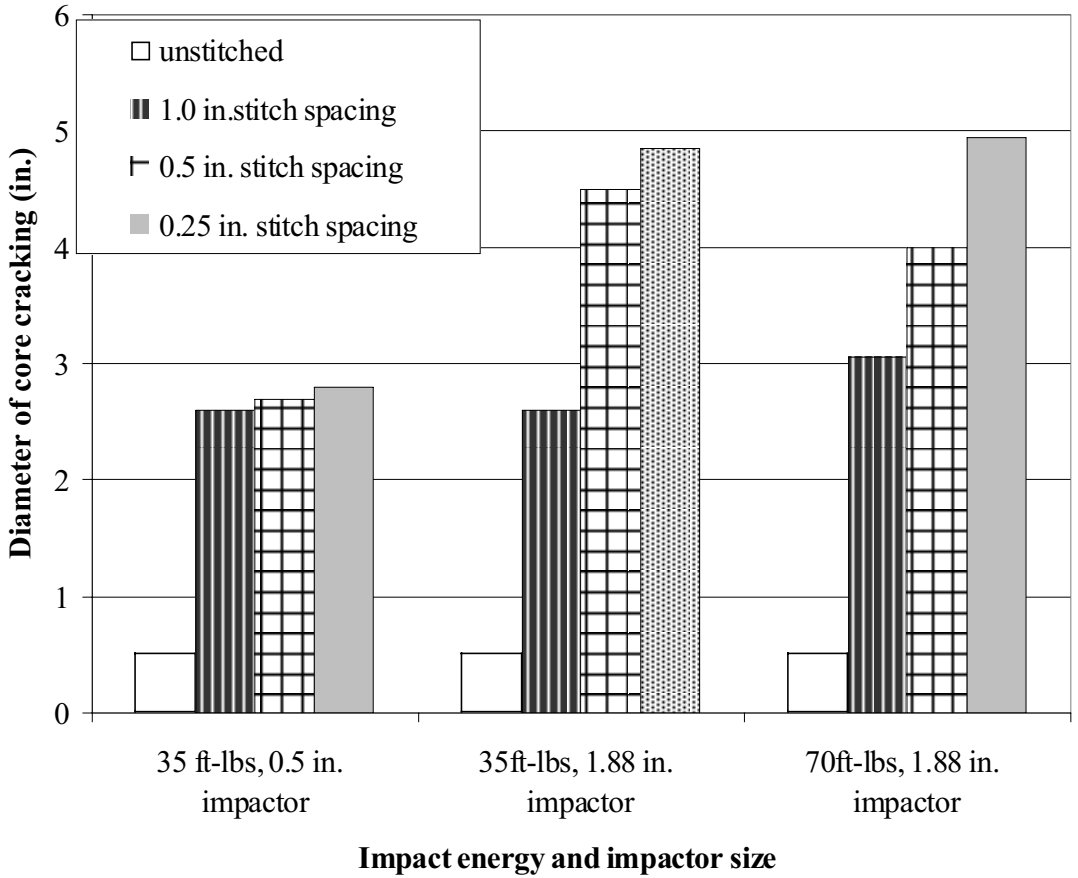

Figure 6.18 Comparison of diameters of crack extent in 1.0 in. core panels.

approximately constant in the unstitched specimens. Comparing the two core thicknesses, a slightly greater diameter of cracking generally occurred in the 0.5 in. core thickness than the 1.0 in. core thickness.

6.4 Compression after impact testing results

As previously explained, two identical specimens were impacted for each of the impact conditions investigated. One specimen was sectioned and photographed whereas the second was used for Compression After Impact (CAI) testing. The test method for CAI testing was similar to the edgewise compression tests, but with larger specimens and with side supports. The NASA CAI test fixture was used for testing the 5 in. wide by 10. in long specimens. Control specimens, not subjected to impact were also tested for comparison. To insure an accurate comparison of CAI strengths, a small hole (0.040 in. diameter) was drilled in the center of the undamaged specimens to match the specimens impacted with the 0.5 in. diameter impactor that were initially evaluated using X-ray inspection. Note that a hole was not drilled in the specimens impacted using the 1.88 in. diameter impactor.

Results of the CAI tests are presented in Table 6.3. The maximum load for each specimen is tabulated along with the percent reduction in maximum load as compared to the same specimen type that was not impacted. Figures 6.19 and 6.20 compare the CAI strengths to the nonimpacted compression strengths for the 0.5 in. and 1.0 in. core specimens, respectively. The nonimpacted specimens showed the same trends as seen

Table 6.3 Results of compression after impact testing.

Specimen type	Maximum load, no impact (lbs)	Maximum load after 35 ft-lb impact, 0.5 in. impactor		Maximum load after 35 ft-lb impact, 1.88 in. impactor		Maximum load after 70 ft-lb impact, 1.88 in. impactor	
		(lbs)	(fraction of no impact)	(lbs)	(fraction of no impact)	(lbs)	(fraction of no impact)
0.5 in.core, unstitched	23,616	21,910	0.928	15,295	0.648	12,860	0.545
0.5 in. core, 1.0 in. stitch spacing	28,437	26,514	0.932	22,376	0.787	22,837	0.803
0.5 in. core, 0.5 in. stitch spacing	32,336	27,674	0.856	26,616	0.823	27,876	0.862
0.5 in.core, 0.25 in. stitch spacing	38,547	34,004	0.882	31,469	0.816	30,789	0.799
1.0 in. core, unstitched	33,554	32,172	0.959	26,155	0.779	22,045	0.657
1.0 in. core, 1.0 in. stitch spacing	36,437	34,342	0.943	32,076	0.880	32,339	0.888
1.0 in. core, 0.5 in. stitch spacing	40,151	37,508	0.934	35,415	0.882	35,234	0.878
1.0 in. core, 0.25 in. stitch spacing	48,156	39,019	0.810	36,828	0.765	35,937	0.746

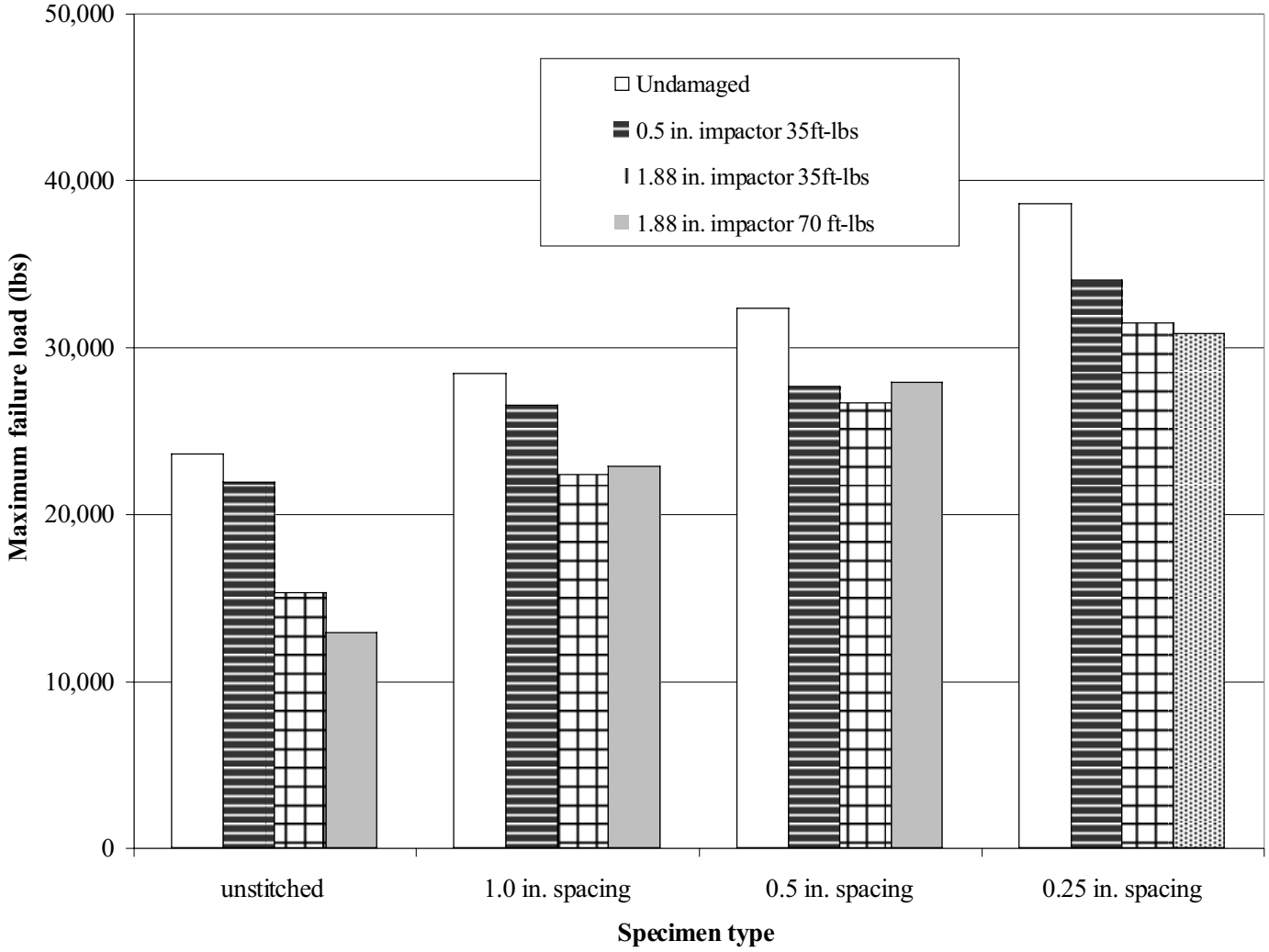

Figure 6.19 Comparison of CAI test results for each stitch configuration, 0.5 in. core thickness.

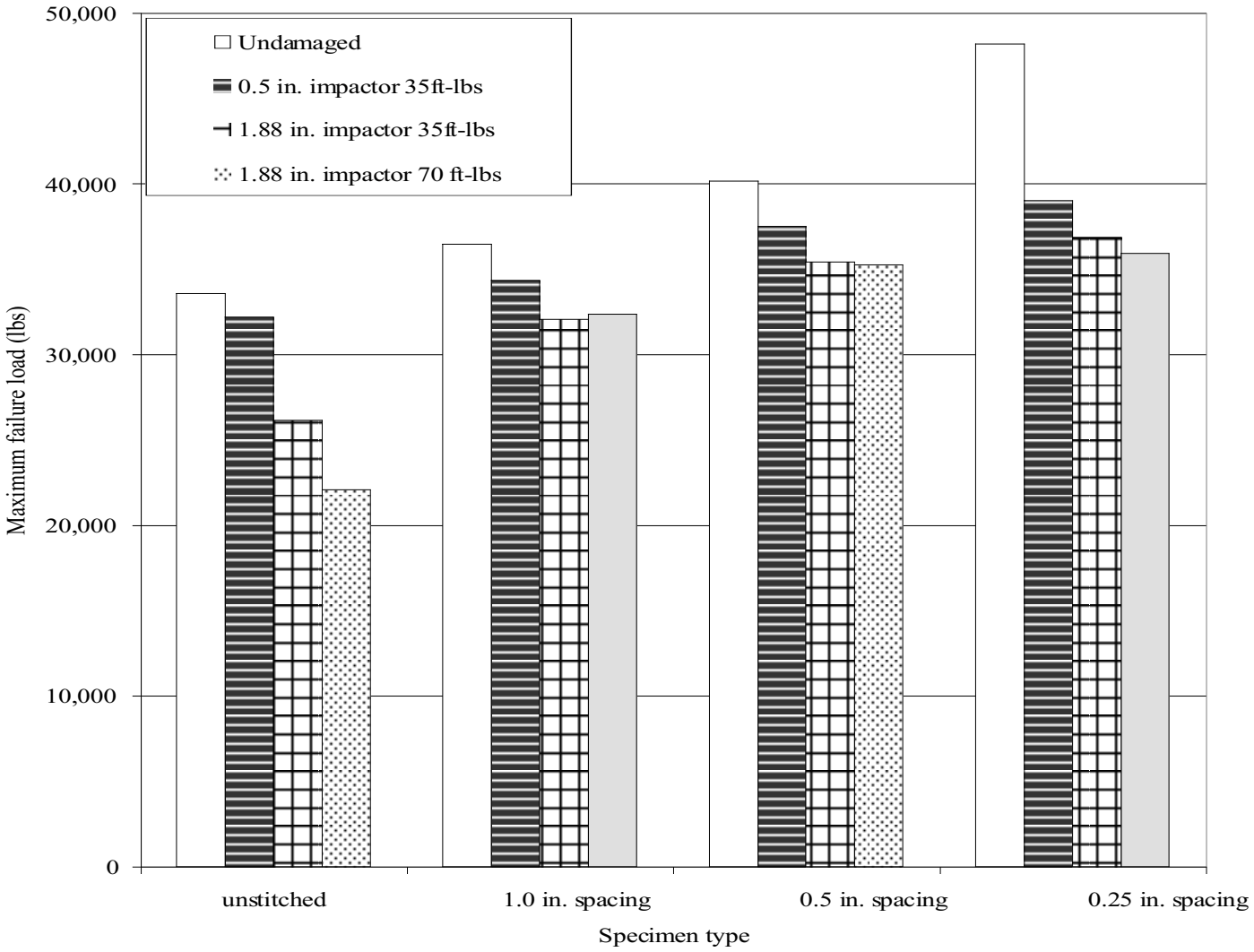

Figure 6.20 Comparison of CAI test results for each stitch configuration, 1.0 in. core thickness.

in the edgewise compression testing; as the stitch spacing decreased, the maximum load increased. All impacted specimens experienced reductions in maximum load as compared to the corresponding nonimpacted case. Reductions in maximum load ranged from a low of 4.1% in the 1.0 in unstitched specimen (35 ft-lb impact, 0.5 in. diameter impactor) to a maximum reduction of 45.5% in the 0.5 in. core unstitched specimen (70 ft-lb impact, 1.88 in. diameter impactor).

For all stitching configurations considered, the larger 1.88 in. diameter impactor produced a greater reduction in CAI strength than the 0.5 in. diameter impactor at the 35 ft-lb energy level. Interestingly, there was no significant difference between the 35 ft-lb impact and the 70 ft-lb impact using the larger 1.88 in. diameter impactor for any of the stitched specimens, although the higher impact energy produced greater reductions in the CAI strength of the unstitched specimens.

Figure 6.21 presents a comparison of the maximum loads for the different specimen types (different core thickness and stitch spacing) grouped according to the impact condition (impact energy and impactor diameter). First, this figure shows that the maximum load increases as the stitch spacing decreases for both core thicknesses. Second, this figure shows that the stitched specimens with the 1.0 in. core produced greater maximum loads than the stitched specimens with the 0.5 in. core. However, both of these observations are also true for the nonimpacted specimens.

To obtain a better understanding of the reductions in strength due to impact, the maximum failure loads for the impacted specimens are nondimensionalized by the corresponding failure load from the nonimpacted specimen with the same core

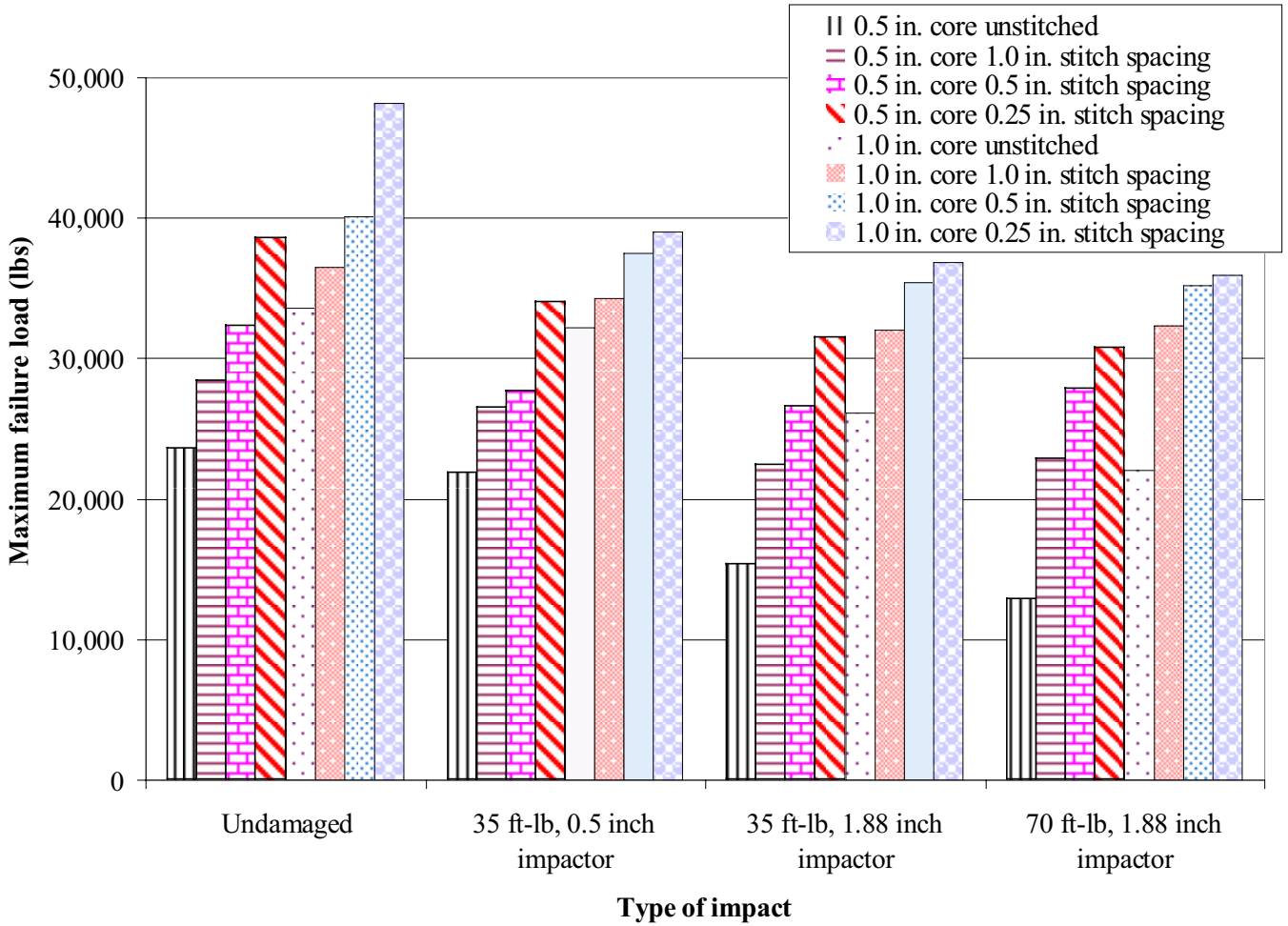

Figure 6.21 Comparison of the maximum compressive failure loads.

thickness and stitch spacing. These nondimensionalized CAI strengths are presented in Figure 6.22.

From the nondimensionalized values, it can be seen that a 35 ft-lb impact with 0.5 in. impactor produced the same or lower relative drop in CAI strength in the unstitched specimens then any of the stitched specimens. It would appear that from this type of impact, stitching does not increase that damage tolerance of the specimens (although the relative strengths are higher for the stitched specimens). A different trend was found with the impacts produced with the larger 1.88 in. impactor. With the 35 ft-lb impact and the larger impactor, nondimensionalized CAI values are much lower for the unstitched panels than for the stitched panels, with the exception of the 1.0 in. core and the lowest stitch spacing. This specimen had about the same CAI fraction as the unstitched specimen. It is noted that this specimen with the greatest amount of core cracking as shown previously in section 6.3. The large amount of core cracking is likely the cause of the low value of nondimensionalized CAI strength.

The stitched specimens impacted with 70 ft-lbs and the larger 1.88 in. impactor all showed greater CAI strength fractions compared to the unstitched specimens of equal thickness. When comparing the 70 ft-lb impact with the larger impactor to the 35 ft-lbs impact with the same impactor, it was revealed that there is no noticeable drop in the fraction of strength for all of the stitched specimens when going to the higher energy impact. Conversely, it was found there is a large drop in the fraction of strength of the unstitched specimens. Results from the CAI specimens impacted show that stitching does increase the damage tolerance of the sandwich panels although it is dependant on the size and type of impactor.

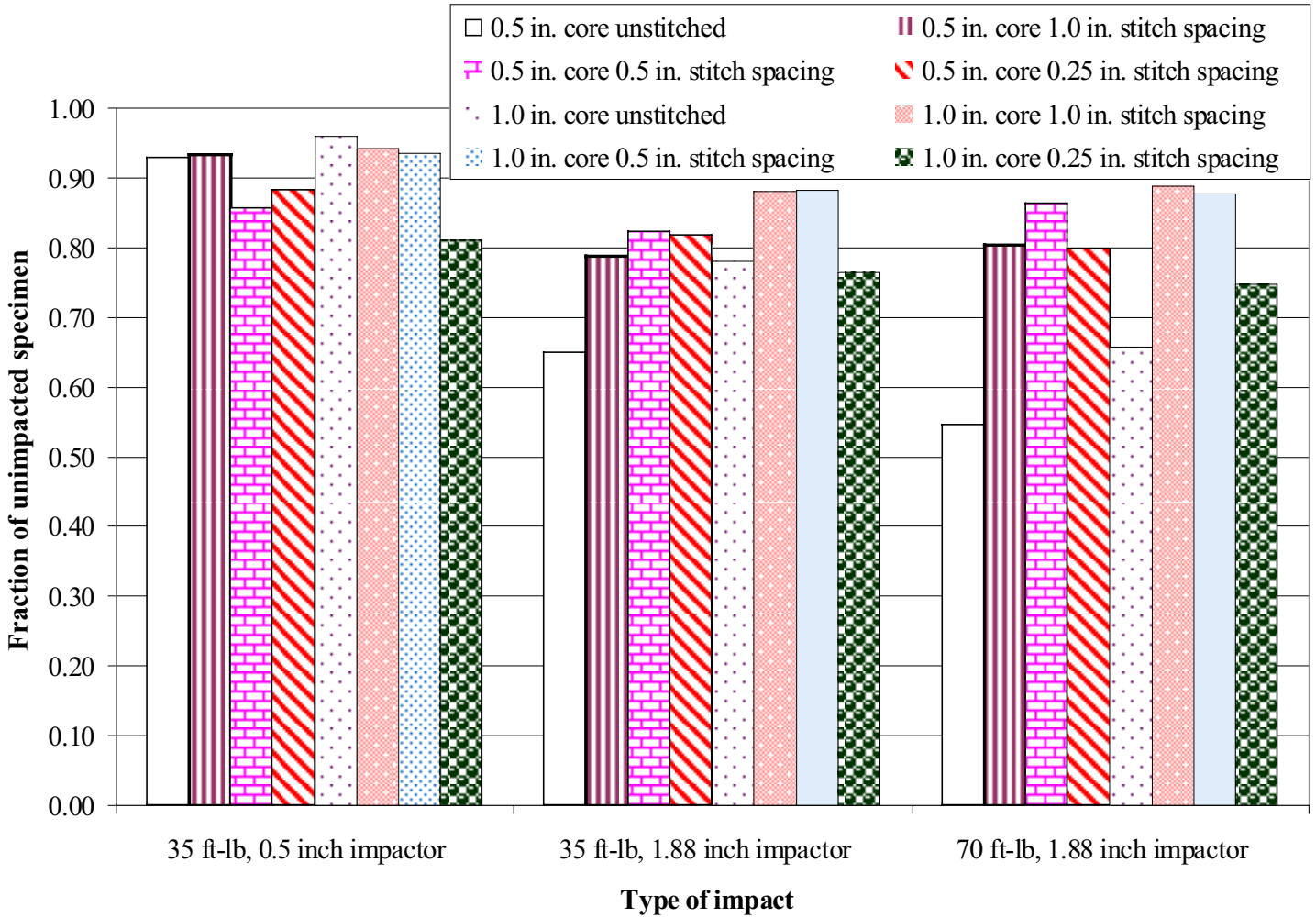

Figure 6.22 Comparison of nondimensionalized CAI strength.

Failure modes of both the impacted and nonimpacted specimens appeared to be the same. Specimen failure during compression loading was associated with a visible inward buckling of one of the facesheets. Inspections of failed specimens support this observation. Following testing, one facesheet was found to remain planar whereas the other facesheet had a shallow inward depression in the center of the specimen relative to the top and bottom edges of the specimen. This inward buckling is shown schematically in Figure 6.23.

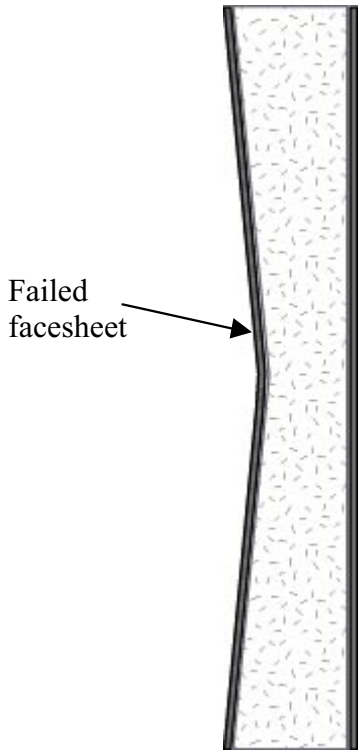

Figure 6.23 Diagram of failed CAI specimen due to inward buckling.

For the face sheet to buckle inward, the core of the sandwich must also fail. The stitches with the resin columns surrounding them appear to have provided additional support to the facesheets to aid in preventing this failure mode. This would explain why stitching significantly increases the failure loads in edgewise compression testing and in the NASA CAI tests without impact damage. This also aids in the understanding of why there is a difference between the different impact types. A delamination between the facesheet and core does not significantly reduce the specimens resistance to an inward buckling failure. Crushed foam, however, does reduce the specimens resistance to inward buckling because the crushed foam cells offer very little rigidity and support to the face sheet. Cracking of the foam core also reduces the support to the facesheet and to the stitch columns although the reduction is not as great a with core crushing. Thus, impacted specimens with greater amounts of core crushing would be expected to have largest drops in CAI strength.

In summary, stitching of sandwich specimens suppressed crushing of the foam core due to impact, but led to more cracking of the foam core. Stitching also increased the compression after impact strength of the sandwich specimens by restraining inward buckling of the facesheets. Additionally in was shown that the type of impact influences the damage tolerance of the sandwich panels. Stitched specimens impacted with the 0.5 in. diameter impactor did not show an increase in damage tolerance although specimens impacted with the 1.88 in. diameter impactor did.

CHAPTER 7

CONCLUSIONS AND RECOMENDATIONS

This study has explored the feasibility and benefits provided by the addition of through-the-thickness stitching to sandwich structures. The four major areas of focus have been in panel fabrication, mechanical testing, damage resistance and damage tolerance evaluation, and tensile testing of Kevlar stitching yarn.

A method of fabrication was developed to produce composite sandwich panels with carbon fiber face sheets and foam cores with through-the-thickness Kevlar stitching. These sandwich panels were fabricated using a low-cost, out-of-autoclave processing method. The sandwich panels were stitched in a dry preform state, vacuum bagged, and infiltrated using Vacuum Assisted Resin Transfer Molding (VARTM) processing. Unstitched sandwich panels were produced using the same materials and manufacturing methodology for comparison testing. Panels were first produced manually at the University of Utah for preliminary use and to prove feasibility. Later panels were produced at NASA Langley Research Center using the information gained during the production of the Utah panels.

Kevlar yarns were infiltrated with epoxy and tested in tension to failure. The maximum load to failure and the yarn stiffness were determined for use in predicting and understanding the results from mechanical testing of stitched sandwich specimens.

Mechanical testing consisted of flexural testing, flatwise tensile testing, core shear testing, and edgewise compression testing. Results from the mechanical testing of stitched sandwich specimens were compared to those from unstitched specimens to evaluate the effect of stitching.

Drop-weight impact testing followed by specimen sectioning was performed to characterize the damage resistance of stitched sandwich panels. Compression after impact (CAI) testing was performed to evaluate the damage tolerance of the sandwich panels.

7.1 Conclusions

Conclusions will be presented according to the four main areas of focus in this investigation: fabrication, Kevlar yarn testing, mechanical testing, and damage resistance/damage tolerance evaluation.

7.1.1. Fabrication

1. Stitched sandwich panels may be fabricated successfully using a low-cost, out-of-autoclave VARTM processing method.
2. The orientation of the stitched sandwich panel with the bobbin side down and against the tooling prevents air bubbles from becoming trapped at the stitch locations during resin infiltration.

7.1.2. Kevlar Yarn testing

1. Infiltration of the Kevlar stitching yarns with epoxy increases the yarn stiffness by an average of 26%.

2. The strength of the Kevlar yarns is increased by an average of 39% following infiltration with epoxy.

7.1.3. Mechanical testing

1. Stitching of sandwich panels significantly increases the maximum failure loads under flexure, core shear, flatwise tensile, and edgewise compression loading. Loads are increased by as much as 174% in flexure, 1659% in flatwise tension, 473% in core shear and 158% in edgewise compression. The greater the stitch density, the greater the increases in failure loads.
2. Stitching of the sandwich panel increases the energy absorption to failure tremendously as much as 40 times in flexure, and 100 times in core shear.
3. Angled stitching through-the-thickness provides significant enhancements in shear strength over normal stitch orientation. This is evidenced by increases as much as 48% over normal stitch orientation in core shear testing.

7.1.4. Damage resistance/damage tolerance

1. Stitching of sandwich panels helps prevent crushing of the core and suppresses facesheet delamination during impact. However, stitching produces a larger region of core cracking than unstitched panels following impacting.
2. Stitching of sandwich panels provides significant increases in compression after impact strength as much as 63%.

7.2 Recommendations

This investigation focused on an initial comparison between stitched and unstitched sandwich panels. Several areas have been identified as topics for further investigation:

1. Modify the VARTM-based infiltration process for use with elevated-temperature curing epoxies.
2. Explore the feasibility of producing stitched sandwich panels with curvature by thermoforming the stitched assembly prior to infiltration.
3. Investigate the strength of the resin column/foam core interface.
4. Investigate the effect of different core materials, facesheet materials and orientations, stitching materials, and resins.
5. Further investigate the use of angled stitching of sandwich structures. Establish design guidelines for determining the optimal stitch angle for prescribed loading conditions.
6. Explore the localized use of stitching around loading points, closeouts, and various stress concentrations found in sandwich structures.
7. Investigate the damage tolerance associated with edgewise impact in the same manner that flatwise impact was investigated in this study.
8. Evaluate the ability of stitched sandwich structures to resist delamination growth by fabricating and testing stitched sandwich panels with an intentional delamination between the core and one facesheet.
9. Develop finite element based analysis capabilities for modeling stitching in sandwich structures.

APPENDIX

SECTIONED IMPACTED SPECIMENS

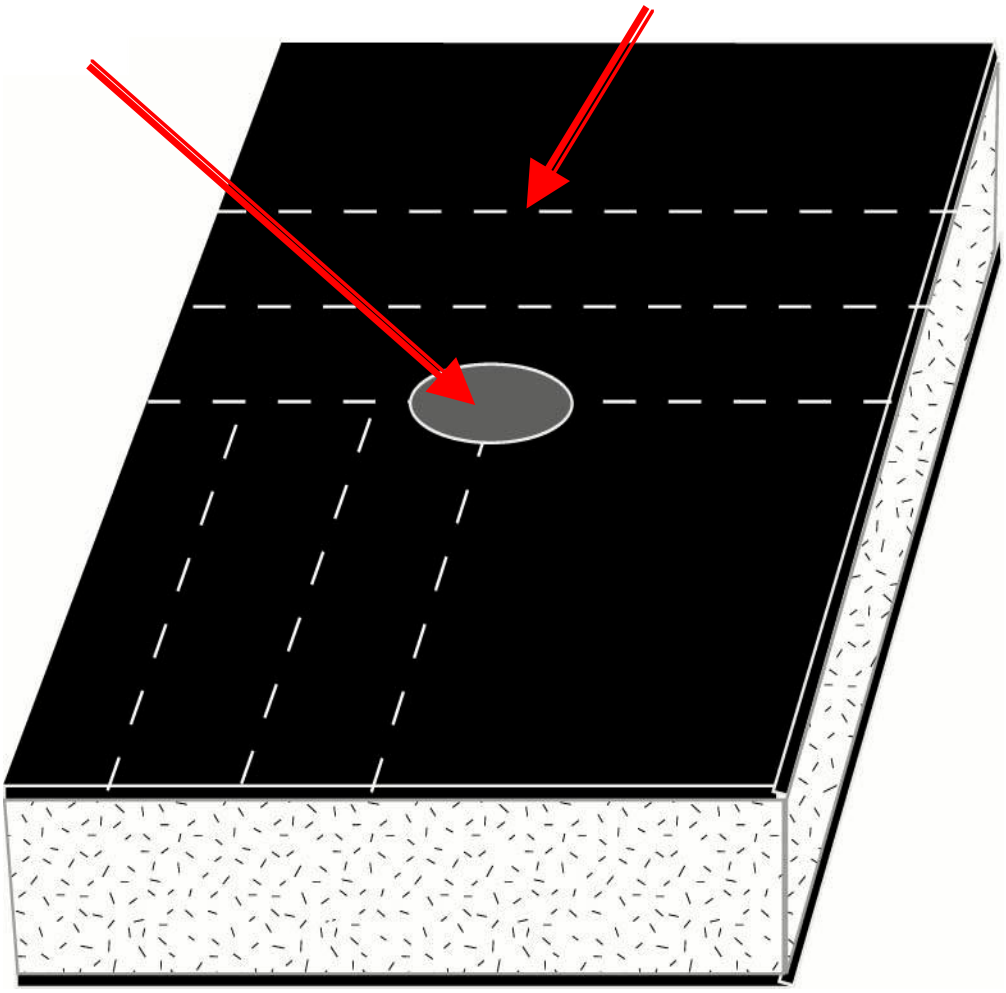

Figure A.1 Diagram of 10 in. long x 5.0 in. wide sandwich panel with sectioning lines.

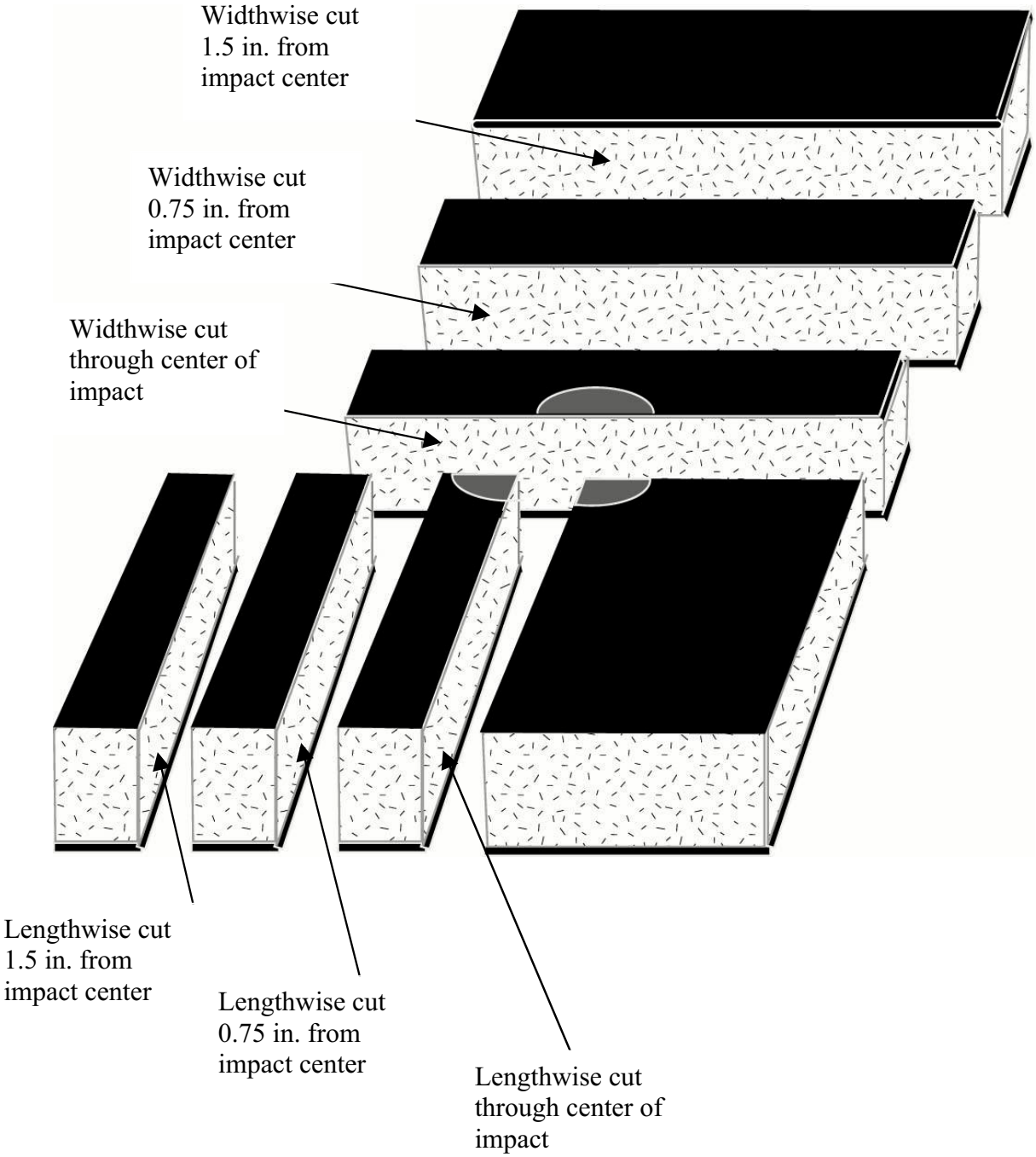

Figure A.2 Diagram of sectioned surfaces

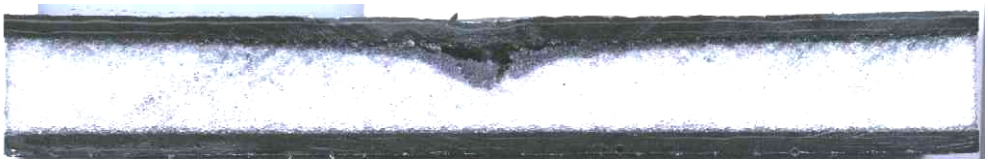

a. Widthwise cut through center of impact.

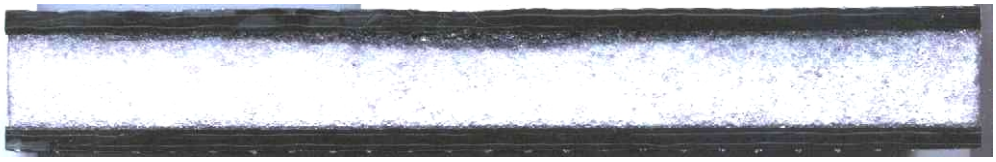

b. Widthwise cut 0.75 in. from center of impact.

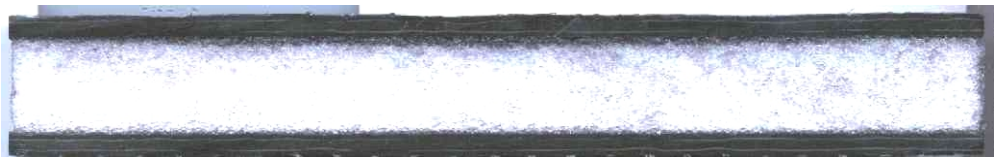

c. Widthwise cut 1.5 in. from center of impact.

d. Lengthwise cut through from center of impact.

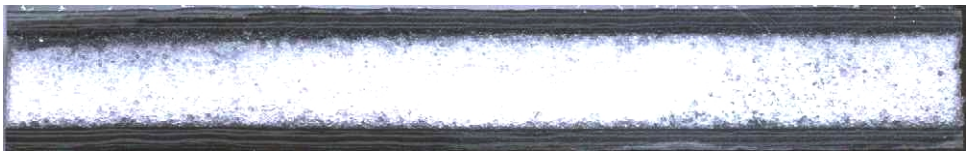

e. Lengthwise cut 0.75 in. from center of impact.

f. Lengthwise cut 1.5 in. from center of impact.

Figure A.3 0.5 in. core, unstitched panel sections after 35 ft-lb impact using 0.5 in. impactor.

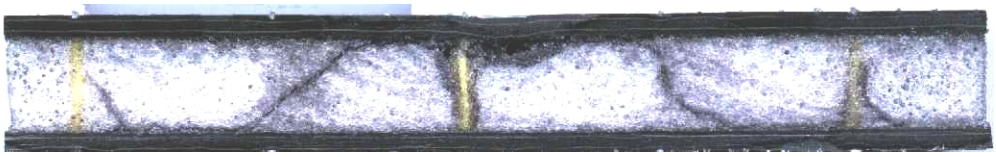

a. Widthwise cut through center of impact.

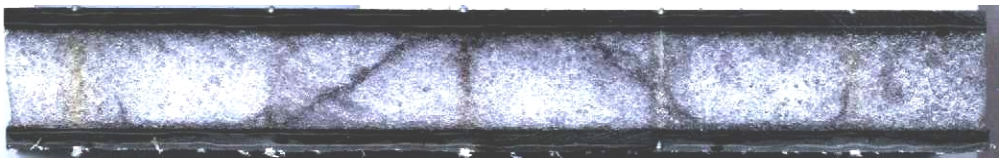

b. Widthwise cut 0.75 in. from center of impact.

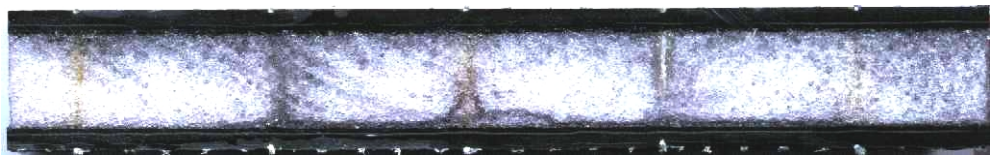

c. Widthwise cut 1.5 in. from center of impact.

d. Lengthwise cut through from center of impact.

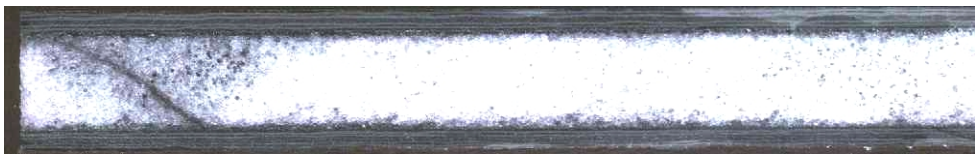

e. Lengthwise cut 0.75 in. from center of impact.

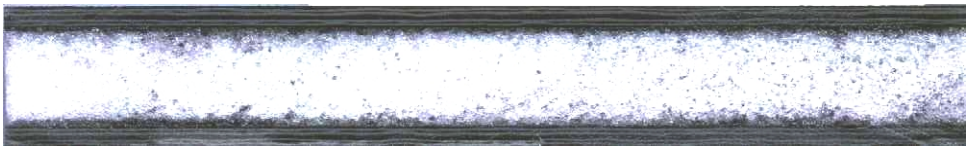

f. Lengthwise cut 1.5 in. from center of impact.

Figure A.4 0.5 in. core, 1.0 in. stitch spacing panel sections after 35 ft-lb impact with 0.5 in. impactor.

a. Widthwise cut through center of impact.

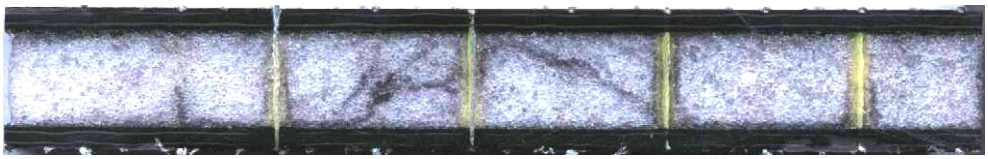

b. Widthwise cut 0.75 in. from center of impact.

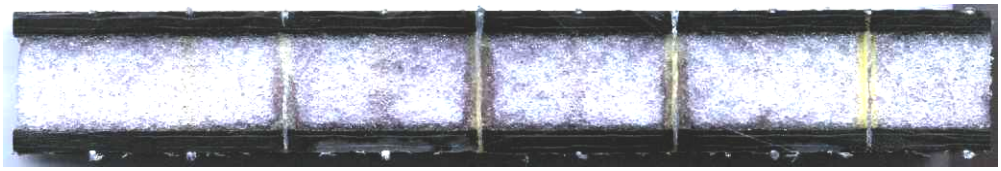

c. Widthwise cut 1.5 in. from center of impact.

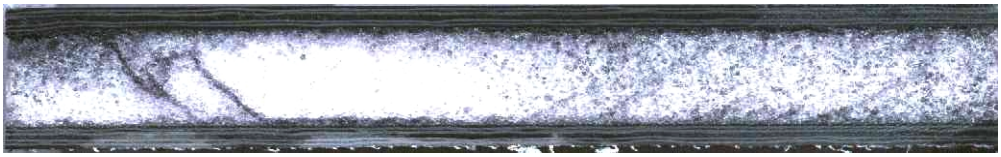

d. Lengthwise cut through from center of impact.

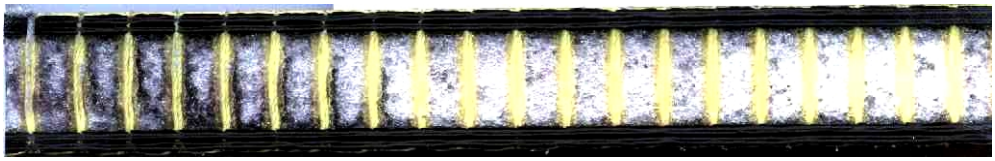

e. Lengthwise cut 0.75 in. from center of impact.

f. Lengthwise cut 1.5 in. from center of impact.

Figure A.5 0.5 in. core 0.5 in. stitch spacing panel sections after 35 ft-lb impact and 0.5 in. impactor.

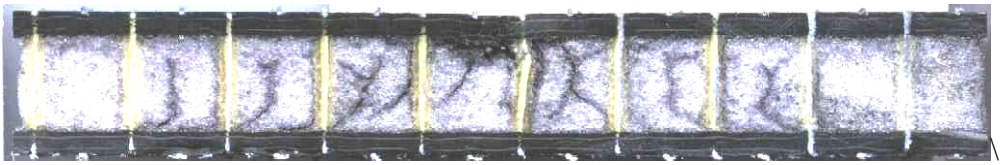

a. Widthwise cut through center of impact.

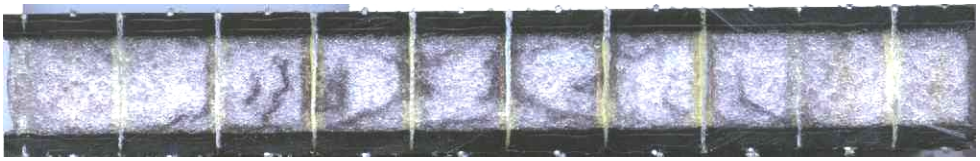

b. Widthwise cut 0.75 in. from center of impact.

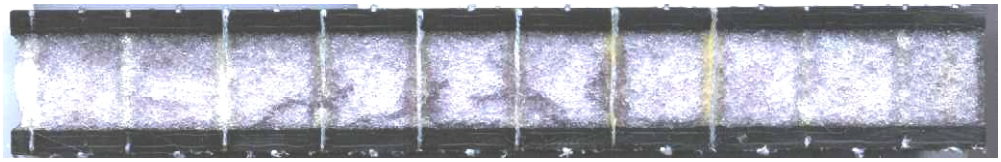

c. Widthwise cut 1.5 in. from center of impact.

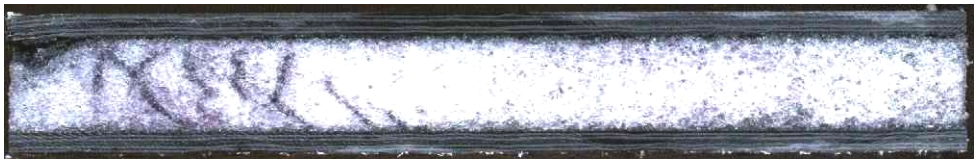

d. Lengthwise cut through from center of impact.

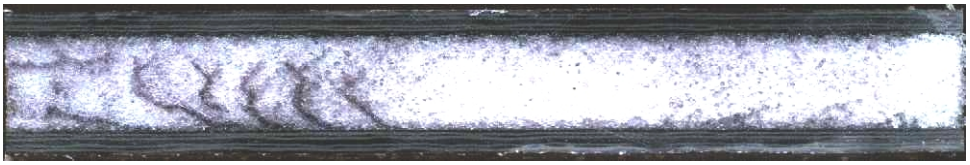

e. Lengthwise cut 0.75 in. from center of impact.

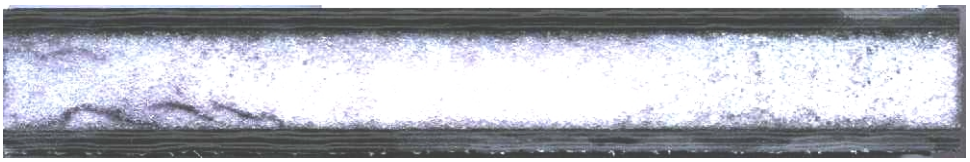

f. Lengthwise cut 1.5 in. from center of impact.

Figure A.6 0.5 in. core 0.25 in. stitch spacing panel sections after 35 ft-lb impact with 0.5 in. impactor.

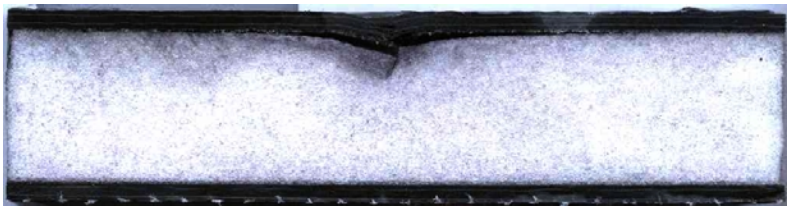

a. Widthwise cut through center of impact.

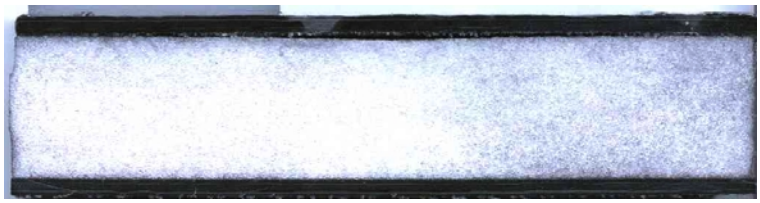

b. Widthwise cut 0.75 in. from center of impact.

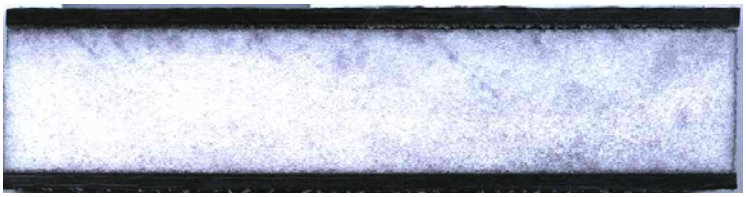

c. Widthwise cut 1.5 in. from center of impact.

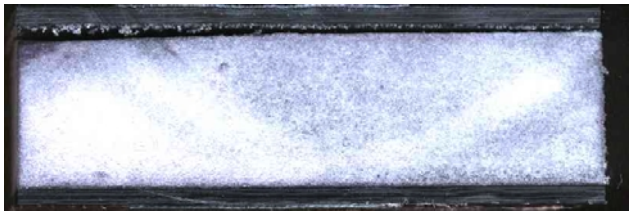

d. Lengthwise cut through from center of impact.

e. Lengthwise cut 0.75 in. from center of impact.

f. Lengthwise cut 1.5 in. from center of impact.

Figure A.7 1.0 in. core, unstitched panel sections after 35 ft-lb impact with 0.5 in. impactor.

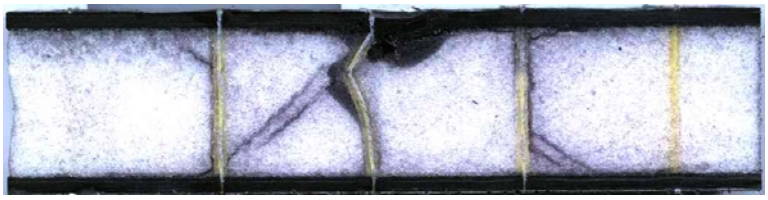

a. Widthwise cut through center of impact.

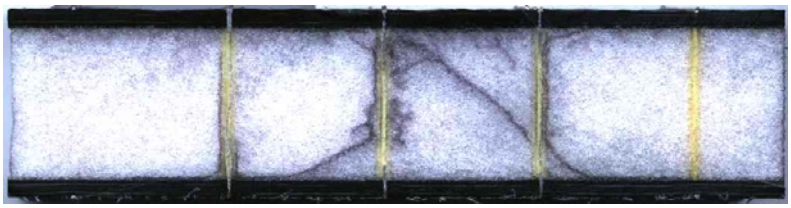

b. Widthwise cut 0.75 in. from center of impact.

c. Widthwise cut 1.5 in. from center of impact.

d: Lengthwise cut through from center of impact on upper left corner

e. Lengthwise cut 0.75 in. from center of impact.

f. Lengthwise cut 1.5 in. from center of impact.

Figure A.8 1.0 in. core, 1.0 in. stitch spacing panel sections after 35 ft-lb impact with 0.5 in. impactor.

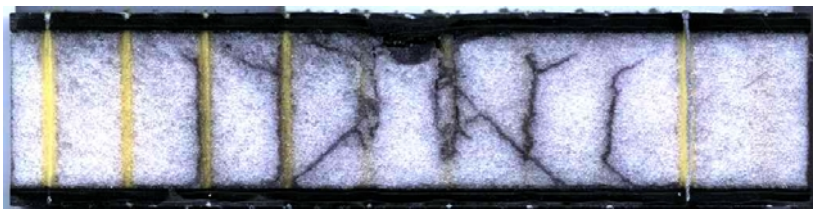

a. Widthwise cut through center of impact.

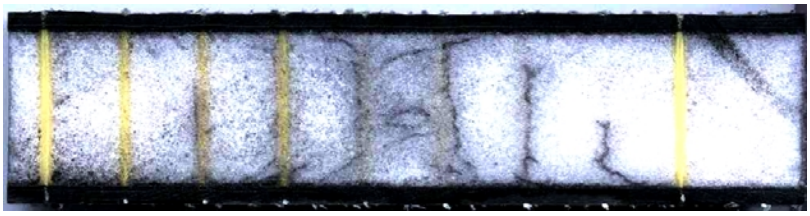

b. Widthwise cut 0.75 in. from center of impact.

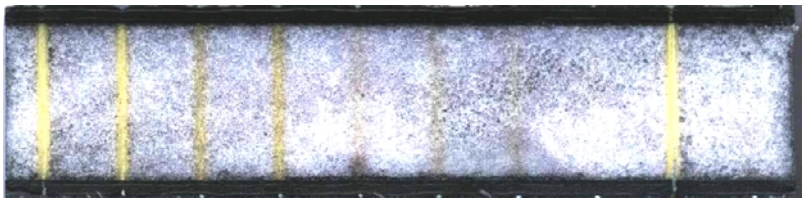

c. Widthwise cut 1.5 in. from center of impact.

d. Lengthwise cut through from center of impact.

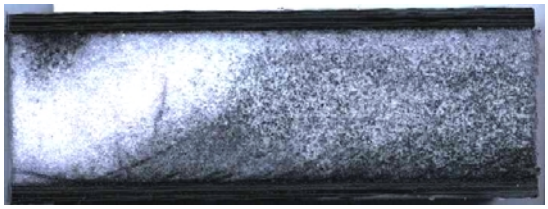

e. Lengthwise cut 0.75 in. from center of impact.

f. Lengthwise cut 1.5 in. from center of impact.

Figure A.9 1.0 in. thick core, 0.5 in. stitch spacing panel sections after 35 ft-lb impact with 0.5 in. impactor.

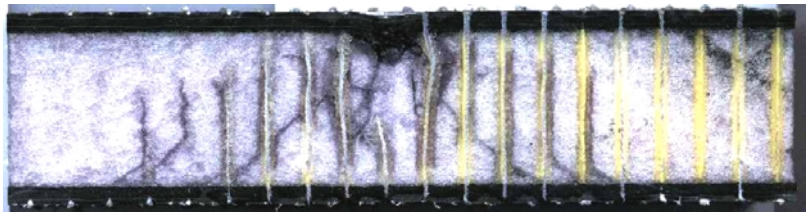

a. Widthwise cut through center of impact.

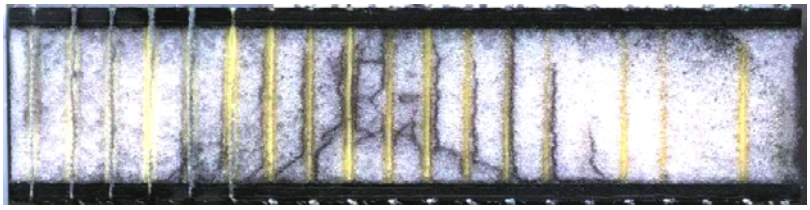

b. Widthwise cut 0.75 in. from center of impact.

c. Widthwise cut 1.5 in. from center of impact.

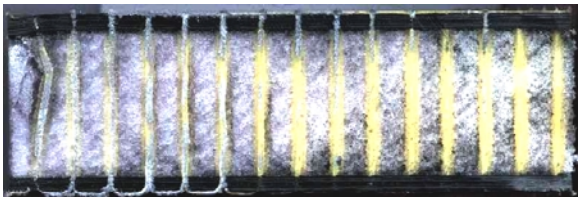

d. Lengthwise cut through from center of impact.

e. Lengthwise cut 0.75 in. from center of impact.

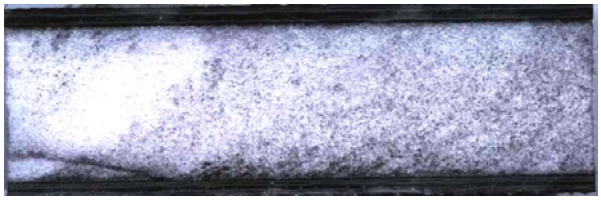

f. Lengthwise cut 1.5 in. from center of impact.

Figure A.10 1.0 in. thick core, _ in. stitch spacing panel sections after 35 ft-lb impact with 0.5 in. impactor.

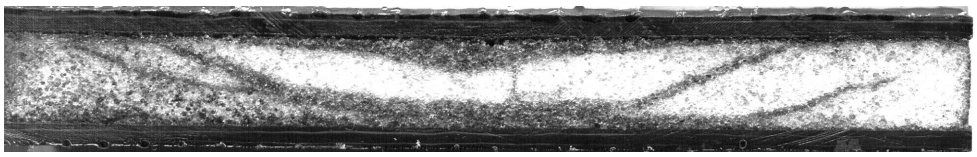

a. Widthwise cut through center of impact.

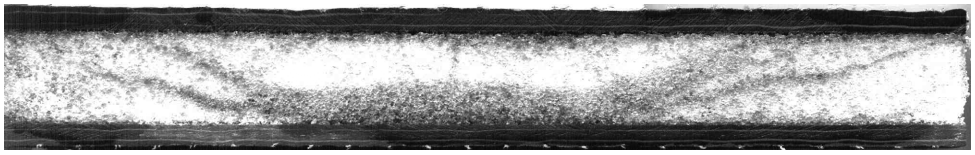

b. Widthwise cut 0.75 in. from center of impact.

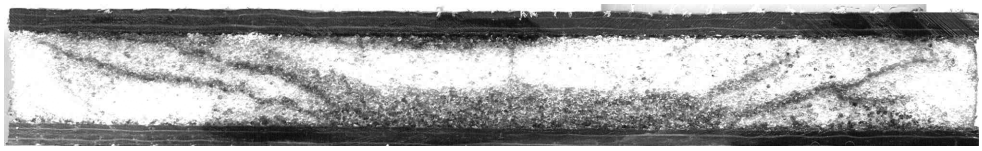

c. Widthwise cut 1.5 in. from center of impact.

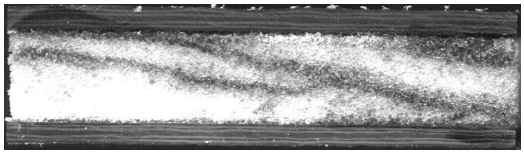

d. Lengthwise cut through from center of impact.

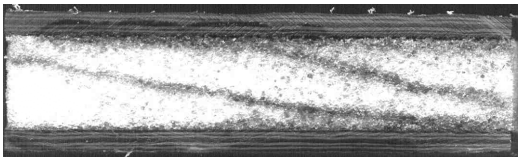

e. Lengthwise cut 0.75 in. from center of impact.

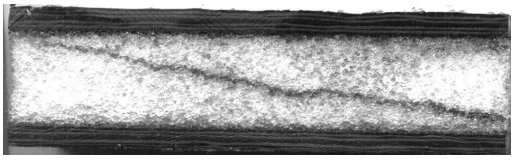

f. Lengthwise cut 1.5 in. from center of impact.

Figure A.11 0.5 in. core, unstitched panel sections after 35 ft-lb impact with 1.88 in. impactor.

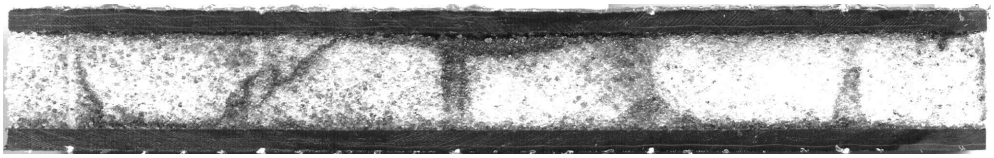

a. Widthwise cut through center of impact.

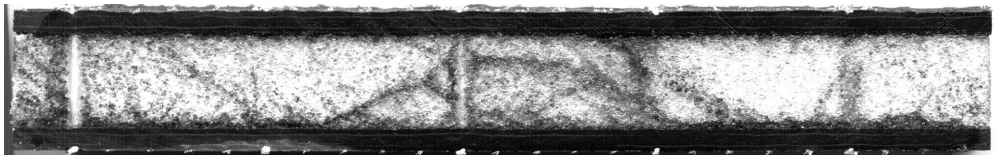

b. Widthwise cut 0.75 in. from center of impact.

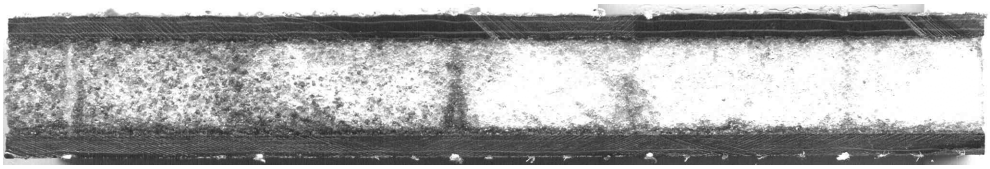

c. Widthwise cut 1.5 in. from center of impact.

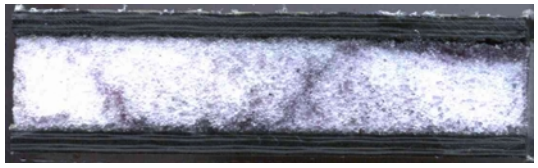

d. Lengthwise cut through from center of impact.

e: Widthwise cut _ in. from center of impact

f. Lengthwise cut 1.5 in. from center of impact.

Figure A.12 0.5 in. core,1 in. stitch spacing panel sections after 35 ft-lb impact with 1.88 in. impactor.

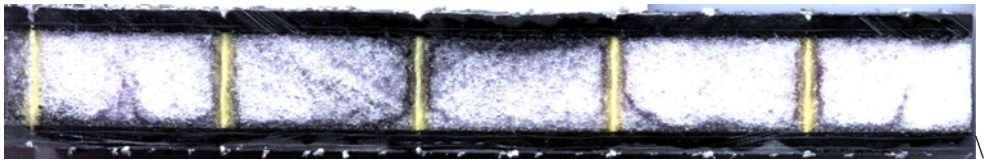

a. Widthwise cut through center of impact.

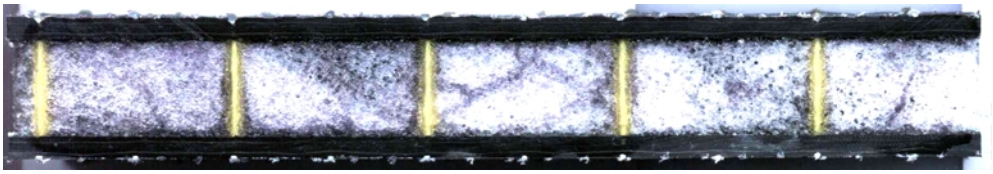

b. Widthwise cut 0.75 in. from center of impact.

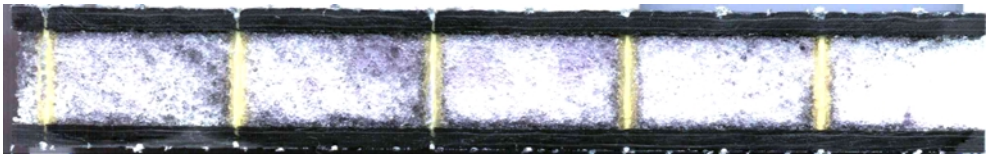

c. Widthwise cut 1.5 in. from center of impact.

d. Lengthwise cut through from center of impact.

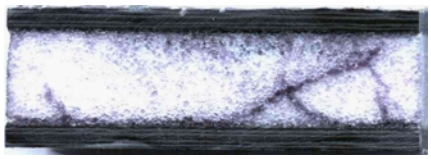

e. Lengthwise cut 0.75 in. from center of impact.

f. Lengthwise cut 1.5 in. from center of impact.

Figure A.13 0.5 in. core 1/2 in. stitch spacing panel sections after 35 ft-lb impact with 1.88 in. impactor.

a. Widthwise cut through center of impact.

b. Widthwise cut 0.75 in. from center of impact.

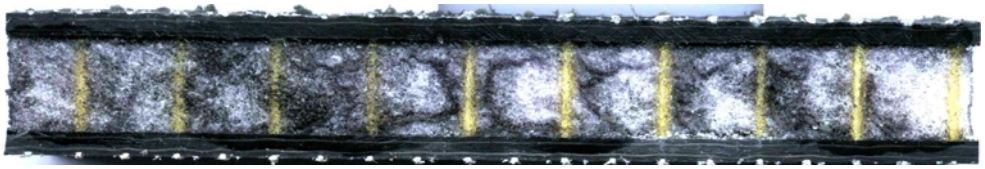

c. Widthwise cut 1.5 in. from center of impact.

d. Lengthwise cut through from center of impact.

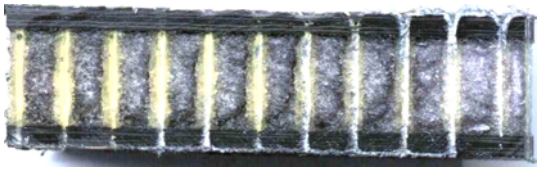

e. Lengthwise cut 0.75 in. from center of impact.

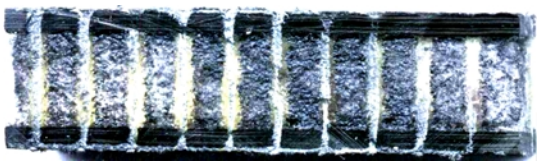

f. Lengthwise cut 1.5 in. from center of impact.

Figure A.14 0.5 in. core 0.25 in. stitch spacing panel sections after 35 ft-lb impact with 1.88 in. impactor.

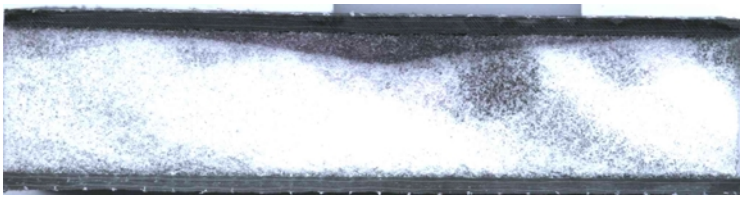

a. Widthwise cut through center of impact.

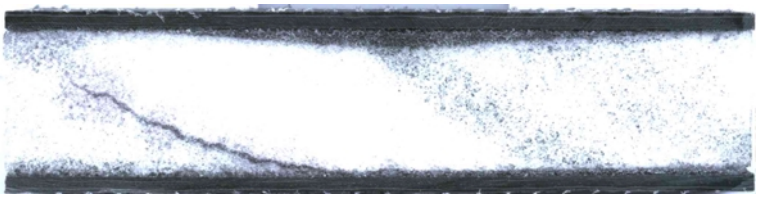

b. Widthwise cut 0.75 in. from center of impact.

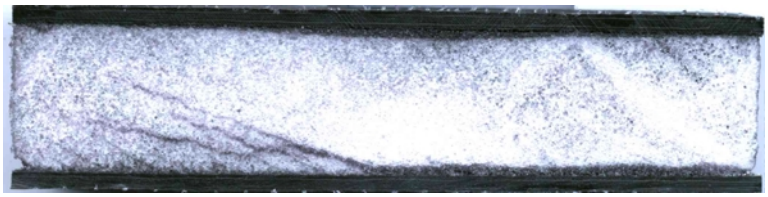

c. Widthwise cut 1.5 in. from center of impact.

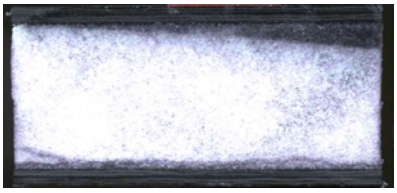

d. Lengthwise cut through from center of impact.

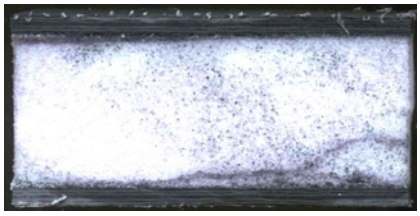

e. Lengthwise cut 0.75 in. from center of impact.

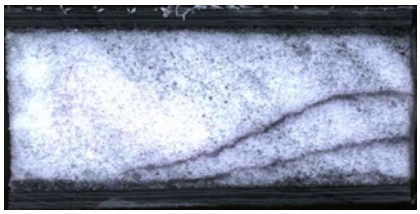

f. Lengthwise cut 1.5 in. from center of impact.

Figure A.15 1.0 in. core, unstitched panel sections after 35 ft-lb impact with 1.88 in. impactor.

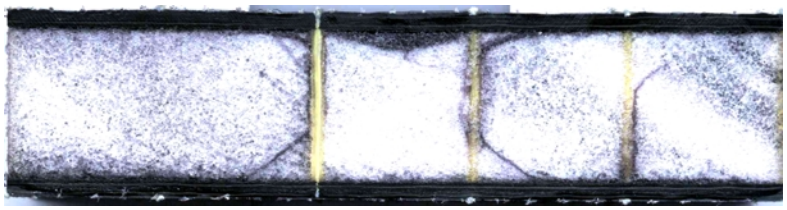

a. Widthwise cut through center of impact.

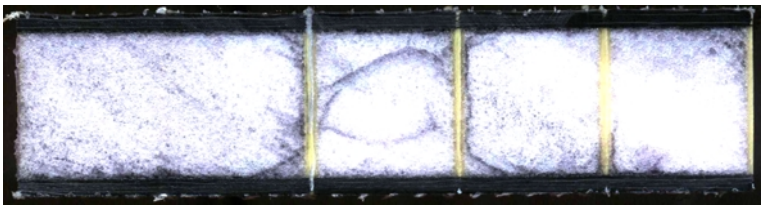

b. Widthwise cut 0.75 in. from center of impact.

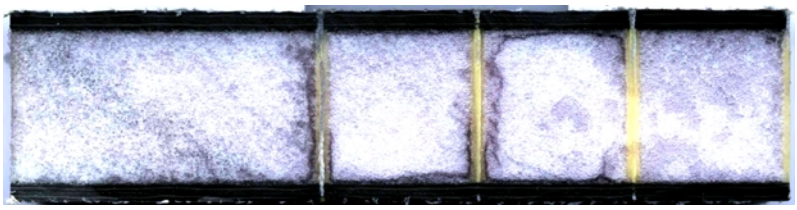

c. Widthwise cut 1.5 in. from center of impact.

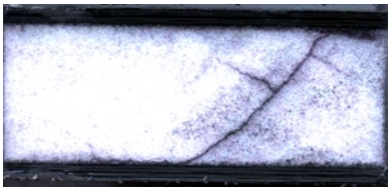

d. Lengthwise cut through from center of impact.

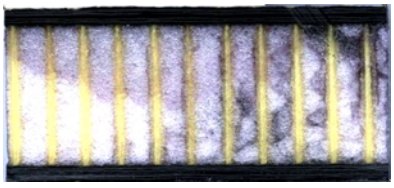

e. Lengthwise cut 0.75 in. from center of impact.

f. Lengthwise cut 1.5 in. from center of impact.

Figure A.16 1in. core, 1.0 in. stitch spacing panel sections after 35 ft-lb impact with 1.88 in. impactor.

a. Widthwise cut through center of impact.

b. Widthwise cut 0.75 in. from center of impact.

c. Widthwise cut 1.5 in. from center of impact.

d. Lengthwise cut through from center of impact.

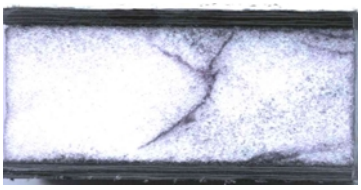

e. Lengthwise cut 0.75 in. from center of impact.

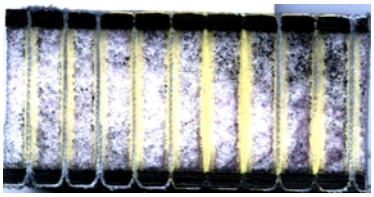

f. Lengthwise cut 1.5 in. from center of impact.

Figure A.17 1.0 in. core 0.5 in. stitch spacing panel sections after 35 ft-lb impact with 1.88 in. impactor.

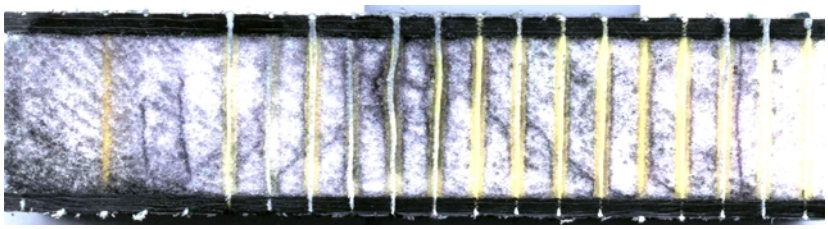

a. Widthwise cut through center of impact.

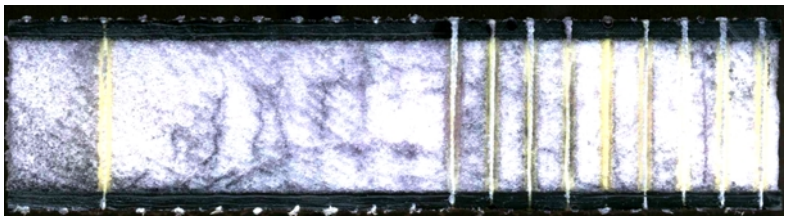

b. Widthwise cut 0.75 in. from center of impact.

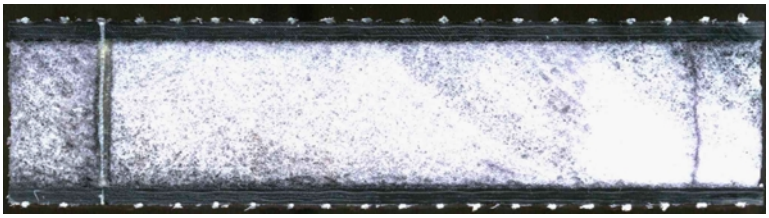

c. Widthwise cut 1.5 in. from center of impact.

d. Lengthwise cut through from center of impact.

e. Lengthwise cut 0.75 in. from center of impact.

f. Lengthwise cut 1.5 in. from center of impact.

Figure A.18 1.0 in. thick core, 0.25 in. stitch spacing panel sections after 35 ft-lb impact with 1.88 in. impactor.

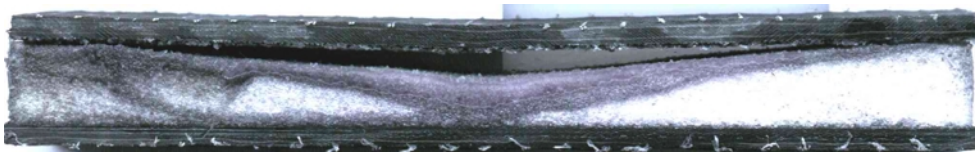

a. Widthwise cut through center of impact.

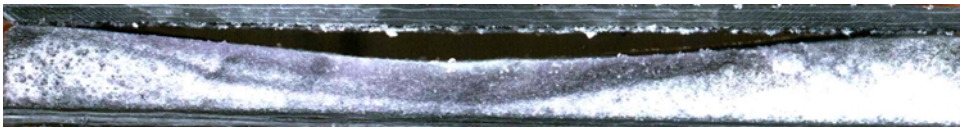

b. Widthwise cut 0.75 in. from center of impact.

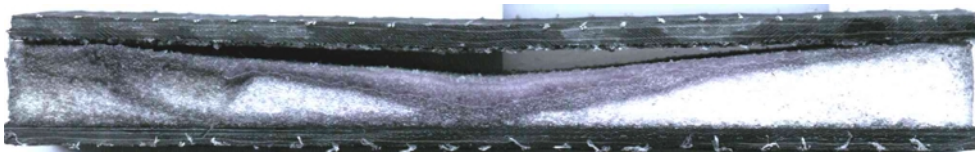

c. Widthwise cut 1.5 in. from center of impact.

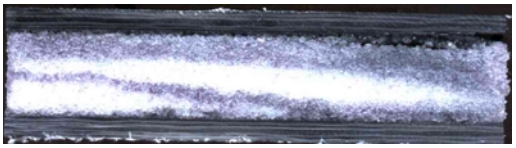

d. Lengthwise cut through from center of impact.

e. Lengthwise cut 0.75 in. from center of impact.

f. Lengthwise cut 1.5 in. from center of impact.

Figure A.19 0.5 in. core, unstitched panel sections after 70 ft-lb impact with 1.88 in. impactor.

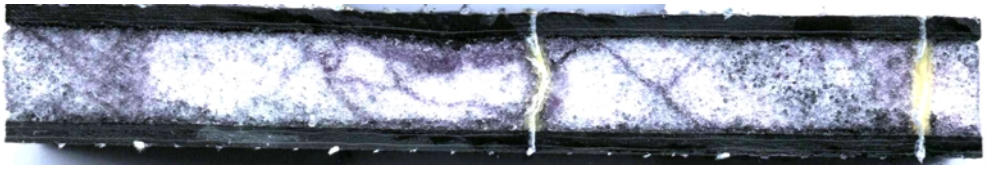

a. Widthwise cut through center of impact.

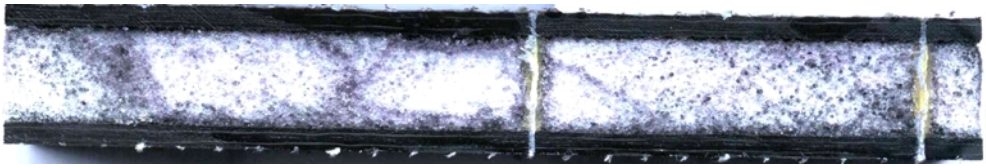

b. Widthwise cut 0.75 in. from center of impact.

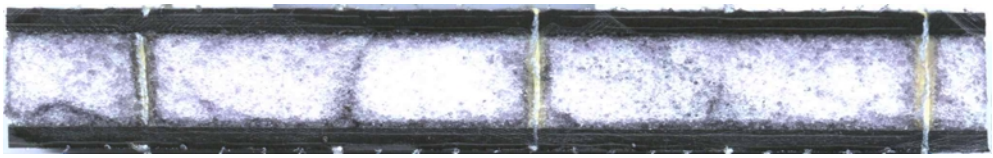

c. Widthwise cut 1.5 in. from center of impact.

d. Lengthwise cut through from center of impact.

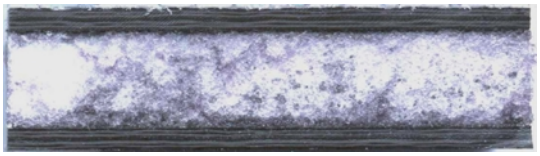

e. Lengthwise cut 0.75 in. from center of impact.

f. Lengthwise cut 1.5 in. from center of impact.

Figure A.20 0.5 in. core, 1.0 in. stitch spacing panel sections after 70 ft-lb impact with 1.88 in. impactor.

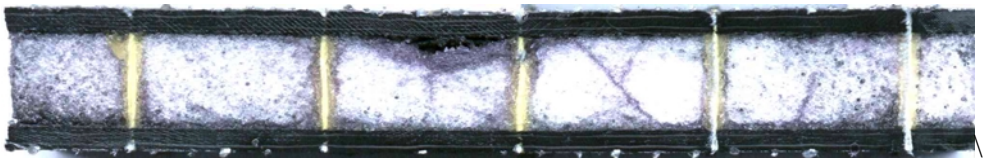

a. Widthwise cut through center of impact.

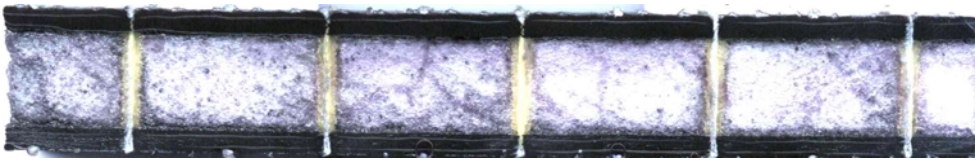

b. Widthwise cut 0.75 in. from center of impact.

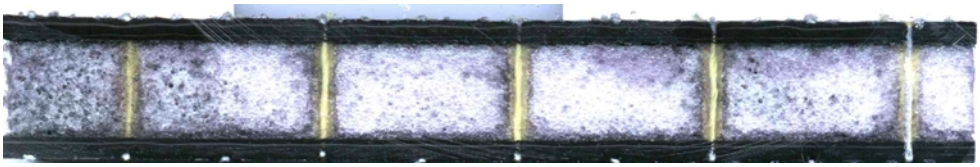

c. Widthwise cut 1.5 in. from center of impact.

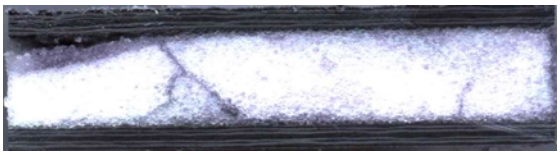

d. Lengthwise cut through from center of impact.

e. Lengthwise cut 0.75 in. from center of impact.

f. Lengthwise cut 1.5 in. from center of impact.

Figure A.21 0.5 in. core 0.5 in. stitch spacing panel sections after 70 ft-lb impact with 1.88 in. impactor.

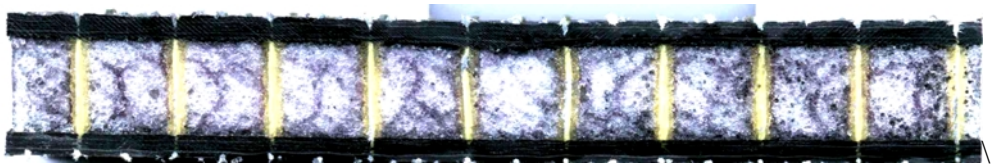

a. Widthwise cut through center of impact.

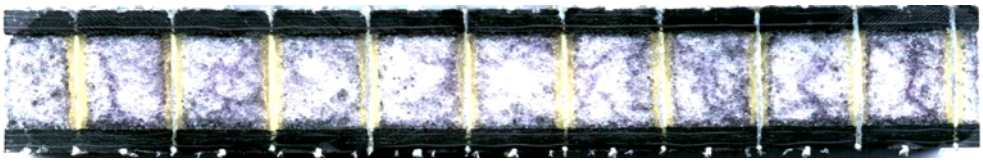

b. Widthwise cut 0.75 in. from center of impact.

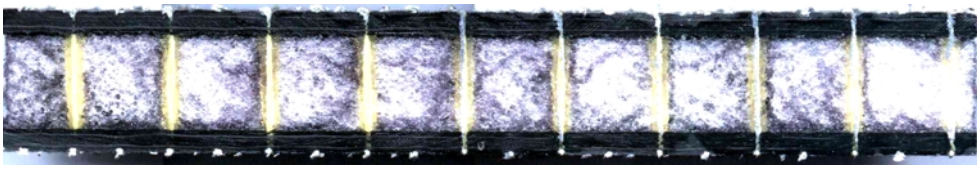

c. Widthwise cut 1.5 in. from center of impact.

d. Lengthwise cut through from center of impact.

e. Lengthwise cut 0.75 in. from center of impact.

f. Lengthwise cut 1.5 in. from center of impact.

Figure A.22 0.5 in. core 0.25 in. stitch spacing panel sections after 70 ft-lb impact with 1.88 in. impactor.

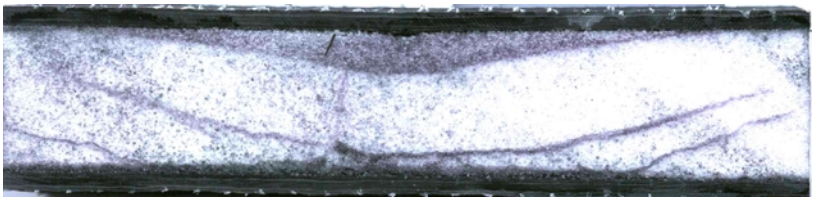

a. Widthwise cut through center of impact.

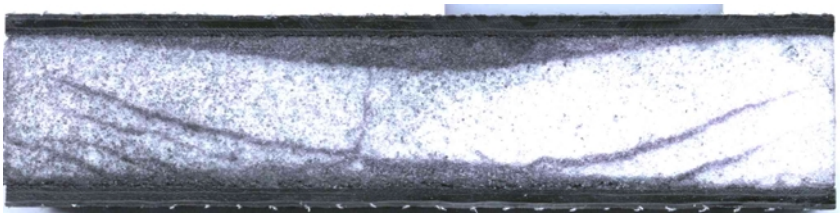

b. Widthwise cut 0.75 in. from center of impact.

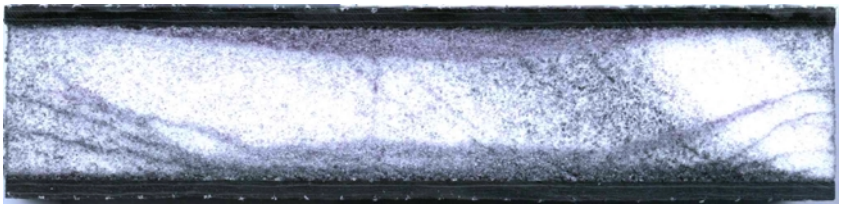

c. Widthwise cut 1.5 in. from center of impact.

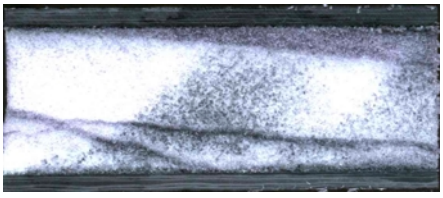

d. Lengthwise cut through from center of impact.

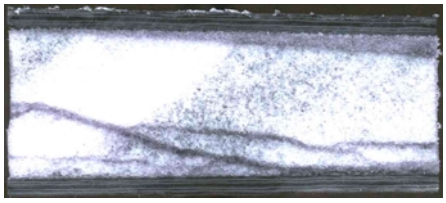

e. Lengthwise cut 0.75 in. from center of impact.

f. Lengthwise cut 1.5 in. from center of impact.

Figure A.23 1.0 in. core, unstitched panel sections after 70 ft-lb impact with 1.88 in. impactor.

a. Widthwise cut through center of impact.

b. Widthwise cut 0.75 in. from center of impact.

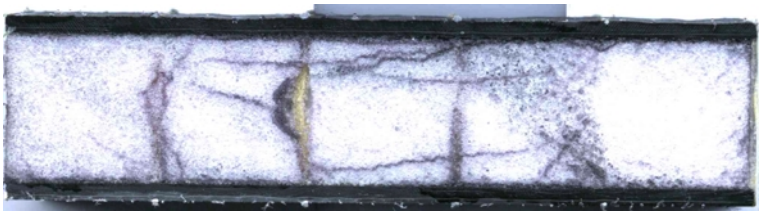

c. Widthwise cut 1.5 in. from center of impact.

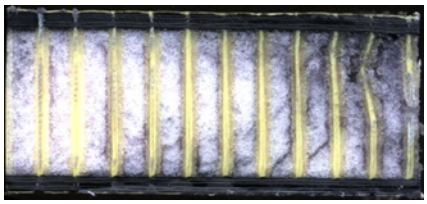

d. Lengthwise cut through from center of impact.

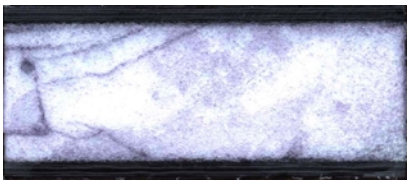

e. Lengthwise cut 0.75 in. from center of impact.

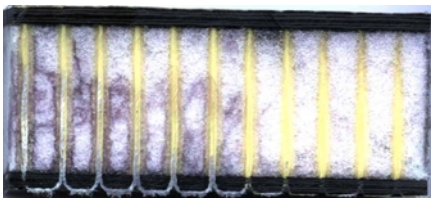

f. Lengthwise cut 1.5 in. from center of impact.

FigureA.24 1.0 in. core, 1 in. stitch spacing panel sections after 70 ft-lb impact with 1.88 in. impactor.

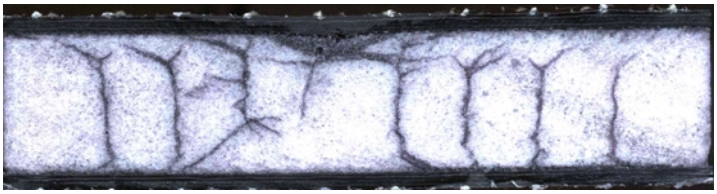

a. Widthwise cut through center of impact.

b. Widthwise cut 0.75 in. from center of impact.

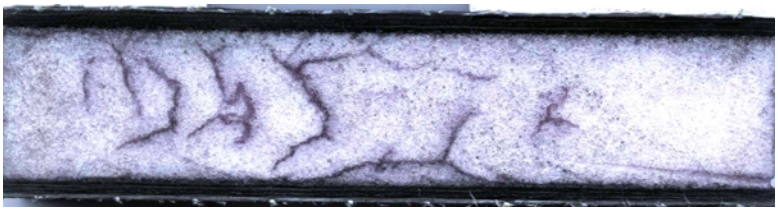

c. Widthwise cut 1.5 in. from center of impact.

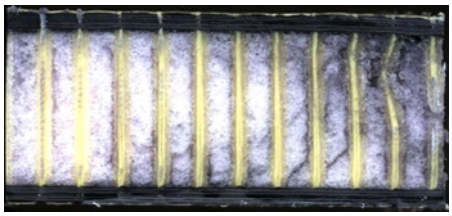

d. Lengthwise cut through from center of impact.

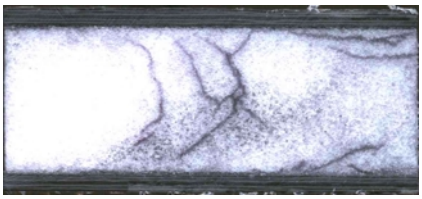

e. Lengthwise cut 0.75 in. from center of impact.

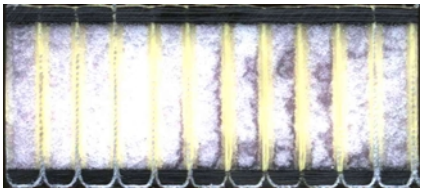

f. Lengthwise cut 1.5 in. from center of impact.

Figure A.25 1.0 in. core 0.5 in. stitch spacing panel sections after 70 ft-lb impact with 1.88 in. impactor.

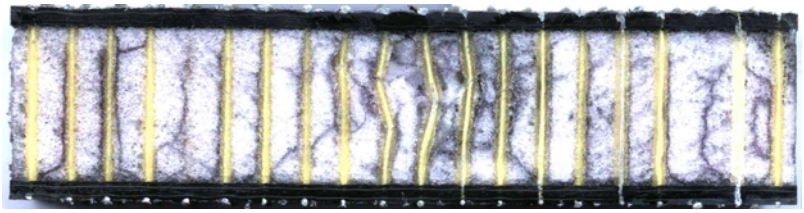

a. Widthwise cut through center of impact.

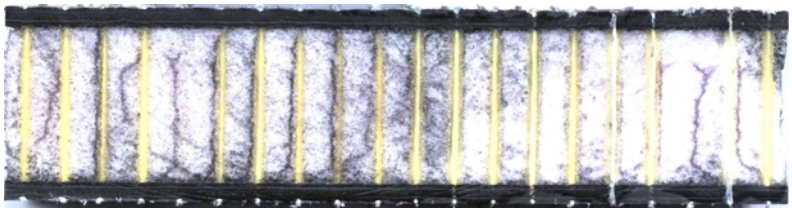

b. Widthwise cut 0.75 in. from center of impact.

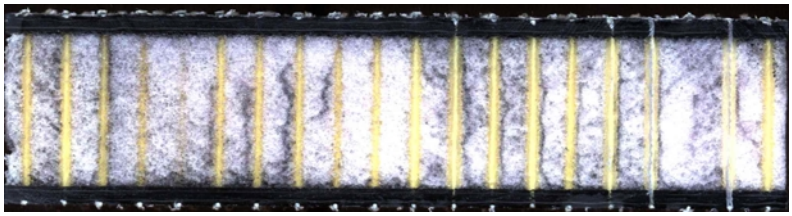

c. Widthwise cut 1.5 in. from center of impact.

d. Lengthwise cut through from center of impact.

e. Lengthwise cut 0.75 in. from center of impact.

f. Lengthwise cut 1.5 in. from center of impact.

Figure A.26 1.0 in. thick core, 0.25 in. stitch spacing panel sections after 70 ft-lb impact with 1.88 in. impactor.

REFERENCES

1. Poe, C.C., Jr. and Harris, C. E., editors, Proceedings of the Mechanics of Textile Composites Conference, NASA Conference Publication 3311, NASA Langley Research Center, October 1995.

2. Sharma, S.K. and Sankar, B.V., "Effects of Through-the-Thickness Stitching on Impact and Interlaminar Fracture Properties of Textile Graphite/Epoxy Laminates," NASA CR-195042, 1995.

3. Sabnis, G. M. Handbook of Composite Construction Engineering, Van Nostrand Reinhold Company, New York, 1979.

4. Nichollos, R. Composite Construction Materials Handbook., Prentice-Hall New Jersey, 1976.

5. Adams, D. O., "Effective Stitch Stiffness in Delaminated Composites" Journal of Reinforced Plastics and Composites, Vol. 19, No 14, 2000.

6. Tanner, M. and Adams, D. O., "Analysis of Damage Development in Stitched Composite Stiffeners," Proceedings of 1999 International SAMPE Technical Conference, Chicago, IL, October 1999.

7. Glaessgen, E. H., Poe, C. C., Jr., and Raju, I. S. "Experimental Verification of Models for Delamination and Stitch Failure in Stitched Composite Joints," proceedings of the 1999 SEM Annual Conference, Cincinnati, OH, June 1999.

8. "Composite Wing Box Tested to Failure," Aviation Week and Space Technology, Vol. 152, No. 25, June 19, 2000, p. 37.

9. Chen, L., Ifju, P.G., Sankar, B. V. and Wallace, B., "Modified DCB Test for High Densty Stitched Composite," Proceedings of 1999 SEM Annual Conference, Cincinnati, Ohio, June 1999.

10. Mignery, L.A., Tan, T.M. and Sun, C.T., "The Use of Stitching to Suppress Delamination in Laminated Composites," ASTM STP 876, 1985, pp. 371-385.

11. Shu, D. and Mai, Y.W., "Effect of Stitching on Interlaminar Delamination Extension in Composite Laminates," Composites Science and Technology, Vol. 49, 1993, pp. 165-171.

12. Jain, L.K. and Mai, Y.W., "Analysis of Stitched Laminated ENF Specimens for Interlaminar Mode II Fracture Toughness," International Journal of Fracture, Vol. 68, 1994, pp. 219-244.

13. Jain, L.K. and Mai, Y. W., "On the Effect of Stitching on Mode I Delamination Toughness of Laminated Composites," Composites Science and Technology, Vol. 51, 1994, pp. 331-345.

14. Lee, H.H., and Hyer, M.W., "Evaluation of Thermal Stresses at the Interface of a Stitch in a Stitched Laminate," Journal of Reinforced Plastics and Composites, Vol. 15, October 1996, pp. 972-987.

15. Sankar, B.V. and Sonik, V., "Modeling End-Notched Flexure Tests of Stitched Laminates," Proceedings of the American Society for Composites, ASC, 1995, pp. 172-181.

16. Tsai, G.C., "Global/Local Stress Analysis of Stitched Composite Laminate," Proceedings of 23rd International SAMPE Technical Conference, 1991, pp. 297-305.

17. Glaessgen, E.H., Raju, I.S., and Poe, C.C., Jr., "Modeling the Influence of Stitching on Delamination Growth in Stitched Warp-Knit Composite Lap Joints," Proceedings of the 12th International Conference on Composite Materials, ICCM-99-449, 1999.

18. Raju, K. S. and Tomblin, J.S. "Energy Absorption Characteristics of Stitched Composite Sandwich Panels," Journal of Composite Materials, vol. 33, no. 8, 1999.

19. LAST-A-FOAM, General Plastics Manufacturing Company, Tacoma Washington,1999.

20. Rohacell foam, Northern Fiber Glass, Hampton New Hampshire, 1999.

21. Dexter, H. B., Palmer, R. J., and Hasko, G. H., Fourth NASA/DoD Advanced Composites Technology Conference, NASA CP-3229, 1993.

22. DERAKANE, Epoxy Vinyl Ester Resin. Dow Chemical Company, Midland Michigan.

23. BPF 862 Epon Resin, RSC 2181 curing agent, Shell Chemical Company, Houston Texas.

24. BYK 505A, BYK-Chemie Additives and Instruments USA. Wallingford, Connecticut.

25. ASTM standard D 2256, Standard Test for Tensile Properties of Yarns. American Society for Testing and Materials Annual Book of ASTM Standards, 1995, Vol. 7.01.

26. ASTM standard C393, Standard Test for Flexural properties of Sandwich Constructions. American Society for Testing and Materials Annual Book of ASTM Standards, 1995, Vol. 03.01.

27. ASTM C297, Standard Test Method for Flatwise Tensile Strength of Sandwich Constructions American Society for Testing and Materials Annual Book of ASTM Standards, 1995, Vol. 03.01.

28. ASTM C273, Standard Test Method for Shear Properties of Sandwich Constructions American Society for Testing and Materials Annual Book of ASTM Standards, 1995, Vol. 03.01.

29. ASTM C364, Standard Test Method for Edgewis Compressive Strength of Sandwich Constructions American Society for Testing and Materials Annual Book of ASTM Standards, 1995, Vol. 03.01.

30. NASA Reference Publication 1092, "Standard Tests for Toughened Resin Composites," NASA Langley Research Center, Hampton, VA, July 1983.

REPORT DOCUMENTATION PAGE

Form Approved
OMB No. 0704-0188

1. AGENCY USE ONLY (Leave blank)	2. REPORT DATE	3. REPORT TYPE AND DATES COVERED
	June 2001	Contractor Report

4. TITLE AND SUBTITLE
Development and Evaluation of Stitched Sandwich Panels

5. FUNDING NUMBERS
P.O. L-11332

WU 242-82-76-10

6. AUTHOR(S)
Larry E. Stanley and Daniel O. Adams

7. PERFORMING ORGANIZATION NAME(S) AND ADDRESS(ES)
University of Utah
Department of Mechanical Engineering
50 S.Central Campus Drive, Room 2202
Salt Lake City, UT 84112

8. PERFORMING ORGANIZATION REPORT NUMBER

9. SPONSORING/MONITORING AGENCY NAME(S) AND ADDRESS(ES)
National Aeronautics and Space Administration
Langley Research Center
Hampton, VA 23681-2199

10. SPONSORING/MONITORING AGENCY REPORT NUMBER
NASA/CR-2001-211025

11. SUPPLEMENTARY NOTES
Langley Technical Monitor: James R. Reeder

12a. DISTRIBUTION/AVAILABILITY STATEMENT
Unclassified-Unlimited
Subject Category 24 Distribution: Standard
Availability: NASA CASI (301) 621-0390

12b. DISTRIBUTION CODE

13. ABSTRACT (Maximum 200 words)
This study explored the feasibility and potential benefits provided by the addition of through-the-thickness reinforcement to sandwich structures. Through-the-thickness stitching is proposed to increase the interlaminar strength and damage tolerance of composite sandwich structures. A low-cost, out-of-autoclave processing method was developed to produce composite sandwich panels with carbon fiber face sheets, a closed-cell foam core, and through-the-thickness Kevlar stitching. The sandwich panels were stitched in a dry preform state, vacuum bagged, and infiltrated using Vacuum Assisted Resin Transfer Molding (VARTM) processing. For comparison purposes, unstitched sandwich panels were produced using the same materials and manufacturing methodology. Test panels were produced initially at the University of Utah and later at NASA Langley Research Center. Four types of mechanical tests were performed: flexural testing, flatwise tensile testing, core shear testing, and edgewise compression testing. Drop-weight impact testing followed by specimen sectioning was performed to characterize the damage resistance of stitched sandwich panels. Compression after impact (CAI) testing was performed to evaluate the damage tolerance of the sandwich panels. Results show significant increases in the flexural stiffness and strength, out-of-plane tensile strength, core shear strength, edgewise compression strength, and compression-after-impact strength of stitched sandwich structures.

14. SUBJECT TERMS	15. NUMBER OF PAGES
Stitched composite; Sandwich; CAI; Strength; Shear; Damage tolerance	166
	16. PRICE CODE: A08

17. SECURITY CLASSIFICATION OF REPORT	18. SECURITY CLASSIFICATION OF THIS PAGE	19. SECURITY CLASSIFICATION OF ABSTRACT	20. LIMITATION OF ABSTRACT
Unclassified	Unclassified	Unclassified	UL